NTNU – Trondheim
Norwegian University of
Science and Technology

Catalytic conversion of biomass

Raquel Calleja Aguado

Chemical Engineering
Submission date: June 2013
Supervisor: De Chen, IKP

Norwegian University of Science and Technology
Department of Chemical Engineering

NTNU – Norges Teknisk-
Naturvitenskapelige Universitet

- Institutt for kjemisk prossesteknologi -

MASTER THESIS 2013

TKP 4900

Catalytic conversion of biomass

Supervisor: Professor De Chen

Co-supervisor: Post-doc Jun Zhu

Master thesis by: Raquel Calleja Aguado

Date: 24/06/2013

This master thesis is written on behalf of the Catalysis group at the Department of Chemical Engineering, NTNU. The work has been performed between February 11, 2013 and June 24, 2013.

I am very grateful to Professor De Chen who provided me with the opportunity to use the catalytic system of Ni-ZnO/CNT for the conversion of biomass. He has been heavily involved in the project and gave new ideas about the experiments, and I thank him for his guidance throughout the project.

Also, I would like to give a big thank you to Post. Doc. Jun Zhu, who has been the most important person during every day in the laboratory work, and also been available at all times for any guidance I have needed. This project would not have been possible without his assistance.

Finally, I would like to thank Ondřej Česák for help me during the preparation of the catalystis and Ying Peng Zhen for analyse with the GC the products of the reaction. It has been a pleasure working with you.

I declare that this is an independent work according to the exam regulations of the Norwegian University of Science and Technology (NTNU).

Raquel Calleja Aguado

1. INDEX

INDEX

2. ABSTRACT

ABSTRACT

Catalytic processes for conversion of biomass to transportation fuels have gained an increasing attention in sustainable energy production. The biomass can be converted to fuels via three platforms, such as fast pylolysis (bio-oil as intermediate), hydrolysis (sugars as intermediates) and gasification (synthesis gas as intimidates). Recently it has been reported that biomass can be directly converted to polyols, such as ethylene glycol and propanediol. Those polyols can be converted to gasoline and diesels via hydrogenolysis, aldol condensation and hydrogenation reactions on multifunctional catalysts. The project will deal with synthesis, characterization and catalytic test of Ni-M/ZnO (M-Cu, Ru, Pt) based catalysts.

A catalyst study investigating Ni-ZnO/CNT catalysts for the conversion of biomass into polyols has been done in this project. The Ni-ZnO/CNT catalysts were prepared by a combination of the pechini method and incipient wetness impregnation. First, the commercial CNT were pretreated with acid to remove remaining growth catalyst and other impurities from production. Second, ZnO was impregnated by wetness impregnation on the pretreated CNT, Finally, nickel was added to the ZnO/CNT catalysts by a nickel nitrate precursor.

Then, catalysts characterization was made. The different types were: BET measures, TGA, TPD, chemisorption and XRD.

To conclude this proyect, the catalysts were tested in one reactor.

3. INTRODUCTION

INTRODUCTION

Nowadays, the demand for transportation fuel is increasing due to the transportation of fuels are based on petroleum-derived liquid hydrocarbons. Future projections by the EIA (the U.S Energy Information Administration) indicate that the use of liquid transportation fuels will increase 45% from 2008 to 2035 [1]. Instead of fossil fuels, it is desired a replacement for the required transportation fuels derived from a renewable feedstock. Two biomass-derived fuels have been successfully implemented in the transportation sector: biodiesel from vegetable oils [2], and ethanol produced from corn and sugar industry [3]. It is expected that production of biofuel will increase as the demand for transportation fuels continue to grow but these two only represent a minor part of transportation energy. Both of them are competing with food industry in terms of feedstock, as well as area, and this is the major disadvantage with these processes. To solve this problem one way is use of non-edible lignocellulosic biomass (such as forestry wastes) for the commercial production of transportation fuels. If methods and infrastructure can be sufficiently advanced, this renewable and abundant supply of biomass (consumes CO_2 during growth) can guarantee stable production of liquid transportation fuels in the future. The composition of lignocellulose depends on which lignocellulosic feedstock that is utilized [4] but normally lignocellulose contain hemicellulose (25-35%), cellulose (40-50%) and lignin (15-20%). Hemicellulose and cellulose is the carbohydrate part of lignocellulose. Hemicellulose is an amorphous polymer, which is easy to break it down, and cellulose is a polymer of C5 and C6 sugars. The hidrogen bonding between chains of cellulose (figure 3.1) makes it harder to desconstruct than hemicellulose. However, the amorphous 3D-polymer structure of lignin consisting of three main units that embeds in and binds to the former two components [4] makes it much more difficult to crack than both cellulose and hemicellulose.

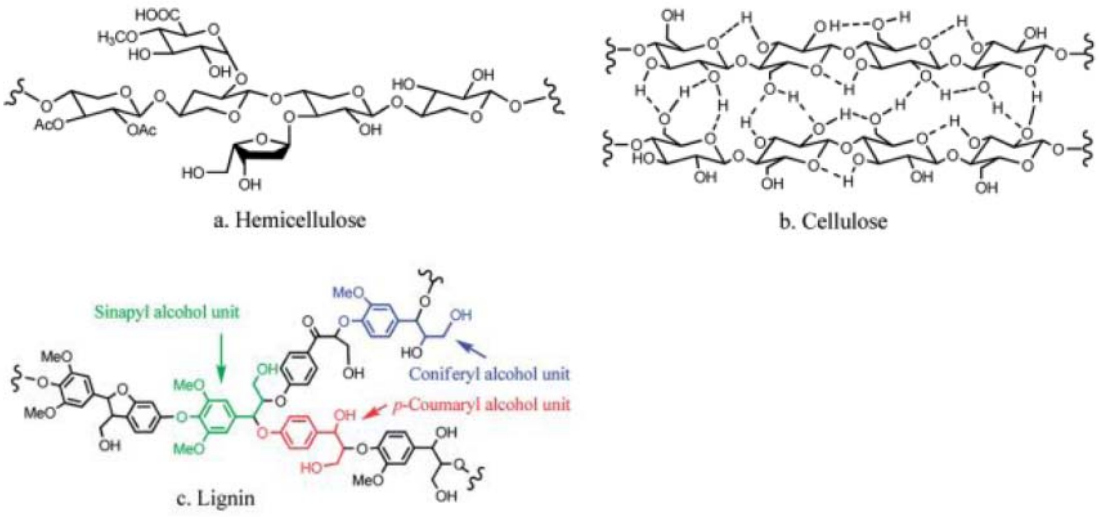

Figure 3.1: structures of hemicellulose, cellulose and lignin

As I say in the abstrac there are a lot of ways for the conversion of biomass to liquid transportation fuels: thermal pathways (pyrolysis and gasification), biological pathways and catalytic pathways (figure 3.2) [5]. These routes represent different processes for the conversion of biomass to hydrocarbon transportation fuels, all in which petroleum carbon is avoided. The enviromental impact whe we use petroleum reserves is higher than if we use lignocellulose as a carbon source. In this study the focus will be on the catalytic conversion of lignocellulosic biomass to polyols.

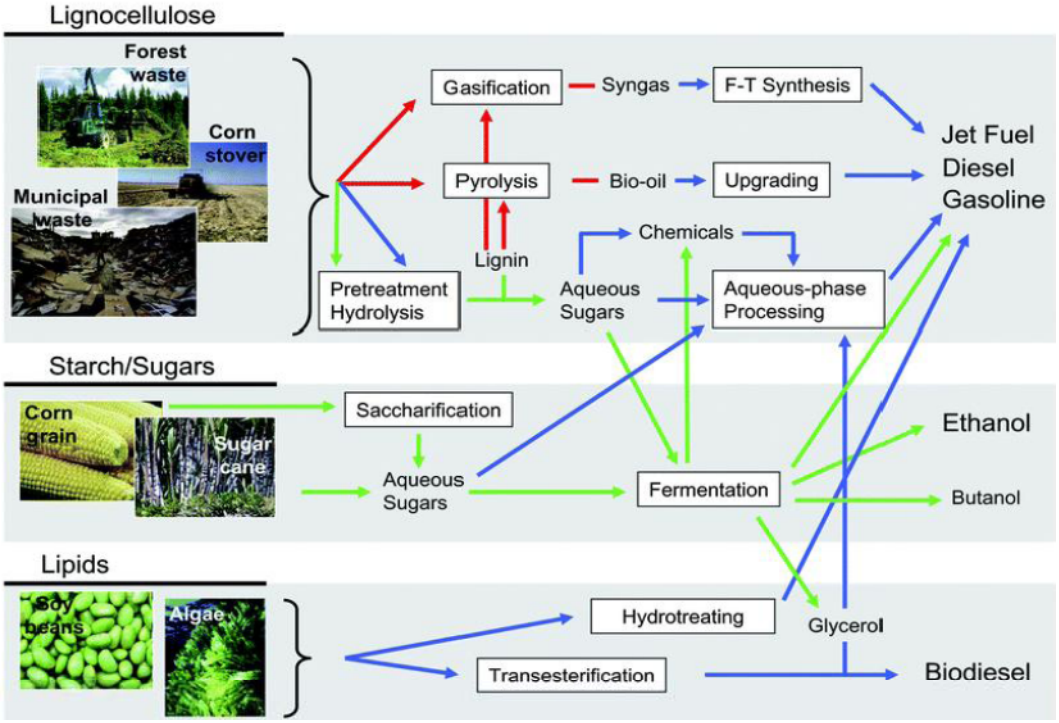

Figure 3.2: conversion of biomass

4. BACKGROUND AND THEORY

BACKGROUND AND THEORY

Chemical transformation from lignocellulosic biomass to polyols.

The interest of the direct conversion of biomass to polyols over a heterogeneous catalyst has increased. Subsequent the polyols can be converted into liquid transportation fuels by deoxygenation and C-C coupling reactions. The best point about this catalytic pathway is that the expensive pretreatment step (required in the aqueous phase pathways [5] for conversion of biomass) is eliminated, and the catalytic system allows high selectivity towards polyol, such as ethylene glycol (EG) and propanediol (1,2-PG). The first people that demonstrate one-pot chemical transformation of biomass to polyols was Fukuoka et al [6]. In this strategy the main priority is the selectivity to a certain polyol, which is highly dependent on the process catalyst. Recently Changzhi Li et al [4] achieved an advance in the catalytic conversion of raw woody biomass to polyols with their previously developed nickel-promoted tungsten catalyst, Ni-W_2C/AC [7]. Cellulose and hemicellulose were converted to EG and other diols (yield up to 75,6%), while the lignin component was converted selectively into monophenols (yield of 46,5%). the composition and structure of the lignocellulosic feedstock affects the catalytic activity significantly. The results indicate that the yield of 1,2-PG increases with the hemicellulose content, and the lignin content can significantly affect the activity of Ni-W_2C/AC for lignocellulose degradation. The higher amount of lignin, the harder it is to degrade. This process shows potential for further development into a commercial process. However, the stability of the Ni–W_2C catalyst remains a challenge. Further investigations have been done to improve the stability of the nickel-promoted tungsten catalyst. In one investigation, the traditional active carbon was replaced by a 3D mesoporous carbon (replicated from commercial silica) which resulted in better resistance to deactivation, and a selectivity towards EG up to 72,9% [9]. Another study that resulted in improved stability was done by Zhijun Tai et al, who developed a temperature-controlled phase-transfer catalyst system; tungsten acid (H_2WO_4) in combination with an activated carbon supported Ru catalyst (Ru/AC), which showed superior reusability and high activity in the one-pot conversion of cellulose to EG [10]. The idea of replacing W_2C by another W source is interesting for future studies.

Very recently another nickel promoted catalyst system was developed for the selective conversion cellulose. Xicheng Wang et al investigated nickel catalysts with different support for the conversion of microcrystalline cellulose to 1,2-alkanediols [12]. The

results show that all the catalysts were effective for the cellulose conversion, but the support determined the product distribution. Among the catalysts tested, the bifunctional ZnO-supported Ni catalysts had the highest selectivity towards 1,2 – alkanediols. The ZnO-supported Ni catalyst showed superior activities and the best result was obtained over a 20% Ni/ZnO catalyst, which exhibited complete conversion of cellulose and up to 70,4% total glycol yields. NH_3-TPR and CO_2 –TPR characterization revealed that Ni/ZnO catalysts possess both acidic and basic sites on the surface, which both changed with the chosen metal loading. The suggested pathway for this process is illustrated in figure 4.1. It is suggested that nickel promotes hydrogenation, while ZnO is active for dehydration. The dehydration step is critical for the formation of intermediates form cellulose, and determines the overall conversion of cellulose. The conversion of cellulose at different reaction times showed that 2 h was enough to gain excellent performance over 20% Ni/ZnO, which is approximately half of the time required for the previous developed 2% Ni-30% W_2C/AC catalyst. The strong basic sites are expected to contribute to the excellent activity and selectivity of the Ni/ZnO catalysts. Especially noteworthy is the high yield obtained for 1,2-PG, 34,4%, which, to the best of my knowledge, is the highest yield reported for 1,2-PG. Correspondingly to the previous mentioned Ni supported tungsten catalyst, the drawback with the 20% Ni/ZnO catalyst is the relatively poor hydrothermal stability. The total glycol yield decreased from 70,4% to 62,0% in the second run, and further dropped to 45,6% in the third run. However, the product distribution did not change significantly.

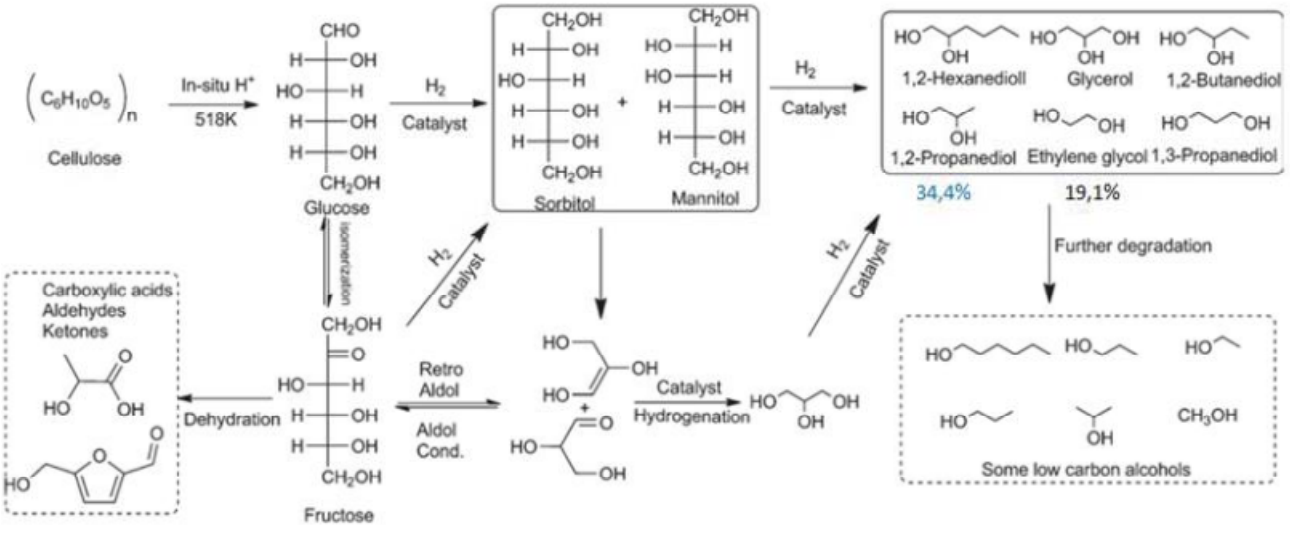

Figure 4.1: catalytic conversion of cellulose over a 20% Ni/ZnO catalyst.

Previous literatures have mostly used EG as the preferred polyol, thus the focus on 1,2-PG (rather than EG) is relatively new, and further improvements are very likely. The high yield of 1,2-PG in the report by Xicheng Wang et al [12] was assigned to surface basicity in the catalytic system. Thus tuning the basic surface using CO_2-TPR characterization might lead to improvements. Additionally the challenge related to the stability of the Ni/ZnO catalyst might be improved by introducing carbon nanotubes as catalyst support. Since this is the first observation of an easily available supported Ni catalyst that effectively catalyze the conversion of high-crystalline cellulose into polyols, further investigations are needed to reveal other parameters related to this catalyst. The motive of this catalyst study is to investigate Ni-ZnO/CNT catalysts for the conversion of cellulose to light oxides to see if the addition of CNT will improve the Ni/ZnO catalyst prepared by Xicheng Wang et al [12].

The ZnO-coating of the CNT

The Sol-gel method is often used to prepare metal oxides, and involves a hydrolysis reaction and a polymerization reaction of metal precursors in liquid phase. This is a possible method for the impregnation of Ni-ZnO on the CNT. Another possibility is using the Pechini method, which is a modified Sol-gel process involving the formation of a 3D polymer resin of a metal complex with subsequent calcination at elevated temperature to obtain the oxides. The key point in Pechini method is the in situ polymerization between CA (citric acid) and EG/PEG (ethylene glycol or 1-2 polyethylene glycol), which leads to the formation of a metal citrate complex, as ilustrated in Figure 4.2. The complex solution can subsequently be impregnated on the CNT, and after drying, the catalyst precursor is heated to initiate pyrolysis of the organic species, and ultimately the desired mixed oxide is obtained. The Pechini method combined with incipient wetness will be tested for the Ni-ZnO/CNT coating of the CNT. In future studies, it would also be interesting to investigate the preparation of Ni-ZnO/CNT catalysts by electrochemical preparation methods.

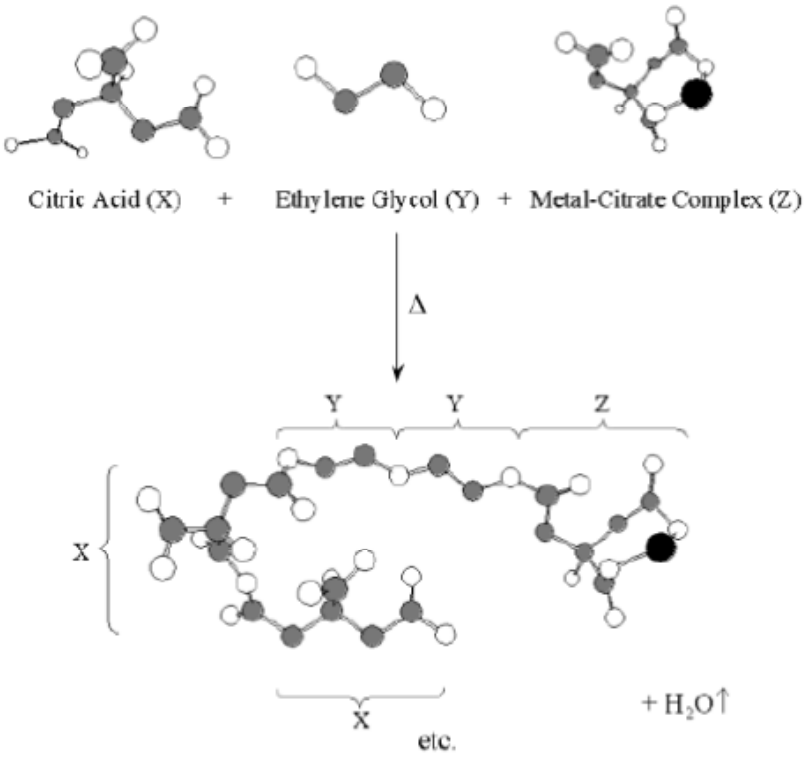

Figure 4.2: formation of a metal citrate complex by the Pechini method.

Catalyst characterization

- BET

A tool for finding the specific surface area [m^2/g] of a catalyst or a support is the BET method, a method based on the isotherm of Brunauer, Emmett and Teller [13]. The main idea of this method is that the surface of the catalyst physisorbs an inert gas such as nitrogen or argon in defined layers. The surface area is determined from the amount of gas needed to fill a monolayer (θ) on the catalyst or support.

The BET equation is derived from the rate equations expressing the equilibrium of the adsorption and desorption. It is assumed that the adsorption and desorption rates are equivalent.

$$\frac{P}{V_a(P_o - P)} = \frac{1}{X \cdot V_o} + \frac{(X-1)}{X \cdot V_o}\frac{P}{P_o}$$

Where:

X is the ratio of the desorption rate constants, k_2 and k_1 for the second and first layers, respectively.

Plotting $P/(V_a(P_0-P))$ versus P/P_0 gives a straight line that intersects the vertical axis at $\eta = 1/(X \cdot V_0)$ and has the slope $\alpha = (X-1)/(X \cdot V_0)$. Usually a relative pressure ranging from 0.05 to 0.30 is used because it gives the best fit [14, 15]. From this the volume adsorbed in the first monolayer, V_0 can be calculated:

$$V_o = \frac{1}{\alpha + \eta}$$

The volume adsorbed in the first monolayer is subsequently used to find the number of molecules adsorbed, N_0:

$$N_o = \frac{P \cdot V_o}{k_B \cdot T}$$

At 77 K, N_2 occupies an area of $A_0 = 0.162$ nm^2 [16]. The BET surface area per gram support or catalyst is found by multiplying N_0 by A_0.

There is a number of assumptions related to the BET method. As already mentioned, the rate of adsorption and desorption are assumed to be equal in any layer. The amount of molecules adsorbed on the first layer is equal to the number of adsorption sites and these adsorbed molecules serve as adsorption sites for the subsequent layer. Possible interactions between the adsorbates are neglected, that is, a molecule that is adsorbed will not prevent another molecule from adsorbing onto the adjacent site due to repulsive forces or steric hindrance. As for the layers above the first ($\theta > 1$), the adsorption-desorption conditions are assumed to be equal for all layers. The adsorption energy for the molecules on these layers is the same as the condensation energy. When the pressure equals the saturation pressure the multilayer will grow to infinite thickness.

The adsorption-desorption isotherms are classified according to IUPAC recommendations [15]. The types of physisorption isotherms can be seen in figure 4.3. A phenomenon which is closely related to filling and emptying of mesopores is hysteresis. The types of hysteresis are shown in figure 4.3 too.

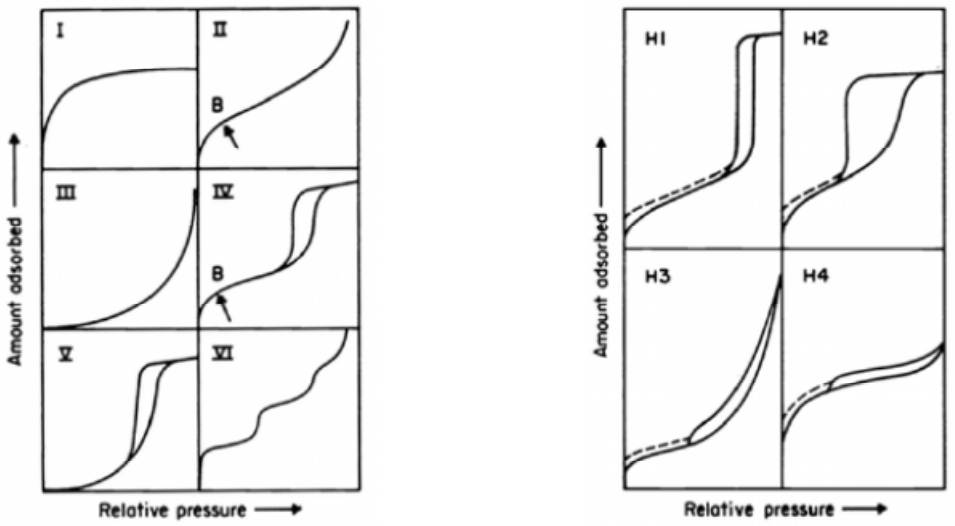

Figure 4.3: different types of sorption isotherms and different types of hysteresis loops

The BET method is often not applicable if the isotherm is Type I or Type III. Type II and Type IV isotherms are well suited for the BET method if the BET plot is linear and contains Point B. The Type II isotherm is attained with a non-porous or macroporous compound. Typical for the Type IV isotherm, which is associated with adsorption in mesoporous structures, is the difference between the adsorption and the desorption in the multilayer range. This is explained by the hysteresis effect, a phenomenon related to pressure needed to fill and discharge the pores [16, 14]. Hysteresis is connected to capillary condensation is mesoporous structures. The lower closure point, that is the lower point where the adsorption and desorption curves meet, depends mainly on the nature of the adsorptive and not so much on the porous adsorbent [15]. The shape of the hysteresis loops are often connected to pore structure. H1 is often associated with compacts of more or less uniform spheres, and gives a rather narrow pore size distribution [15].

Hysteresis is usually not seen in the monolayer-micropore filling range. In the case of micropores, the accessibility of the pores limits the nitrogen uptake, not the total surface area. The BET method does not take the filling of micropores into account, meaning that the result may be a wrong representation of the truth [15].

The adsorption-desorption method is also applied in order to retrieve information about the pores such as the pore volume, the pore size distribution and the average pore size. Pores are classified according to their width [17]. Micropores are smaller than 2 nm, mesopores are between 2 and 50 nm, whereas macropores are larger than 50 nm. The

method most frequently applied for calculation of the pore size and pore volume of mesopores is the Barrett-Joyner-Halenda (BJH) method [18]. The method assumes cylindrical pores. The Kelvin equation takes capillary condensation into account. Although it is generally accepted that the Kelvin equation is not suitable for micropores, the validity of the Kelvin equation is not clearly defined [14, 18]. Some claim that the lower pore size limit is as low as 7.5 nm [14].

- H_2 chemisorption

Within catalyst characterization chemisorption is widely used technique to measure the active metal area and the particle size of supported metal catalysts [19].

Chemisorption is a term used for chemical adsorption of a probe molecule, typically hydrogen. Chemisorption is a strong, more or less permanent, adsorption where the molecules or atoms form a chemical bond with the surface. Physical adsorption, physisorption, is another type of adsorption. Physisorption is characterized by weak reversible interactions between the adsorbate and adsorbent [16].

The chemisorption technique is based on assumptions such as a specific H/M stoichiometry and particle geometry, and the fact that the hydrogen must only adsorb on the active metal, which is not necessarily correct or easy to retrieve in all situations [19, 20]. Still this cheap and easy method is widely applied. The scope of the analysis is to measure the amount of H_2 adsorbed at different pressures at a specific temperature. The quantity adsorbed is plotted against the pressure from which a smooth adsorption isotherm should be obtained. The amount of hydrogen adsorbed is found by extrapolating the linear part of the isotherm to zero pressure.

Chemisorption is mainly used to estimate the dispersion D of a catalyst. The dispersion is the percentage of the metal exposed and is defined as the ratio between the number of surface atoms of the active metal and the total number of metal atoms in the sample, given in this equation:

$$D = \frac{v_{ads} \cdot M_m \cdot F}{x_m \cdot 22400}$$

Where v_{ads} [cm^3/g STP] is the adsorbed gas (e.g. H_2, CO, O_2), M_m is the molecular weight of the metal, F is the stoichiometric factor and x_m is the weight loading of the metal on the catalyst support.

The dispersion can subsequently be used to estimate the metal particle size. The relation between the dispersion and particle size is given in the following equation. It is assumed that the particles are spherical and uniform, with a site density of 14.6 nm^{-2} [21].

$$D = \frac{f_s \cdot M_m}{\rho \cdot A_m \cdot N_A} \frac{S}{V}$$

Where f_s, taking the value 1, is the surface fraction of the active phase, A_m is the cross sectional area of one metal atom, N_A is Avogadro's number, equal 6,022·1023 atoms/mol and ρ is the density of the metal [21]. S/V is the surface to volume ratio, which for spherical particles with diameter d_m is equal to $6/d_m$.

Inserting the known numbers:

$$d_m = \frac{99{,}6}{D}\ nm$$

Another application of the dispersion is to find the site-time yield, STY, which is a measure of the catalyst's average activity. The definition of the STY is the number of molecules of a specified product made per active catalyst surface site and time [22], and it is calculated with:

$$STY = \frac{r \cdot M_m}{x_m \cdot D}$$

Where r is the apparent rate of reaction.

The STY is an alternative to the more common turn over frequency (TOF), which is defined as the number of revelations of the catalytic cycle per unit time [22]. The TOF is only valid under differential conditions.

H_2 spillover

The migration of hydrogen atoms from the metal to the support is termed hydrogen spillover.

In presence of a metal the activation temperature might be much lower, as for instance with rhodium where spillover is observed at room temperature [23]. Hydrogen spillover can be detected by comparing the calculated particle size to the one obtained by CO adsorption, X-ray diffraction or transmission electron microscopy (TEM). If hydrogen spillover has taken place, the particles size will be significantly lower than the one

found with one of the other techniques [20]. However, these techniques also have their limitations and should be used thereafter.

- X-ray diffraction (XRD)

X-ray diffraction (XRD) is used for identification of the crystalline phases in catalysts and to determine the particle size. One major advantage of this technique is that it can be performed in situ, and therefore give a good impression of the state and composition of the catalyst. The technique is one of the most applied methods in characterization of catalysts [16].

In XRD X-ray beams are sent towards a crystalline sample. Photons are elastically scattered by atoms in the periodic lattice of the crystal. The monochromatic scattered X rays (X-rays with a single wavelength) that are in phase will give constructive interference when they collide with a crystal plane that is faced at an angle θ to the incident beam. The strength and angles of the scattered X-ray beams are measured as a function of the angle 2θ.

The lattice spacing, d, between two planes can be derived by using the Bragg relation:

$$n \cdot \lambda = 2d \sin \theta;\ n = 1, 2, \ldots$$

Where λ is the wavelength of the X-rays and θ is the angle between the X-ray beam and the normal to the lattice plane. n is the order of reflection. The lattice spacing can be used to calculate the lattice parameters/constants by the following equation:

$$a = d\sqrt{h^2 + k^2 + l^2}$$

Where h, k and l are known as the Miller indices describing the orientation of the crystallographic planes. The lattice constant is the distance between the corners in a unit cell. For a cubic structure all lattice constants are equal.

The width of the diffraction peaks provide information about the dimensions of the reflecting planes, and thus the size of the particles. The relation between the peak width and the size is given by the Scherrer formula:

$$< L \geq \frac{K \cdot \lambda}{\beta \cdot \cos(\theta}$$

< L > is the length of the particle in the direction which is perpendicular to the reflection plane, λ and θ have the same definitions as mentioned above, β is the full width at half maximum (FWHM) of the specific peak of the XRD plot and K is a constant that depends on the crystallite shape. It often takes the value 1 [16].

XRD can not detect amorphous particles or particles that are too small. This means that it is impossible to be sure that no other phases are present. Additionally, the surface is not detected by XRD either.

- TGA (Thermal gravimetric analysis)

Thermogravimetric analysis (TGA) is an analytical technique used to determine a material's thermal stability and its fraction of volatile components by monitoring the weight change that occurs as a specimen is heated. The measurement is normally carried out in air or in an inert atmosphere, such as Helium or Argon, and the weight is recorded as a function of increasing temperature. Sometimes, the measurement is performed in a lean oxygen atmosphere (1 to 5% O_2 in N_2 or He) to slow down oxidation. In addition to weight changes, some instruments also record the temperature difference between the specimen and one or more reference pans (differential thermal analysis, or DTA) or the heat flow into the specimen pan compared to that of the reference pan (differential scanning calorimetry, or DSC). The latter can be used to monitor the energy released or absorbed via chemical reactions during the heating process. In the particular case of carbon nanotubes, the weight change in an air atmosphere is typically a superposition of the weight loss due to oxidation of carbon into gaseous carbon dioxide and the weight gain due to oxidation of residual metal catalyst into solid oxides.

In most cases, TGA analysis is performed in an oxidative atmosphere (air or oxygen and inert gas mixtures) with a linear temperature ramp. The maximum temperature is selected so that the specimen weight is stable at the end of the experiment, implying that all chemical reactions are completed. This approach provides two important numerical pieces of information: ash content (residual mass, M_{res}) and oxidation temperature (T_o) (Figure 4.3). While the definition of ash content is unambiguous, oxidation temperature can be defined in many ways, including the temperature of the maximum in the weight loss rate (dm/dT_{max}) and the weight loss onset temperature (T_{onset}). The former refers to the temperature of the maximum rate of oxidation, while the latter refers to the

temperature when oxidation just begins. The use of the former definition, To = dm/dT_{max}, is preferred for two reasons.

First, due to the gradual initiation of transition (sometimes up to 100ºC, Figure 4.3) it may be difficult to determine T_{onset} precisely. Gradual onset is believed to be due to nanotubes being contaminated with amorphous carbon and other types of carbonaceous impurities that oxidize at temperatures lower than that of nanotubes. In these cases, T_{onset} describes the properties of the impurities rather than the nanotubes. Second, weight loss due to carbon oxidation is often superimposed on the weight increase due to catalyst oxidation at low temperatures. In some cases this leads to an upward swing of the TGA curve prior to the bulk of the weight loss, which makes the definition of T_{onset} even more difficult and ambiguous. However, determining dm/dT_{max} is relatively straightforward. Therefore, oxidation temperature is herein defined as $T_o = dm/dT_{max}$.

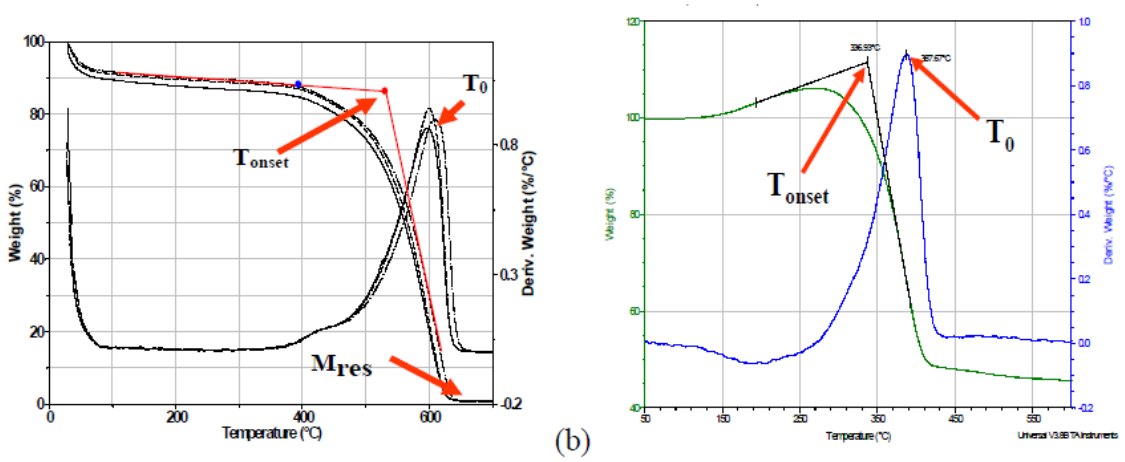

Figure 4.3: (a) TGA of purified SWCNTs; 3 specimens sampled from the same batch. (b) Graph illustrating the ambiguity in determining T_{onset}.

TGA measurement of as-produced nanotube material in air usually produces only one peak in the dm/dT curve, as fluffy raw nanotubes oxidize rapidly in an oxygen-rich environment. However, analysis of purified nanotube material in air may produce more than one peak. These additional peaks are likely due to the fact that purified material contains a fraction of nanotubes with damage and/or with functional groups (i.e., the material is oxidized at lower temperatures) or because purified material is more compacted after drying. The position of each peak is also strongly affected by the amount and morphology of the metal catalyst particles and other carbonbased impurities, as well as their distribution within a specimen. A lean oxygen environment can be used to better separate these peaks. In addition, these peaks have also been attributed to various components in the nanotube material (amorphous carbon,

nanotubes, graphitic particles), and it may be possible to quantify these components by deconvolution of peaks.

Oxidation temperature, T_o, is basically a measure of the thermal stability of nanotubes in air and depends on a number of parameters. For example, smaller diameter nanotubes are believed to oxidize at lower temperature due to a higher curvature strain. Defects and derivatization moiety in nanotube walls can also lower the thermal stability. Active metal particles present in the nanotube specimens may catalyze carbon oxidation, so the amount of metal impurity in the sample can have a considerable influence on the thermal stability. It is impossible to distinguish these contributions, but, nevertheless, thermal stability is a good measure of the overall quality of a given nanotube sample. Higher oxidation temperature is always associated with purer, lessdefective samples.

- Temperature programmed desorption (TPD)

Thermal desorption spectroscopy (TDS), also known as temperature programmed desorption (TPD) is the method of observing desorbed molecules from a surface when the surface temperature is increased.

The basic experiment is very simple, involving: adsorption of one or more molecular species onto the sample surface at low temperature (frequently 300 K, but sometimes sub-ambient) and heating of the sample in a controlled manner (preferably so as to give a linear temperature ramp) whilst monitoring the evolution of species from the surface back into the gas phase.

Since TDS observes the mass of desorbed molecules, it shows what molecules are adsorbed on the surface. Moreover, TDS recognizes the different adsorption conditions of the same molecule from the differences between the desorption temperatures of molecules desorbing different sites at the surface. TDS also obtains the amounts of adsorbed molecules on the surface from the intensity of the peaks of the TDS spectrum, and the total amount of adsorbed species is shown by the integral of the spectrum.

To measure TDS, one needs a mass spectrometer, such as a quadrupole mass spectrometer or a time-of-flight (TOF) mass spectrometer, under ultrahigh vacuum (UHV) conditions. The amount of adsorbed molecules is measured by increasing the temperature at a heating rate of typically 2 K/s to 10 K/s. Several masses may be

simultaneously measured by the mass spectrometer, and the intensity of each mass as a function of temperature is obtained as a TDS spectrum.

Thermal desorption is described based on the Arrhenius equation.

$$r(\sigma) = -\frac{d\sigma}{dt} = v(\sigma)\sigma^n \cdot e^{-\frac{E_{act}(\sigma)}{RT}}$$

Where

r (σ): the desoption rate [mol/cm^2 sec] as a function of σ

n: order of desorption

σ: surface coverage

v(σ): pre-exponential factor [Hz] as a function of σ

E_{act} (σ): activation energy of desorption [kJ/mol] as a function of σ

R: gas constant [J K^{-1} mol^{-1}]

T: temperature [K]

This equation is difficult in daily practice while several variables are a function of the coverage and influence each other. The complete analysis method calculates the pre-exponential factor and the activation energy at several coverages. This calculation can be simplified. First we assume the pre-exponential factor and the activation energy to be independent of the coverage.

We also assume a linear heating rate:

$$T(t) = T_o + (\beta \cdot t)$$

Where:

β: the heating rate in [K/s]

T_o: the start temperature in [K]

t: the time in [s]

We assume that the pump rate of the system is indefinitely large, thus no gasses will absorb during the desorption. The change in pressure during desorption is described as:

$$\frac{dP}{dt} + \frac{P}{\alpha} = \frac{dP}{dt} + \frac{P}{V/S} = \frac{d(a \cdot r(t))}{dt} = \frac{d((\frac{A}{KV}) \cdot r(t))}{dt} =$$

Where:

P: the pressure in the system

t: the time in [s]

A: the sample surface [m^2]

K: a constant

V: volume of the system [m^3]

r(t): the desoption rate [mol/cm^2 sec]

S: the pump rate

V: volume of the system [m^3]

We assume that S is indefinitely large so molecules do not re-adsorpt during desorption process and we assume that P/α is indefinitely small compared to dP/dt and thus:

$$a \cdot r(t) = \frac{dP}{dt}$$

The desorption rate is a function of the change in pressure. One can use data in an experiment, which are a function of the pressure like the intensity of a mass spectrometer, to determine the desorption rate.

Since we assumed the pre-exponential factor and the activation energy to be independent of the coverage. Thermal desorption is described with a simplified Arrhenius equation:

$$r(t) = -\frac{d\sigma}{dt} = v_n \sigma^n \cdot e^{-\frac{E_{act}(\sigma)}{RT}}$$

Where:

r (t): the desorption rate[mol/cm^2 sec]

n: order of desorption

σ: surface coverage

v_n: pre-exponential factor [Hz]

E_{act}: activation energy of desoption [kJ/mol]

R: gas constant

T: temperature [K]

Using the before mentioned Redhead method (a methode less precise as the complete analysis or the leading edge method) and the temperature maximum T_m one can determine the activation energy: for n=1

$$\frac{E_{act}}{R \cdot T_m^2} = \frac{v_1}{\beta} \cdot e^{-\frac{E_{act}(\sigma)}{RT}}$$

for n=2

$$\frac{E_{act}}{R \cdot T_m^2} = \frac{\sigma_0 v_2}{\beta} \cdot e^{-\frac{E_{act}(\sigma)}{RT}}$$

M. Ehasi en K. Christmann have described a simple method to determine the activation energy of the second order.

$$\ln(\sigma \cdot T_m^2) = -\frac{E_{act}}{RT} + \ln \frac{\beta \cdot -E_{act}}{v_2 R}$$

Where: σ_o is the surface area of a TDS or TPD peak.

A graph of $\ln(\sigma_o \cdot T_m)$ versus $1/T_m$ results in a straight line with an angle of $-E_{act}/R$.

Thus in a first order reaction the T_m is independent of the surface coverage. Changing the surface coverage one can determine n. Usually a fixed value of the pre-exponential factor is used and is β known, with these values one can derive the E_{act} iteratively from T_m

5. EXPERIMENTAL

EXPERIMENTAL

1. Pretreatment of the CNT

The commercial CNF (bought from Chengdu Organic Chemicals Co. Ltd) were pretreated with nitric acid 65% to remove remaining growth catalyst and other impurities. 10 g of CNF were treated with nitric acid for each batch. Then 250ml of nitric acid were added to the different batches. The number of treatments for each batch were 3 for the CNT and 2 for the CNF. Each treatment of each batch was heated until 110ºC during 1 hour. The acid treated CNF were subsequently washed with destillated water, and dried at 110˚C overnight. In total five different batches of CNT were pretreated.

BATCH	TYPE	NUMBER OF PRETEATMENTS	HNO_3 (ml)
1	CNT	3	250
2	CNT	3	250
3	CNT	3	250
4	CNF	2	250
5	CNF	2	250

Table 5.1: pretreatment of the CNT with nitric acid (HNO_3)

2. Preparation of Ni-ZnO/CNT catalysts

To prepare the eight ZnO/CNT catalysts, the Pechini method was used, followed by rapid incipient wetness impregnation. The catalysts were dried overnight and calcined in 10% O_2 in N_2 flow. By incipient wetness impregnation, a Nickel precursor was added. The eight Ni-ZnO/CNT catalysts were calcined in 10% O_2 in N_2 flow and reduced in pure H_2 flow.

- **The complex metal solution.**

The complex metal solution was prepared by mixing citric acid (CA), ethylene glycol (EG), distillated water (10ml) and zinc nitrate hexahydrate ($Zn(NO_3)_2 \cdot 6H_2O$), by ultrasonic treatment. The complex metal solution was immediately impregnated on the pretreated CNT by incipient wetness impregnation, and dried at 110ºC overnight. To make the calculation the ZnO loading was supossed. To calculate the amount of CA and EG, the molar ratio between Zn:CA:EG is 7:8:8. (Calculations in appendix A) The first

table show the type of CNT and the ZnO loading while the second table show the amount of each component of the complex solution.

CATALYSTS	TYPE	ZnO LOADING (%)
1	CNF	20
2	CNF	20
3	CNF	10
4	CNF	10
5	CNT	26
6	CNT	20
7	CNT	20
8	CNT	0

Table 5.2: ZnO loading

CATALYST	CNT (g)	$Zn(NO_3)_2 \cdot 6H_2O$ (g)	CA (g)	EG (g)	WATER (*ml*)	COMPLEX SOLUTION (*ml*)
1	2,4	2,1930	1,7690	0,5222	10	2
2	2,4	2,1930	1,7690	0,522	10	1,8
3	2,7	1,0965	0,8841	0,2610	10	2
4	2,7	1,0965	0,8841	0,2610	10	1,8
5	2,2	2,8509	2,2999	0,6758	10	2
6	1,8	2,1930	6,1320	1,8100	10	6
7	2,4	2,1930	1,7690	0,5222	10	8
8	2,4	0	0	0	0	0

Table 5.3: complex metal solution and impregnation in the CNT.

As we can see, the last catalyst hasn't complex solution because is a Ni/CNT.

- **Calcination.**

Calcination of the catalysts was done in 10% O_2 in N_2 flow. All the samples were heated up to 400ºC in Argon flow with a heating rate of 10ºC/min during 1 hour, then 10 minutes with the same flow of 10% O_2 in N_2 and then cooling down in Argon flow until room temperature.

- **The Nickel impregnation of the calcined ZnO/CNT catalysts.**

Nickel was impregnated, by incipient wetness, on the calcined ZnO/CNT catalysts. The precursor used was Nickel (II) nitrate hexahydrate. Each catalyst has 20% Nickel-loading (calculations in appendix B). Then calcination at similar conditions that before was used. The following table shows details related to the incipient wetness impregnation of Ni on the ZnO/CNT catalysts.

CATALYST	ZnO/CNT (g)	Ni (g)	DESTILLATED WATER (ml)
1	1,3869	1,7178	2,77
2	1,3869	1,7178	2,77
3	1,3404	1,6602	2,68
4	1,4853	1,8397	2,97
5	1,5196	1,8821	3,03
6	1,3869	2,1222	2,77
7	3	0	0
8	2,4	2,9700	4,8

Table 5.4: Ni-impregnation on the catalysts

As we can see the catalyst 7 hasn't Ni because it is a ZnO/CNT catalyst.

- **Reduction of the Ni-ZnO/CNT catalysts.**

The Ni-ZnO/CNT catalysts were reduced in pure H_2 flow at 400°C for 2 hours. The heating rate used was 10ºC/min, and then for cooling down argon was used with the same cooling rate.

6. CATALYST CHARACTERIZATION

CATALYST CHARACTERIZATION

1. N_2-adsorption measurements (BET)

The physical properties of the calcined ZnO/CNT and the calcined Ni-ZnO/CNT catalysts were investigated by N_2-adsorption measurements in a Micrometrics Tristar II 3020. Each sample was degassed at 200°C overnight. The samples were analyzed at liquid nitrogen temperature. The surface area was calculated by the Brunauer-Emmet-Teller (BET) method, and the pore volume and pore size distribution were obtained from N_2-adsorption using Barett-Joyner-Halenda (BJH) method.

Figure 6.1: BET

The main idea of BET is that the surface of the catalyst physisorbs an inert gas such as nitrogen or argon in defined layers. The surface area is determined from the amount of gas needed to fill a monolayer on the catalyst or support.
The adsorption method is also applied in order to retrieve information about the pores such as the pore volume, the pore size distribution and the average pore size. The method most frequently applied for calculation of the pore size and pore volume of mesopores is the Barrett-Joyner-Halenda (BJH) method [18]. The method assumes cylindrical pores.

2. Chemisorption

Hydrogen Chemisorption was carried out in a Micromeritics ASAP 2020 instrument to measure the nickel dispersion. The temperature was controlled with a thermocouple placed between the reactor and the inner wall of the furnace. It is assumed that hydrogen adsorbs dissociatively, that is, one hydrogen atom per metal surface area atom [24].

Figure 6.2: chemisorption

A sample (~200 mg) was weighed before put into a U-shaped quartz reactor which was already loaded with some loosely packed quartz wool. To encapsulate the sample, quartz wool was also put on top of the sample. The reactor was attached to the apparatus. To ensure that

the reactor was completely closed to the atmosphere, vacuum was introduced and a leak test was performed.

The chemisorption technique is based on assumptions such as a specific H/M stoichiometry and particle geometry, and the fact that the hydrogen must only adsorb on the active metal, which is not necessarily correct or easy to retrieve in all situations [19, 20]. Still this cheap and easy method is widely applied. The scope of the analysis is to measure the amount of H_2 adsorbed at different pressures at a specific temperature. The quantity adsorbed is plotted against the pressure from which a smooth adsorption isotherm should be obtained. The amount of hydrogen adsorbed is found by extrapolating the linear part of the isotherm to zero pressure.

3. X-Ray Diffraction (XRD)

XRD measurements were carried out using a Bruker-AXS D8-focus instrument with a D8 gonimeter with Cu Kα radiation and a Lynxeye detector. Diffractograms were obtained in the 2θ range of 20-70° with a step size of 0,020° and a step time of 1,5 s.

Figure 6.3: XRD

X-ray diffraction (XRD) is used for identification of the crystalline phases in catalysts and to determine the particle size. One major advantage of this technique is that it can be performed in situ, and therefore give a good impression of the state and composition of the catalyst.

XRD can not detect amorphous particles or particles that are too small. This means that it is impossible to be sure that no other phases are present. Additionally, the surface is not detected by XRD either.

4. TGA (Thermal gravimetric analysis)

TGA was carried out in a TGA/DSC instrument (NETZSCH STA499C). The sample of the Ni-ZnO/CNT was heated from 30ºC to 1000ºC with a rate of 10ºC/min in air.


Figure 6.4: TGA

TGA is a method of thermal analysis in which changes in physical and chemical properties of materials are measured as a function of increasing temperature (with constant heating rate), or as a function of time (with constant temperature and/o constant mass loss). TGA can provide information about physical phenomena.

5. Temperature programmed desorption (TPD)

CO_2-TPD was carried out on the calcined ZnO/CNT catalysts and the calcined Ni-ZnO/CNT catalysts. A thermogravimetric analyzer (Netzch STA-429 instrument) was used, and Argon was used as purge gas (PG). The samples were heated in Ar flow (50ml/min) to 300°C (10ºC/min) and kept at 300°C for 1h before they were cooled down to 30°C (10ºC/min). The samples were then exposed to CO_2 (50ml/min, PG: Ar 50) for 1h, followed by 30 min with PG:50 and 1 h with PG:25. The samples were finally heated to 900°C (10ºC/min) with PG:25.

7. CATALYSTS TEST

CATALYSTS TEST

The catalytic conversion of cellulose into polyols was carried out mixing cellulose with the Ni-ZnO/CNT in a stainless-steel bacht reactor (Parr, 100 mL). The procedure of this reaction is:

1. Open the reactor and add 200 ml H_2O, 0,5g cellulose, 2g catalyst in the reactor.
2. Close the reactor properly.
3. Check the leakage by N_2 (by gradually increase the pressure from 20 to 85 or 90 bar).
4. Release the pressure gradually.
5. Purge the reactor three times with 5 bar of N_2 in order to remove the remaining oxygen in the reactor.
6. Purge the reactor with hydrogen.
7. Add 20 bar of hydrogen in the reactor.
8. Increase the temperature to 245ºC with stirring in the reactor (600 rpm).
9. Keep the temperature in 245ºC for 30 minutes.
10. Set the temperature to 0ºC.
11. After the temperature goes down to room temperature, release the hydrogen slowly.
12. Purge the reactor with N_2 for three times to remove the remaining hydrogen.
13. Open the reactor and collect the product.
14. Analyse the products with the GC.

The temperature inside the reactor increased to 263ºC after introducing the H_2, and was kept at 263ºC to the end. This happens due to the heat of the reaction.

The process flow diagram of the plant is show below:

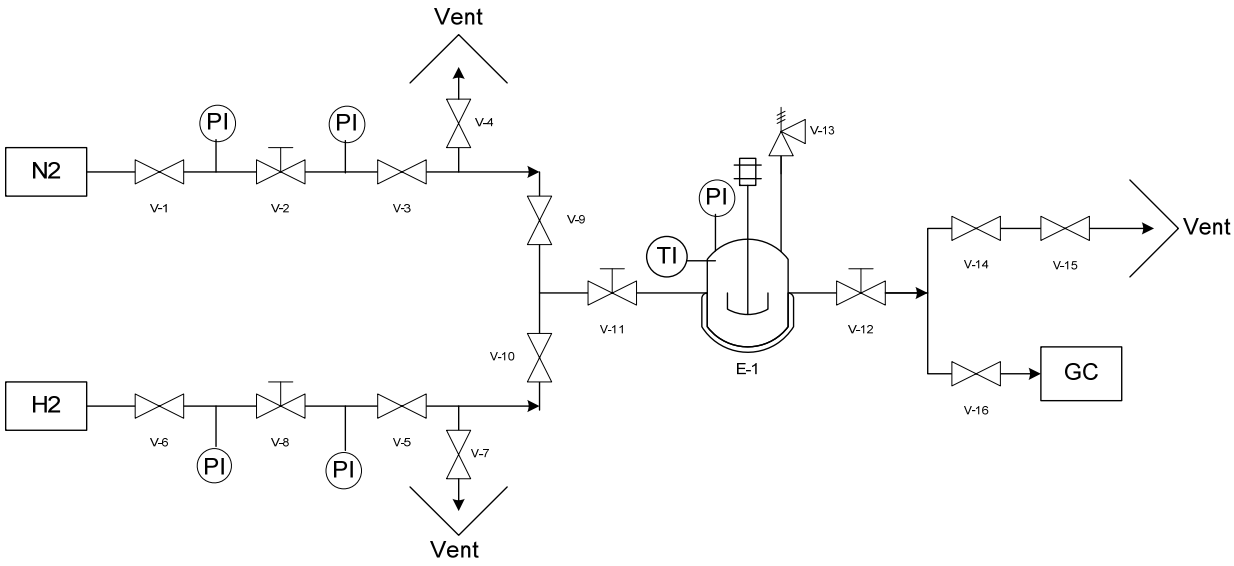

Figure 7.1: PFD of conversion of cellulose

With the valves V-2 and V-8, the inlet flow is controlled. If the pressure is high we can use valves V-4 and V-7 to decrease it.

The reactor has a safety valve. If the pressure in the reactor is very high, the safety valve open and the gases go to the ventilation to decrease the inside pressure.

Then, when the reaction has finished, the gases inside the reactor are remaining to the ventilation with the valves V-14 and V-15.

After remain the gasses, the product is collected in a glass container and analyse which kind of products are inside by liquid inyection in the GC.

8.RESULTS AND DISCUSSION

RESULTS AND DISCUSSION

1. The Brunauer-Emmet-Teller (BET) method

The Brunauer-Emmet-Teller (BET) method was used to calculate the surface area, and the pore volume and pore size distribution were obtained from N_2-adsorption using Barett-Joyner-Halenda (BJH) method. Each catalysts were tested, including the ZnO/CNT catalyst and Ni/CNT catalyst. The results for the different catalysts are presented in the following table.

CATALYST	ZnO LOADING (%)	BET SURFACE AREA (m^2/g)	PORE VOLUME (cm^3/g)	PORE SIZE (Å)	t-PLOT MICROPORE VOLUME (cm^3/g)
1	20	162,0879	0,169944	47,792	0,009247
2	20	166,9475	0,195713	49,670	0,010084
3	10	168,9443	0,184775	49,796	0,011379
4	10	165,7748	0,160501	45,208	0,012168
5	26	163,9367	0,175928	49,419	0,011914
6	20	80,7357	0,106743	55,164	0,000729
7	20	22,2119	0,024038	50,800	-0,000004
8	0	104,6299	0,130983	49,913	0,001072

Table 8.1: BET measurements for the ZnO/CNT catalyst and the Ni-ZnO/CNT catalysts

As we can see in the table 8.1, the BET surface area is, more or less, stable in the first 5 catalyst, this means that the surface area doesn't depend on the amount of ZnO that is added. We cas see also that the BET surface decrease if the ZnO loading is higher (in the catalyst 3, with only 10% of ZnO, the area is 168,9443 m^2/g, while in the catalyst 5 that has 26% of ZnO the surface area is 163,9367 m^2/g).

We can also observe that if the Zn and Ni are added together (catalyst 6) the BET surface area decrease a lot.

Now the comparison between catalyst 7 (20%ZnO/CNT) and catalyst 1 (20%Ni-20%ZnO/CNT) is done. As we can see, after the Ni is added the BET surface are increase so much (the catalyst 1 has an area of 162,0879 m^2/g while the area ot catalyst 7 is 22,2119 m^2/g).

With the catalyst 8 we can see that the presence of Ni or not influence very much on the BET surface area. The difference between the catalyst 8 and the catalysts from 1 to 5 is less than the difference between catalyst 7 and the rest of them. So we can say that the Ni increase the surface area.

By comparing the micropore volume for catalysts 7 and 1, it is observed that the micropore volume increases from -0,000004 to 0,009247 cm^3/g. One possible explanation is that the strong acidic nickel nitrate might have destroyed parts of the ZnO-layer and created the measured miscropores in the catalyst.

In relation with the adsorption plots, we can say that the amount adsorbed increases at higher pressures.

The adsorption-desorption isotherms and the BJH Adsorption dV/dD Pore Volume plots from the BET measurements for each catalysts are given in appendix C.

2. Chemisorption

H_2-Chemisorption was carried out on Ni-ZnO/CNT to determine the nickel dispersion in the catalyst. The following table shows the results of the metal dispersion and the metal particle size:

CATALYSTS	DISPERSION (%)	PARTICLE SIZE (nm)
1	1,1002	92,01338
2	1,3054	77,55081
3	1,0625	95,27318
4	1,2294	82,34293
5	0,9742	103,91378
6	0,0601	1685,12604
7	-0,2241	-451,74773
8	4,8678	20,79619

Table 8.2: chemisorption measurements for the ZnO/CNT catalyst and the Ni-ZnO/CNT catalysts

The nickel dispersion is not particularly high, and this might be due to the high amount of metal added (20%) to the ZnO/CNT catalysts.

As we can see in the table 8.2, in the first five catalysts the dispersion is stable. We also can see that the dispersion of the Ni decreases if there is more ZnO loading (for example the dispersion of the catalyst 3 is 1,3054% while the dispersion of catalyst 5 is 0,9742%). In relation with the particle size is the contrary. The particle size increases when the ZnO loading is higher.

Another special thing is that we added together the Ni and ZnO (catalyst 6) the dispersion decreases so much, but the particle size increase very much (1685,12604 nm). These differences may be caused by the different electrical charges between the Ni and Zn.

In the catalyst 7, we can observe that the dispersion and the particle size is 0 because this catalyst is 20%ZnO/CNT, so no contains Ni.

In catalyst 8, the dispersion is very high and the particle size is very low. This catalyst only contain 20% of Ni so we can say that the presence of diferents amounts of ZnO decrease the dispersion and increase the particle size.

The adsorption plots show an increased hydrogen consumption at higher pressures. This might be an indication of hydrogen spillover into the ZnO. The adsorption data will thus probably include the total adsorption of H_2 on both the active metal and ZnO. A way to circumvent the spillover effect is to decrease the analysis temperature and use low pressures within a narrow range,

The adsorption plots and detailed data are found in appendix D.

3. X-Ray Diffraction (XRD)

X-ray diffraction analysis was carried out to identify the components in the catalysts, to compare the peaks of the different samples and to determine the particle size.

The XRD measurements of the Ni-ZnO/CNT (catalysts 1 to 6) are illustrated in figure 8.1. The first biggest peak is carbon in the Ni-ZnO/CNT.

According to the XRD results zinc nickel oxide was formed, or at least it is very hard to separate nickel from zinc oxide. Two peaks with oxides are located after the first carbon peak. The green line symbolizes zinc nickel oxide and the blue line symbolizes nickel oxide. The blue line, nickel oxide, is placed left next to the green line, zinc nickel oxide, and one has to zoom in to actually notice the blue line, as illustrated in figure 8.2. In this

figure the zinc nickel oxide (gree) and the nickel oxide (blue) are identified right next to each other, and additionally zinc oxide (violet) is identified to the left for these compounds. A similar distribution is found in the other peaks with zinc nickel oxide, and it is not straight forward to determine how the zinc, nickel and oxides are separated or combined in these catalysts. If, in fact, zinc nickel oxide is formed it might make it more difficult to reduce the catalysts.

Catalyst 1 has the sharpest peaks which indicate that this catalyst also has the biggest particles. (The particle size will be describe later).

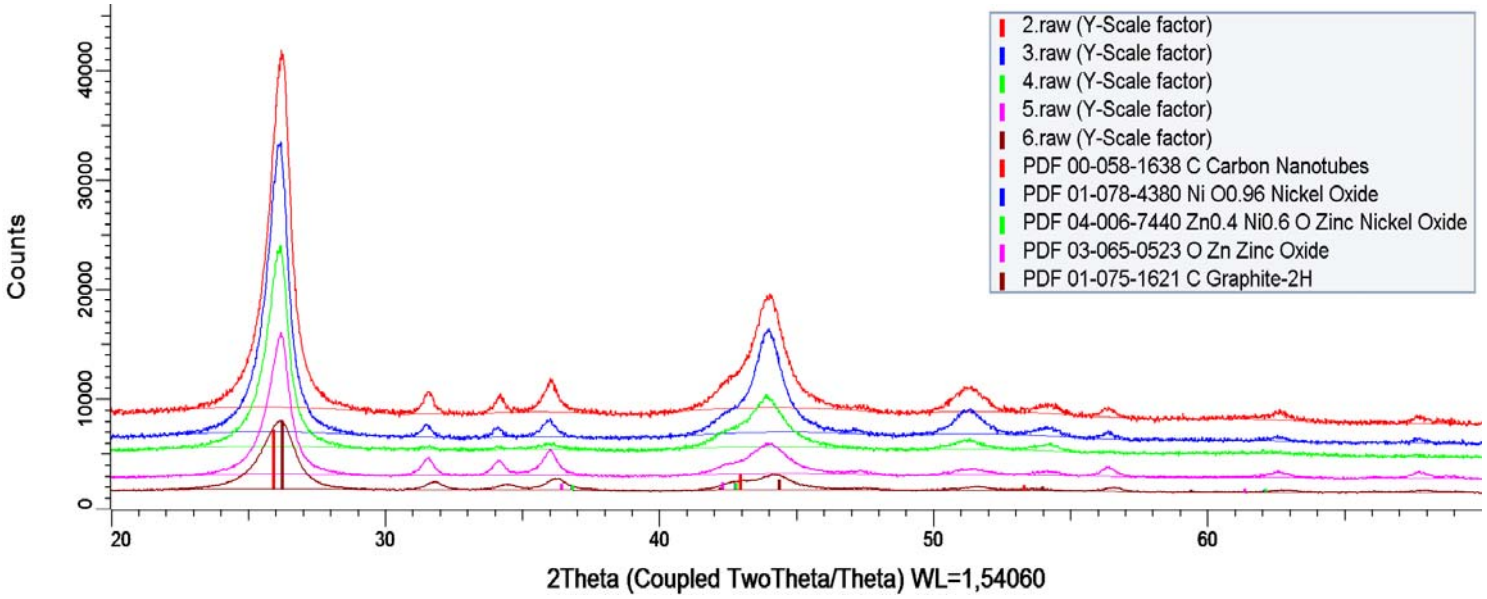

Figure 8.1 The XRD patterns for the Ni-ZnO/CNT catalysts

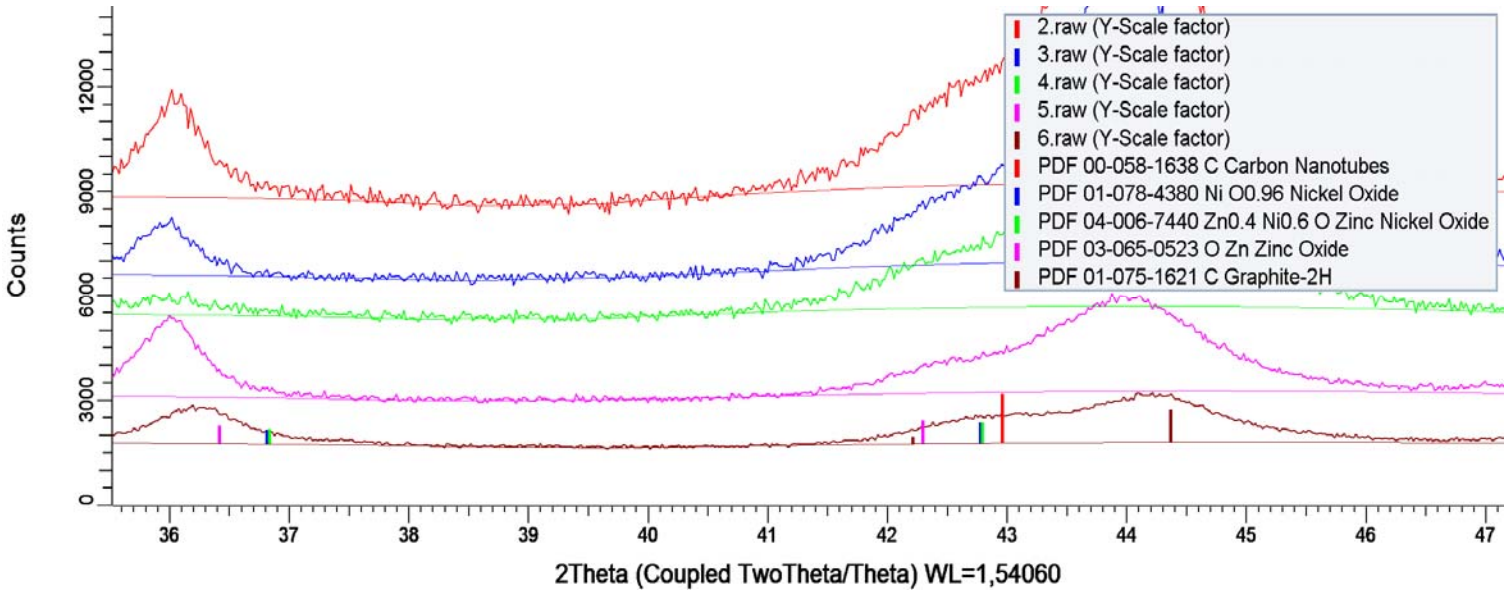

Figure 8.2 The XRD patterns for one peak in the Ni-ZnO/CNT catalysts (zoomed in from Figure 7.1)

The XRD measurements of the ZnO/CNT (catalyst 7) is illustrated in figure 8.3. The first biggest peak is carbon in the ZnO/CNT.

The diffraction pattern of the ZnO/CNT catalyst shows one peak identified as ZnO, followed by some smaller peaks of carbon.

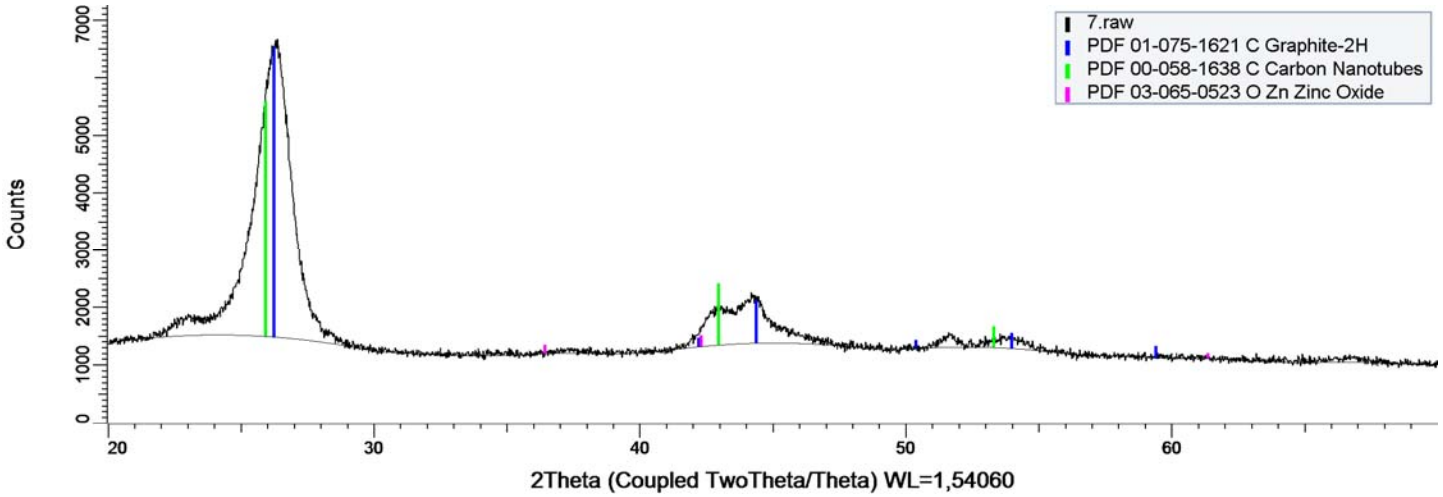

Figure 8.3 The XRD pattern for the ZnO/CNT catalyst

The XRD measurements of the Ni/CNT (catalyst 8) is illustrated in figure 8.4. The first biggest peak is carbon in the ZnO/CNT.

The diffraction pattern of the Ni/CNT catalyst shows three peaks identified as nickel oxide. In the second peak we can see that the nickel oxide and the carbon nanotubes are together and its separation is difficult.

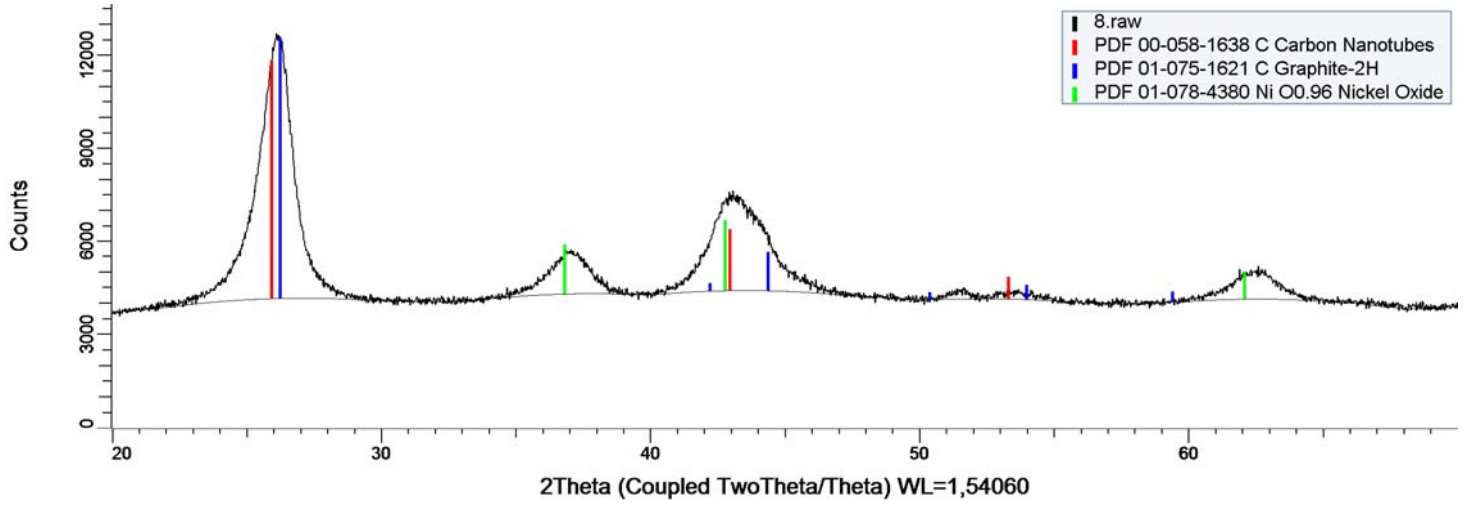

Figure 8.4: The XRD pattern for the Ni/CNT catalyst

The XRD patterns of the catalysts 1 to 6 are described in the appendix E.

As I said before, the particle size can be determined by the XRD method. In the next table the values of this particle size are shown.

CATALYSTS	PARTICLE SIZE (nm)
1	10,7
2	10,25
3	10,3
4	10,18
5	10,2
6	6,54
7	6,39
8	6,62

Table 8.3: XRD particle size

As the table shows, the particle size is stable from the catalyst 1 to 5. So acording to the XRD measurements, the ZnO loading doesn't affect the particle size.

In the catalyst 6, we see that there is a special influence if we added the Ni and Zn together. The particle size decrease if we added this two components together.

In relation with the catalyst 7, the particle size decrease if the Nickel isn't added. So the adition of Ni increase the particle size. This conclusion is also suported by the results of the chemisorption.

With the catalyst 8 occurs the same that with the catalyst 7. If we don't add Zn the particle size decrease, so the adition of Zn increase the particle size. This is also suported by chemisorption.

4. TGA (Thermal gravimetric analysis)

Thermal gravimetric analysis was carried out with two different samples of pretreated CNT and CNF to determine the remaining mass from the commercial CNT and CNF synthesis, and to investigate how the acid treatment effected the CNT. The results are presented in table 8.4:

BATCH	TYPE	NUMBER OF PRETEATMENTS	HNO_3 (ml)	REMAINING MASS (%)
1	CNT	3	250	5,65
2	CNF	2	250	7,64

Table 8.4: TGA results for the pretreated CNT.

The results from the TGA of the CNT demonstrate the importance of the amount of HNO_3 used for the pretreatment. When the CNT were pretreated with 250 ml for 1 h three diferent times, 5,65% of the mass remained in the samples, while when 250 ml was used two time in the CNF the remaining mass was increase to 7,64%. Thus it is important to use a sufficient amount of acid for the pretreatment of the CNT. It would be reasonable to expect that the percentage of the remaining mass would decrease with increasing acid treatments. The pretreatment of the CNT was not the motive of this study, therefore this observation was not investigated further. The explanation might be related to the production of the commercial CNT used in this study. The CNT synthesis require metal catalysts for the CNT growth, and quite large amounts of these metals might be left on the CNT in addition to other impurities form production.

Determination of calcinations temperatures by TGA.

Termo gravimetric analysis (TGA) was carried out to investigate the decomposition temperature of the ZnO-precursor, and thus determine a suitable calcination temperature for the catalysts. The following plots show the calcination temperature for all the catalysts. The calcination temperature has to be balanced in a way so that the temperature is high enough to burn off the unwanted components from the complex metal precursor solution.

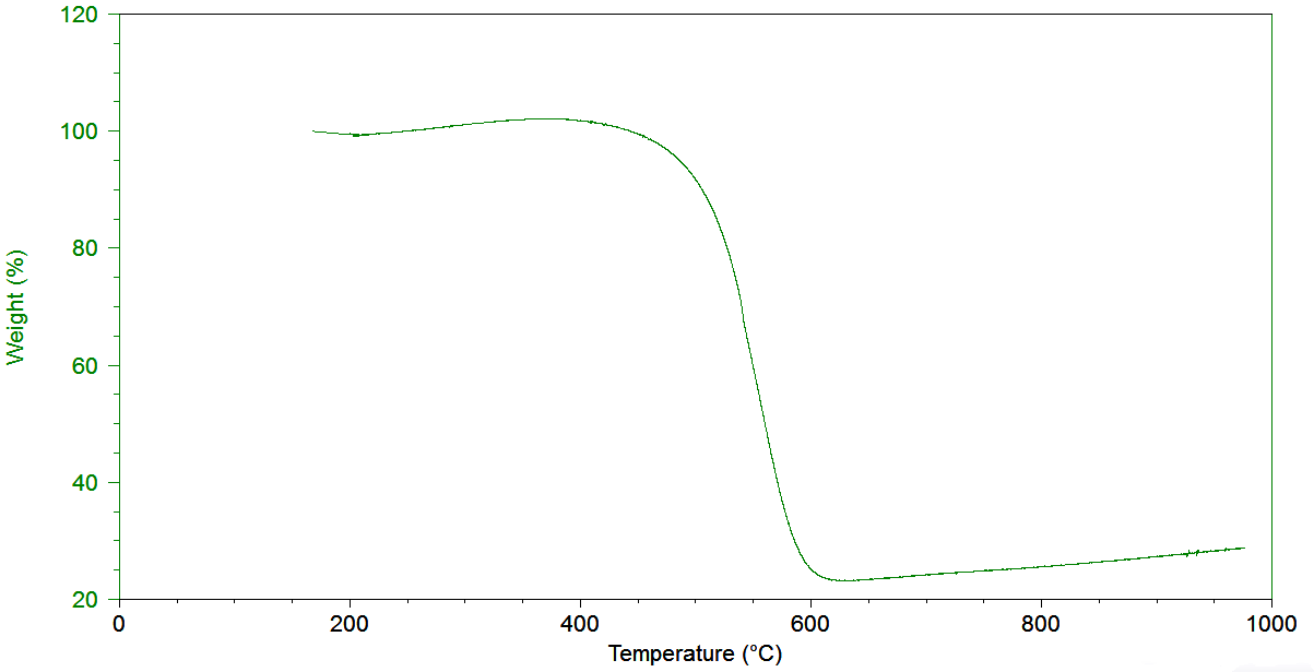

Figure 8.5: %weight vs temperature catalyst 2

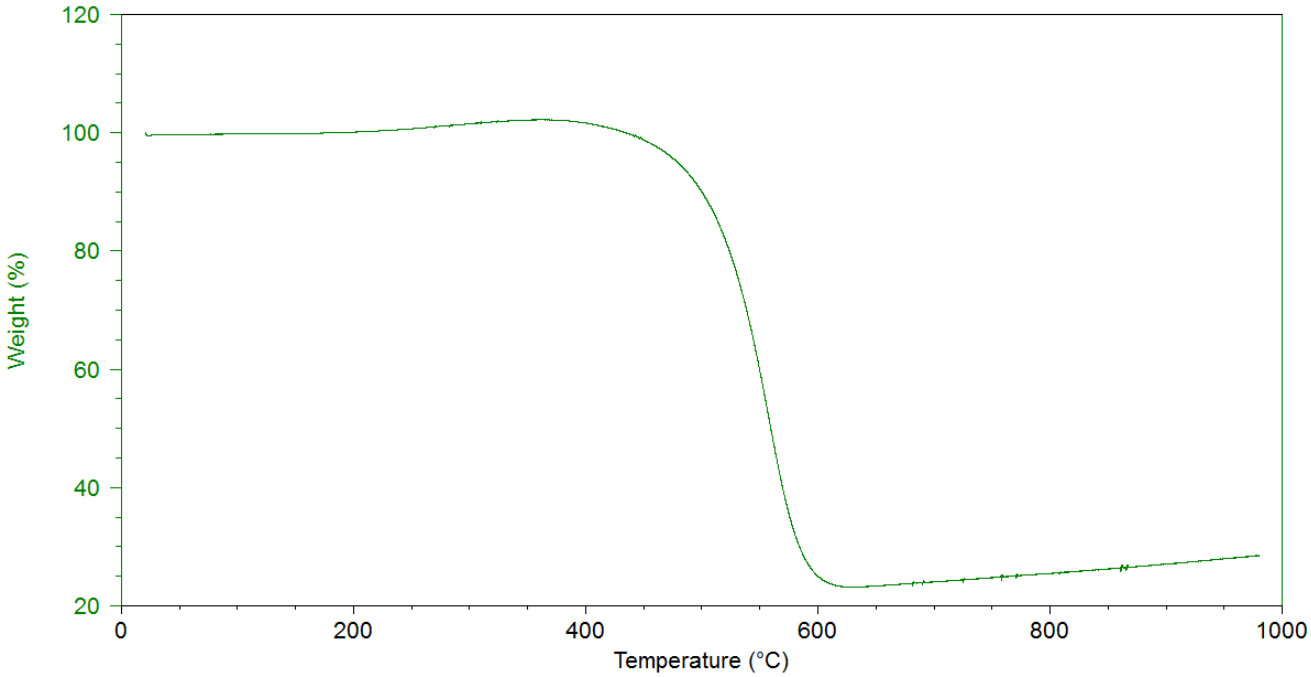

Figure 8.6: %weight vs temperature catalyst 4

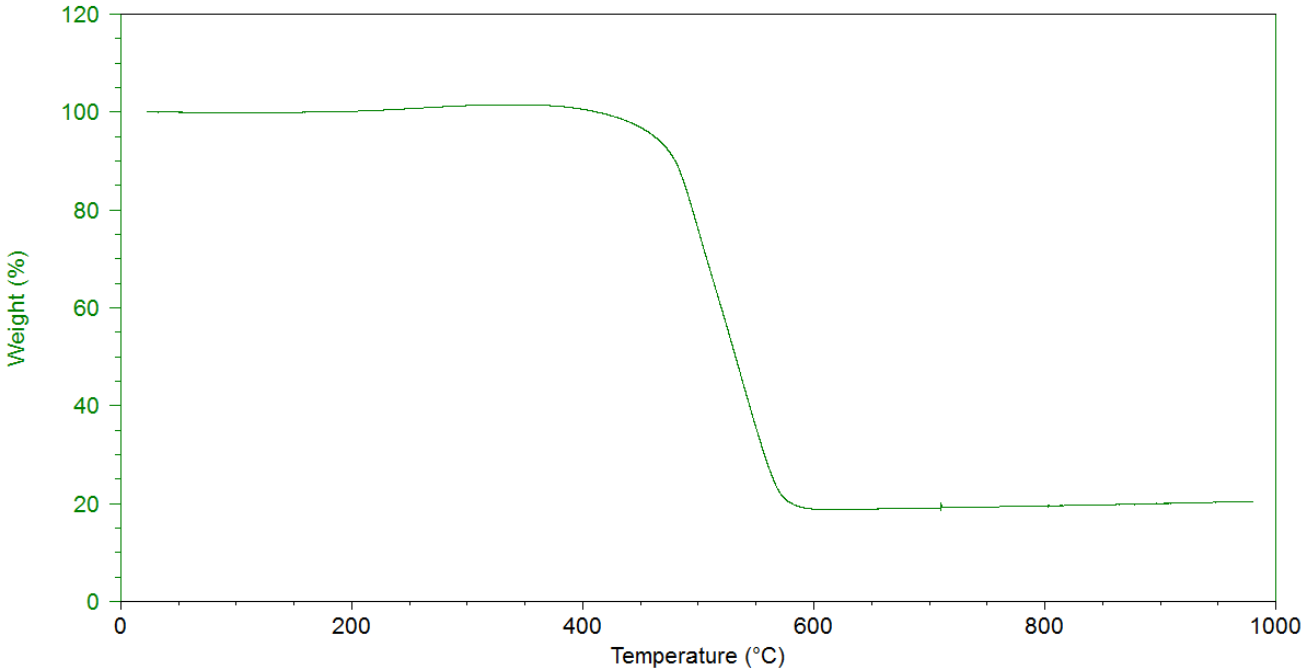

Figure 8.7: %weight vs temperature catalyst 5

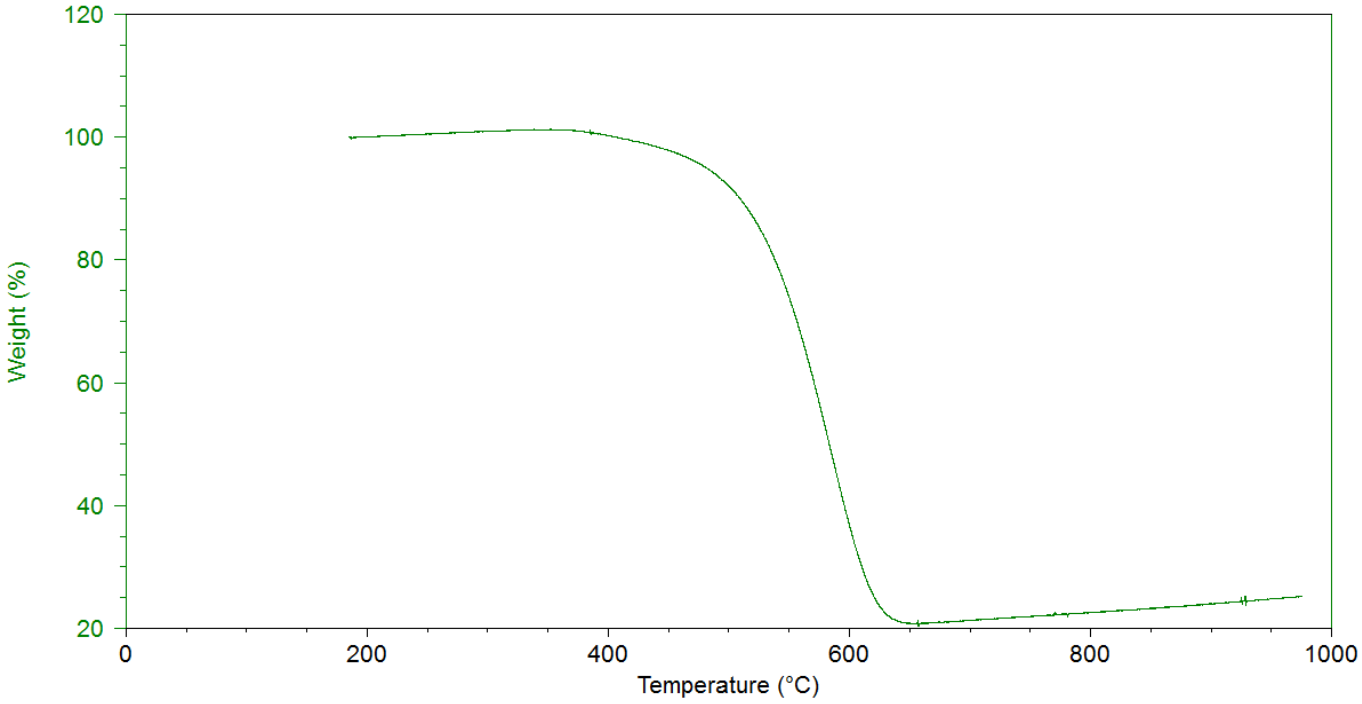

Figure 8.8: %weight vs temperature catalyst 6

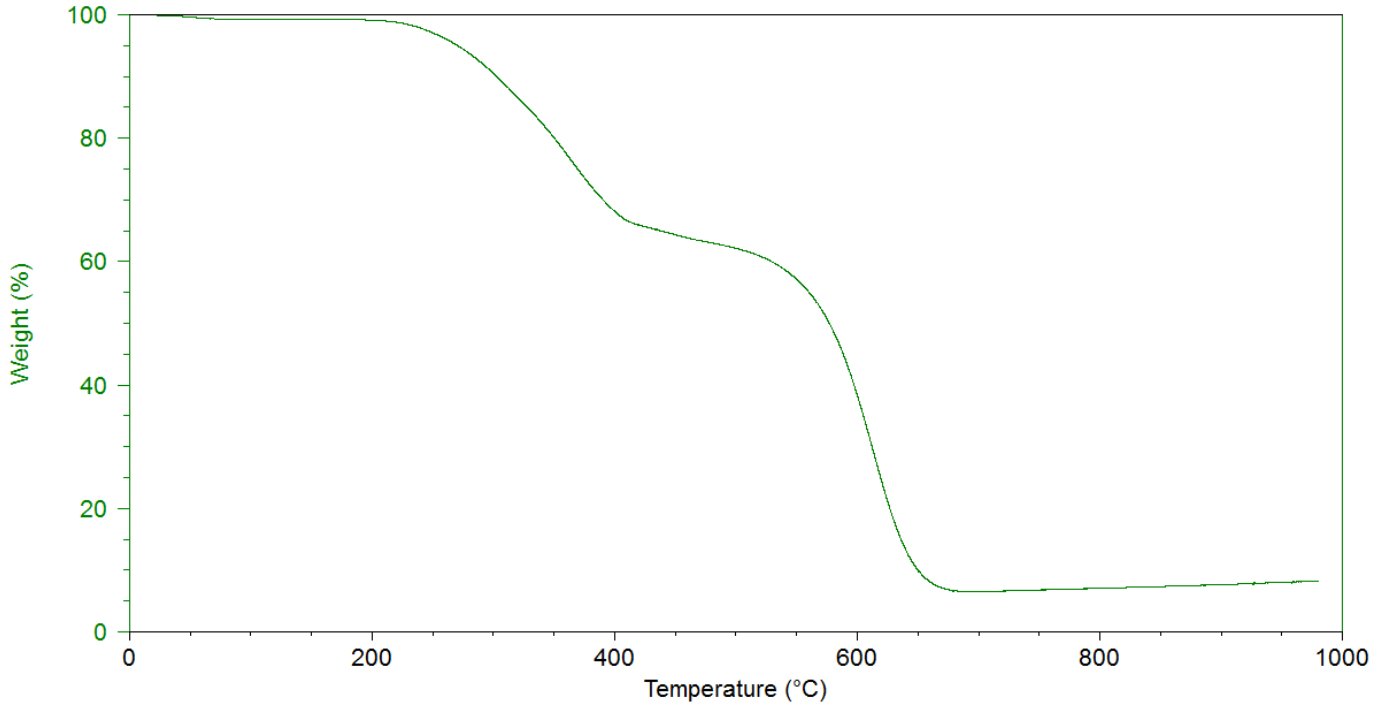

Figure 8.9: %weight vs temperature catalyst 7

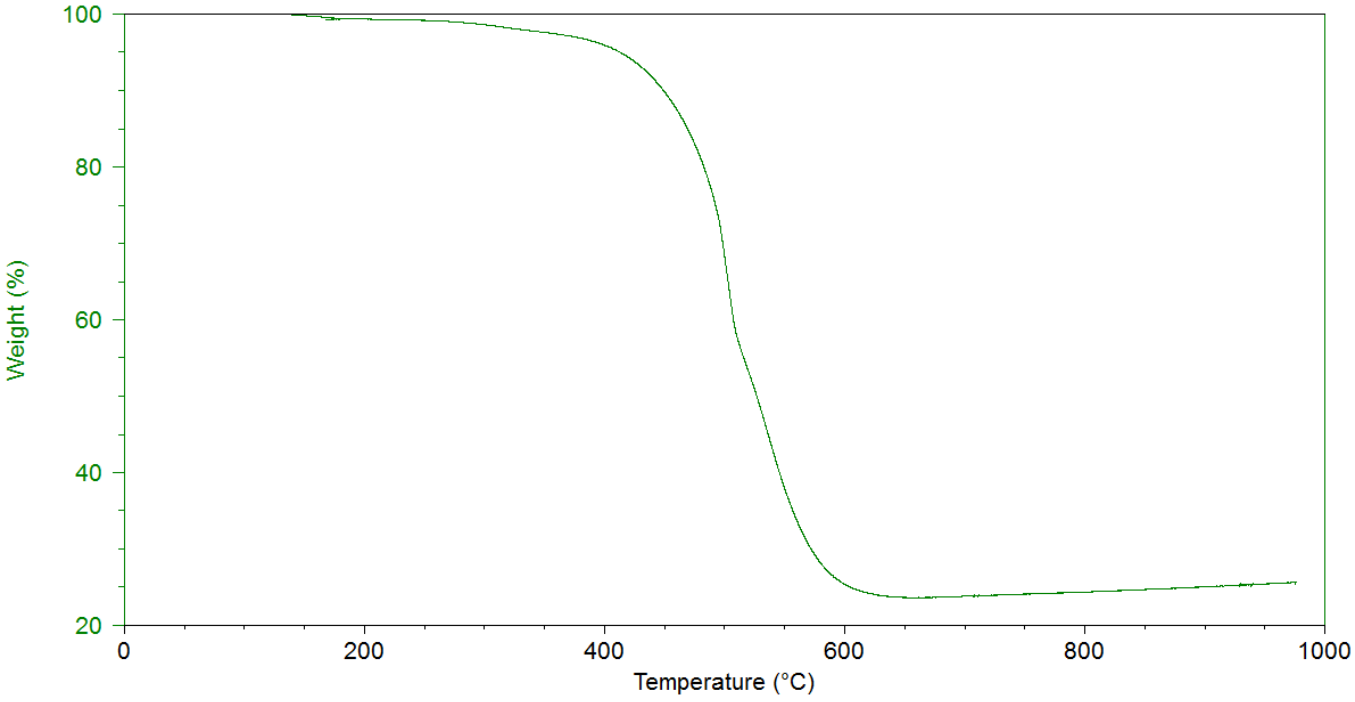

Figure 8.10: %weight vs temperature catalyst 8

So the calcination temperature for these catalyst and the remaining mass are shown in the following table:

CATALYSTS	CALCINATION TEMEPERATURE (ºC)	REMAINING MASS (%)
2	440	28,8
4	440	28,51
5	415	20,47
6	410	25,2
7	210	8,236
8	400	25,72

Table 8.5: TGA results for then Ni-ZnO/CNT

The calculated loading according to the TGA measurements for the ZnO/CNT-catalyst and the Ni-ZnO/CNT are presented in the table 8.6. The calculations can be found in Appendix F. From the comparison with the calculated loading from the impregnation (Appendix A) it is clear that the calculated loading from the TGA measurements does not correspond to the values from impregnation. The author has not managed to determine the explanation of the different values obtained from impregnation and TGA calculations. One possibility is that the noted impregnation values from the laboratory work are wrong, but it seems highly unlikely that they would be that far off. Another possibility is that there is an overlooked error in the calculations that no one has discovered.

CATALYSTS	ZnO-LOADING IMPREGNATION (%)	ZnO-Ni LOADING TGA (%)
2	20	31,2
4	10	31,51
5	26	20,24
6	20	27,74
7	20	2,98
8	0	28,59

Table 8.6: Calculated loading according to the TGA for the ZnO/CNT and Ni-ZnO/CNT catalysts

5. TPD (Temperature programmed desorption)

CO_2-TPD was carried out for the catalysts 1, 3, 5 before Ni impregnation. Additionally, a sample of the pretreated CNT was tested with CO_2-TDP to be able to compare with the ZnO-loaded samples. The results are shown in figure 8.11

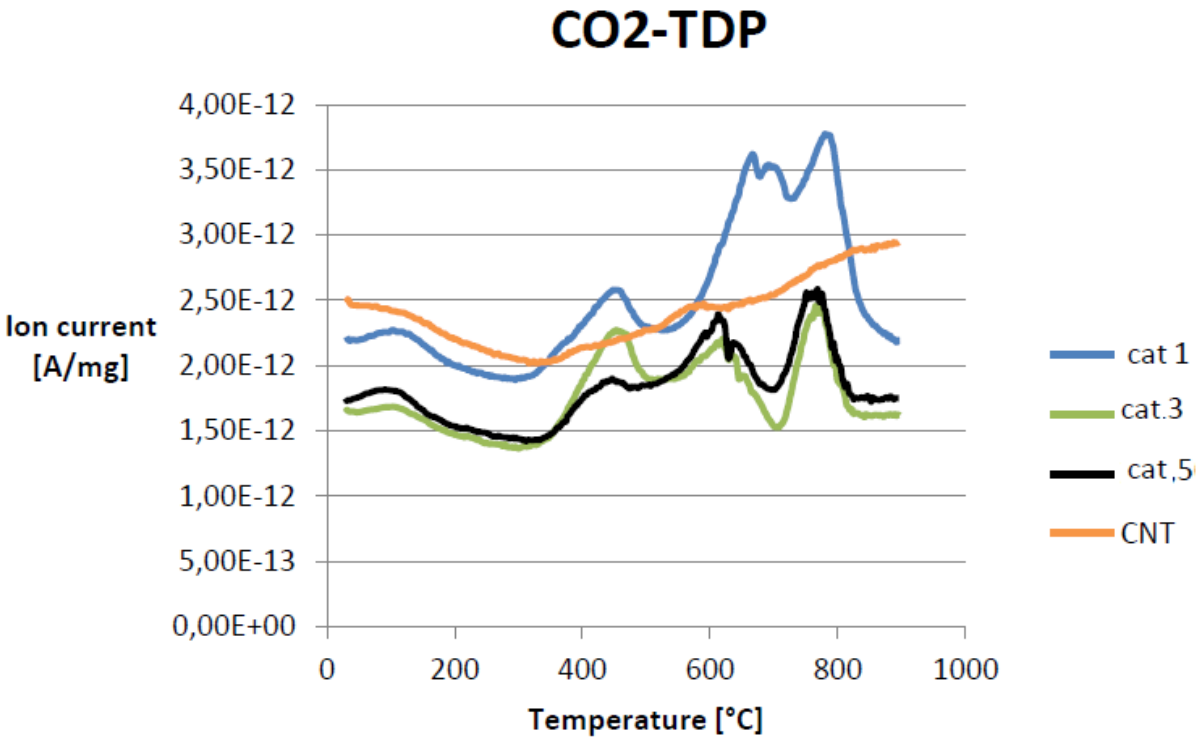

.Figure 8.11: CO_2-TPD measurements of the ZnO/CNT catalysts and the CNT

It is observed that there are three peaks for the ZnO/CNT catalysts, while the CNT has two small peaks. To compare the three peaks for the ZnO/CNT catalysts, the mass % as a function of temperature was plotted. The change in mass% was found from the corresponding mass% vs temperature plots (Appendix H). Catalyst 1 has the highest total difference in mass%, 13%, which corresponds to highest CO_2-desorption. The other two catalysts, 3 and 5, both have a total difference in mass% close to 8,2%, which indicate that these have similar basic sites that are not as strong as the basic sites in the catalyst 1.

The mass % as a function of temperature (during CO_2-TPD analysis of the catalysts) are given below, and the plots of DCS and DTG vs temperature can be found in Appendix H.

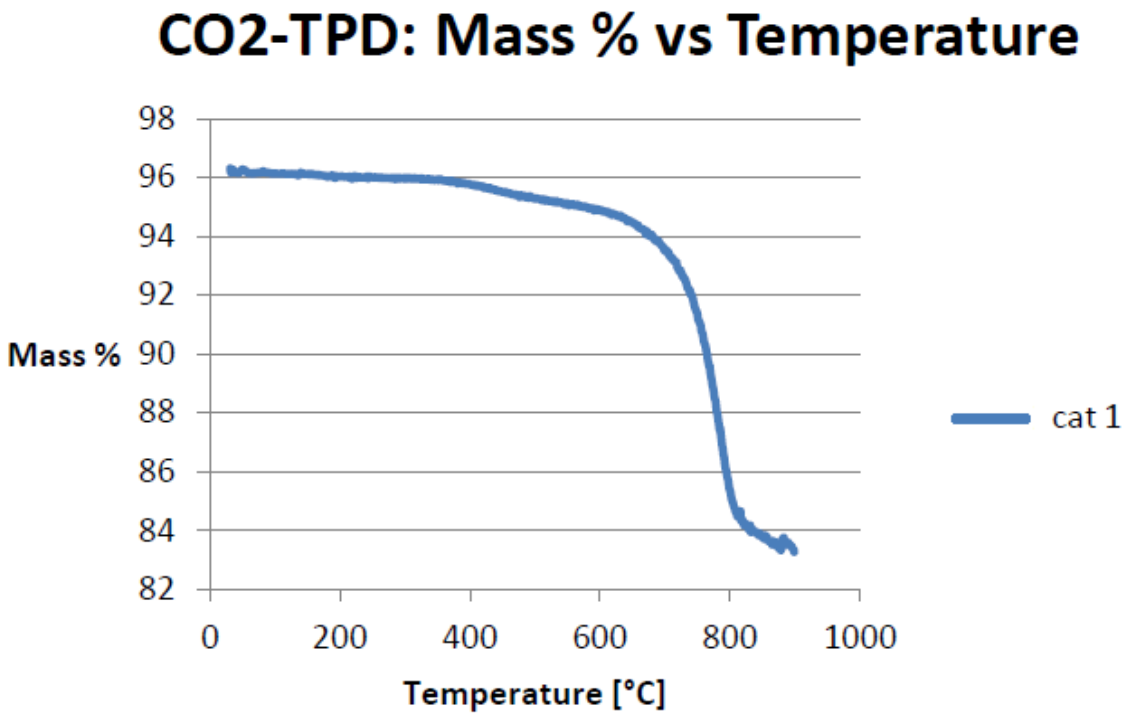

Figure 8.12: CO_2-TPD for catalyst 1 describing Mass% as a function of temperature

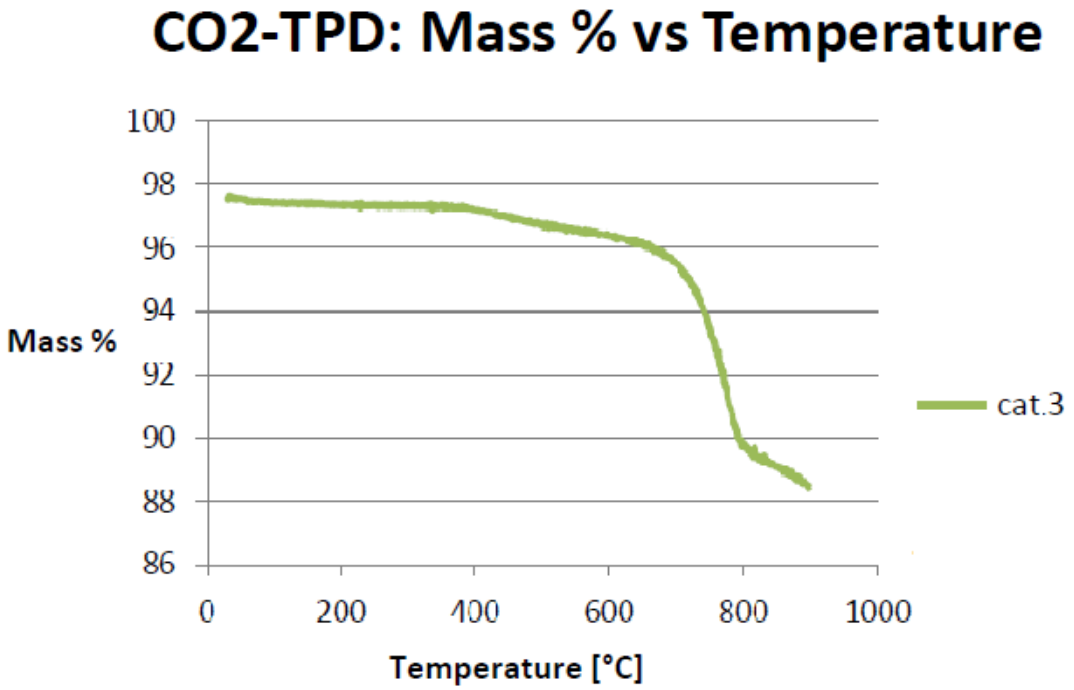

Figure 8.13: CO_2-TPD for catalyst3 describing Mass% as a function of temperature

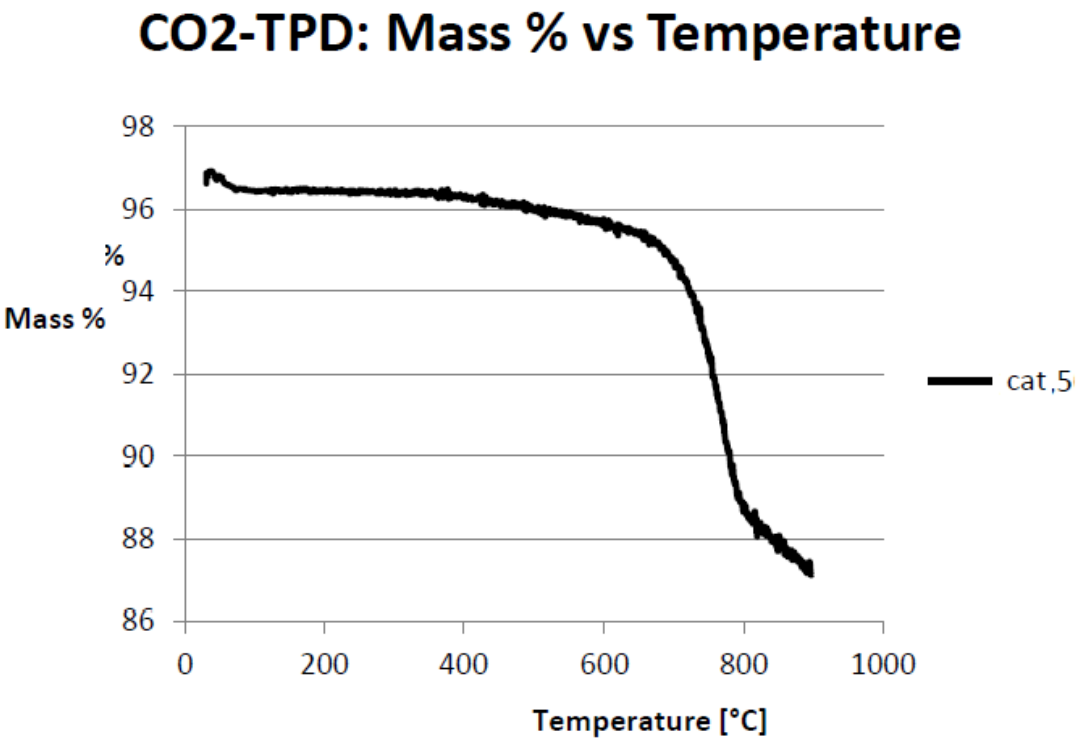

Figure 8.14: CO_2-TPD for catalyst 5 describing Mass% as a function of temperature

CATALYST	1ST PEAK	2ND PEAK	3RD PEAK	TOTAL DIFFERENCE MASS (%)
1	1	3	9,5	13,5
3	0,5	1,2	6,5	8,2
5	0,4	1,5	6,3	8,2

Table 8.7: Difference in Mass % in the three peaks

After this analysis, Ni was added to the same catalyst. The results of TPD after Ni impregnation is show below (catalyst 8 is included in this analysis).

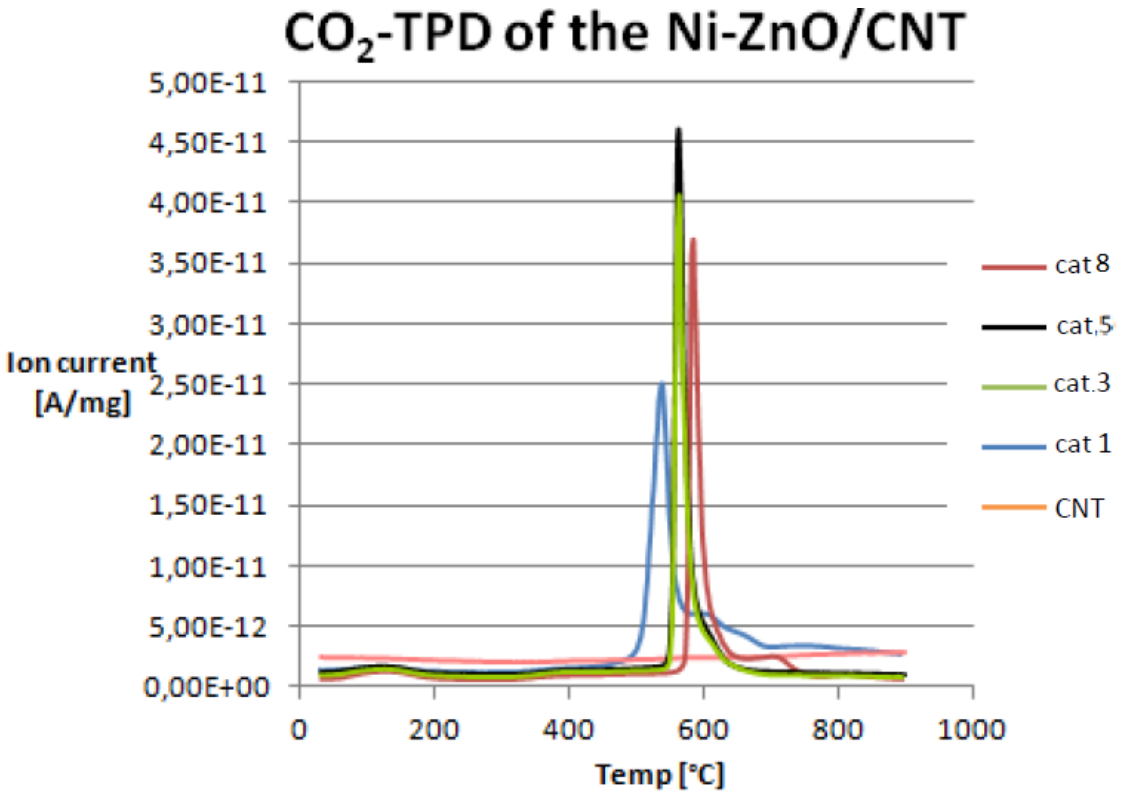

Figure 8.15: CO2-TPD measurements of the Ni-ZnO/CNT catalysts and the CNT

The CO_2-TPD measurements of the Ni-ZnO/CNT catalysts demonstrate a significant difference from the measurements of the ZnO/CNT catalysts before nickel impregnation. The ZnO/CNT catalysts all have three peaks. However, after nickel impregnation only one big peak is observed. The mass % as a function of temperature was plotted for the Ni-ZnO/CNT catalysts. The difference in mass% was compared for the Ni-ZnO/CNT catalysts by the same procedure as for the ZnO/CNT catalysts, and the calculations can be found in Appendix H. These results indicate that there has been a change in which catalysts that are most basic. Before nickel impregnation the catalyst 1 has the highest difference in mass%, but after nickel impregnation this catalyst show similar difference in mass% as the catalyst 3 (which had smaller mass% before nickel was impregnated). The results indicate that catalyst 8 has the highest difference in mass during CO_2-TPD suggesting that this catalyst might have the strongest basic sites of the four Ni-ZnO/CNT catalysts.

The mass % as a function of temperature (during CO_2-TPD analysis of the catalysts) are given in the following figures, and the plots of DCS and DTG vs temperature can be found in Appendix H.

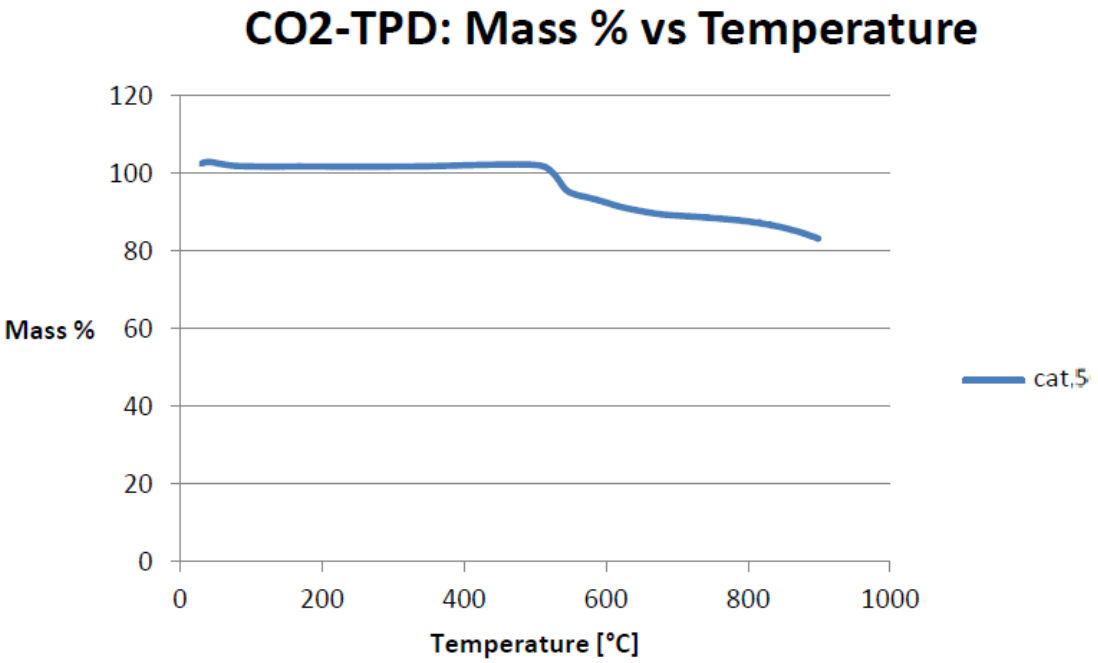

Figure 8.16: CO2-TPD for catalyst 5 describing Mass% as a function of temperature

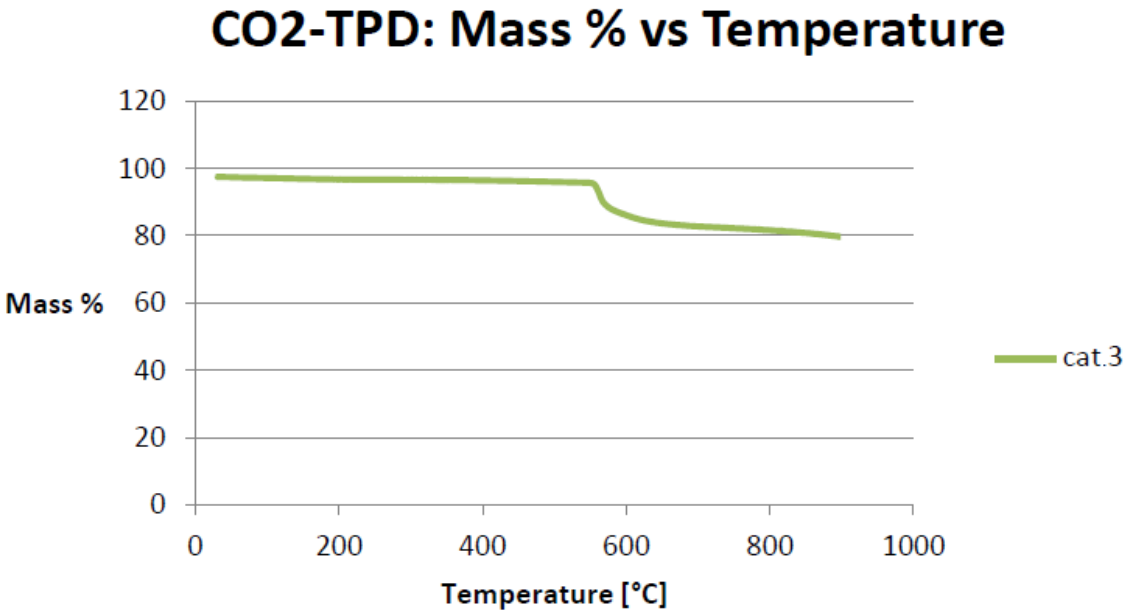

Figure 8.17: CO2-TPD for catalyst 3 describing Mass% as a function of temperature

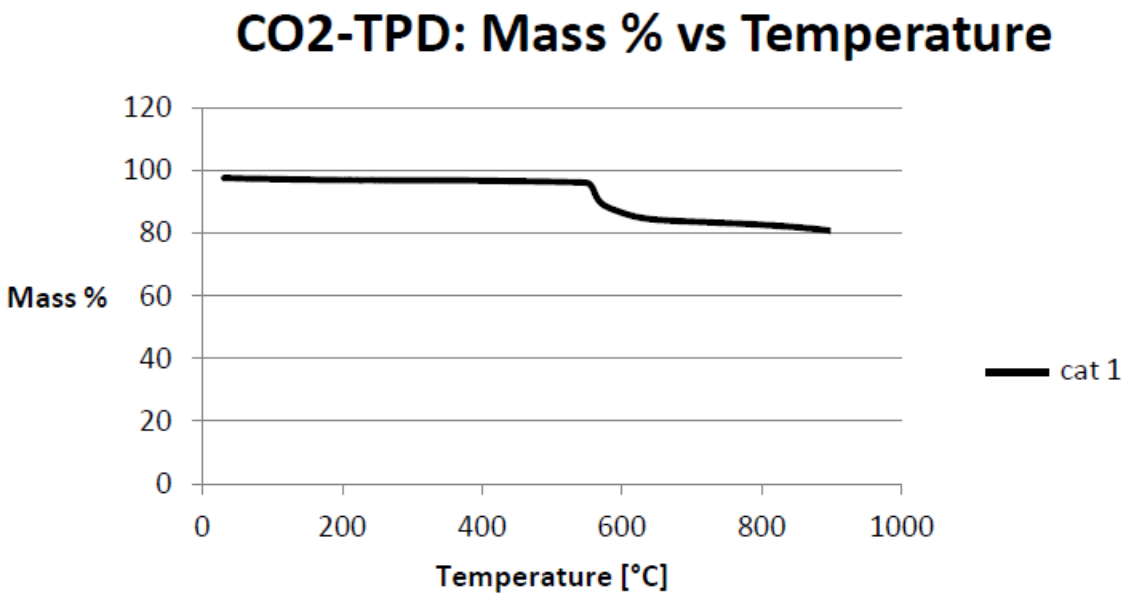

Figure 8.18: CO2-TPD for catalyst 1 describing Mass% as a function of temperature

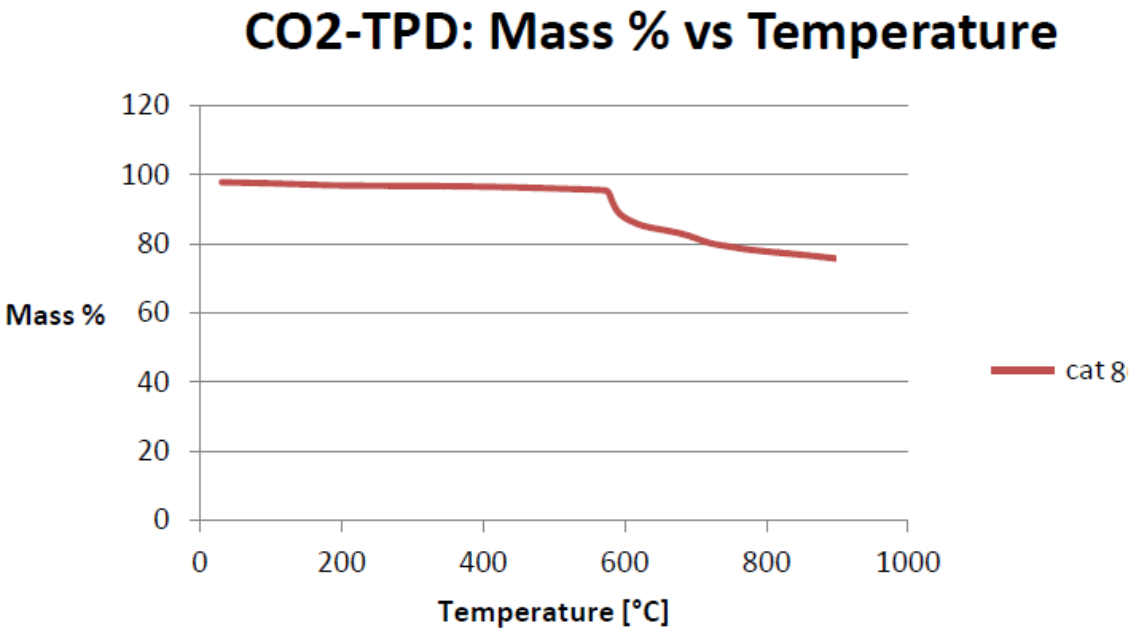

Figure 8.19: CO2-TPD for catalyst 8 describing Mass% as a function of temperature

CATALYST	DIFFERENCE IN MASS (%)
8	18
1	13
3	12,7
5	11,8

Table 8.8: Difference in Mass % in the peaks

6. Catalysts test

As the part 7 of this report said, a batch reactor was used to transform cellulose into polyols by catalytic action. The reactor was charged with cellulose, catalyst and water. These chemicals were heated up 263ºC and stirring at 600 rpm. Then the polyols that were obtained of this reaction were collected in a glass container and analyse with a GC.

The objective of this analysis is try to guess which polyols are in the products. To do this, some of the pure polyols were analised before. The result of the GC is a graph with different peaks. These peaks indicate the time and the chemical that go out the GC column. The graphs of the pure polyols are shown in appendix G.

- Catalyst 5: the graph that is obtained with the GC is the following figure:

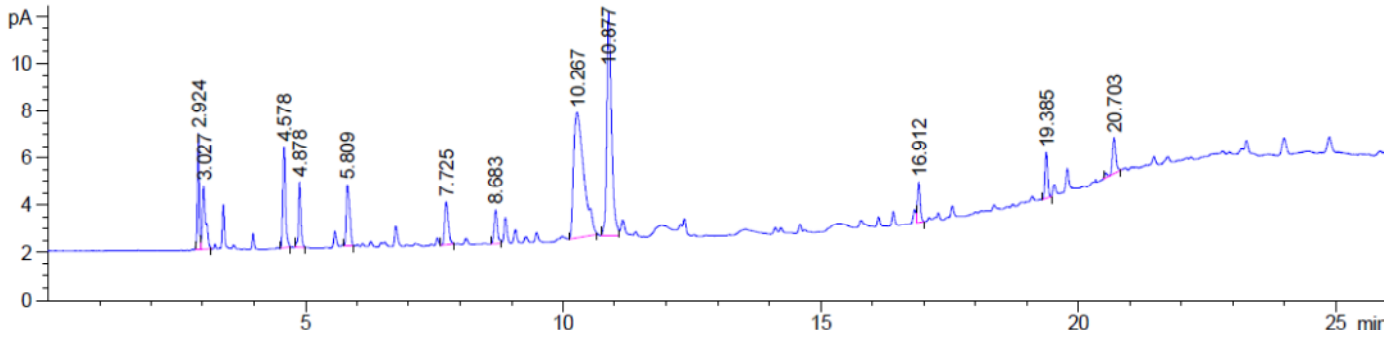

Figure 8.20: GC analysis catalyst 5

As we can see, the most important peaks are in the following times: 2,924 min, 3,027 min, 4,578 min, 5,809 min, 10,267 min, 10,877 min, 16,912 min

Comparing these times with the time of the pure components (Appendix G), we can decide which kind of chemicals are. These chemicals are:

- Peak 2,924 min: 2-propanol (3,156 min).
- Peak 3,027 min: ethanol (3,235 min), 1-propanol (3,545 min).
- Peak 4,578 min: 3-pentanol (3,804 min).
- Peak 5,809 min: 1-hexanol (6,256 min).
- Peak 10,267 min: EG and PG (10,305 min).
- Peak 10,877 min: EG (11,712 min).
- Peak 16,912 min: 1,3 propanodiol (13,537 min).

- Catalyst 6: the graph that is obtained with the GC is the following figure:

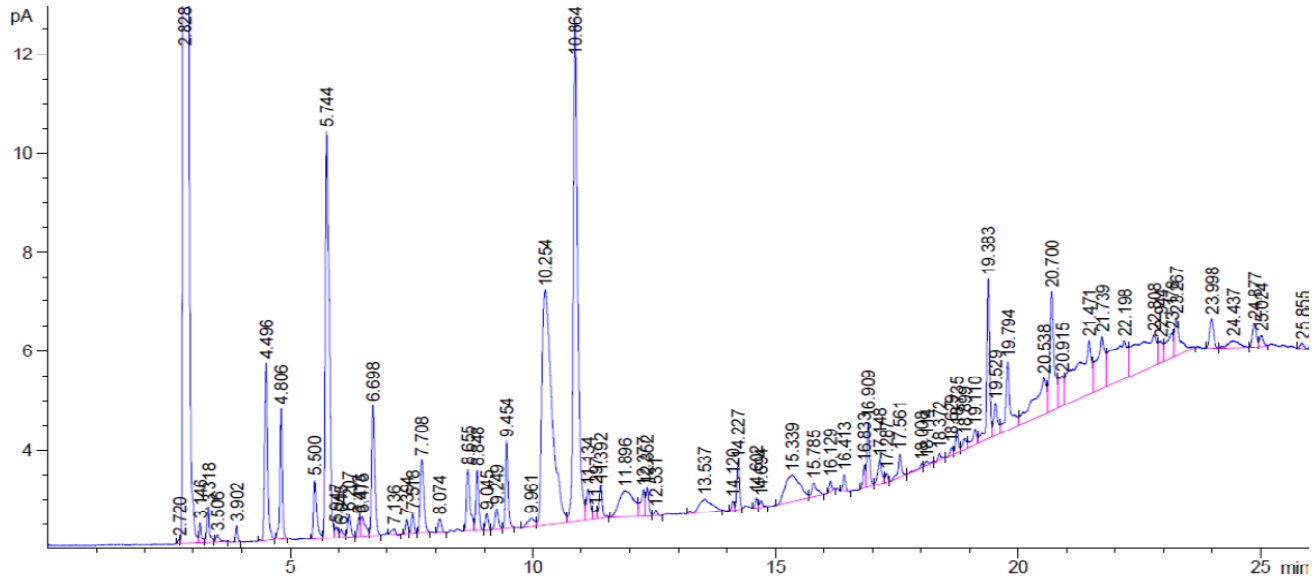

Figure 8.21: GC analysis catalyst 6

As we can see, the most important peaks are in the following times: 2,828 min, 5,744 min, 10,254 min, and 10,664 min.

Comparing these times with the time of the pure components (Appendix G), we can decide which kind of chemicals are. These chemicals are:

- Peak 2,828 min: 2-propanol (3,156 min).
- Peak 5,744 min: 1-hexanol (6,256 min).
- Peak 10,254 min: EG and PG (10,305 min).
- Peak 10,664 min: PG (11,044 min)

- Catalyst 7: the graph that is obtained with the GC is the following figure:

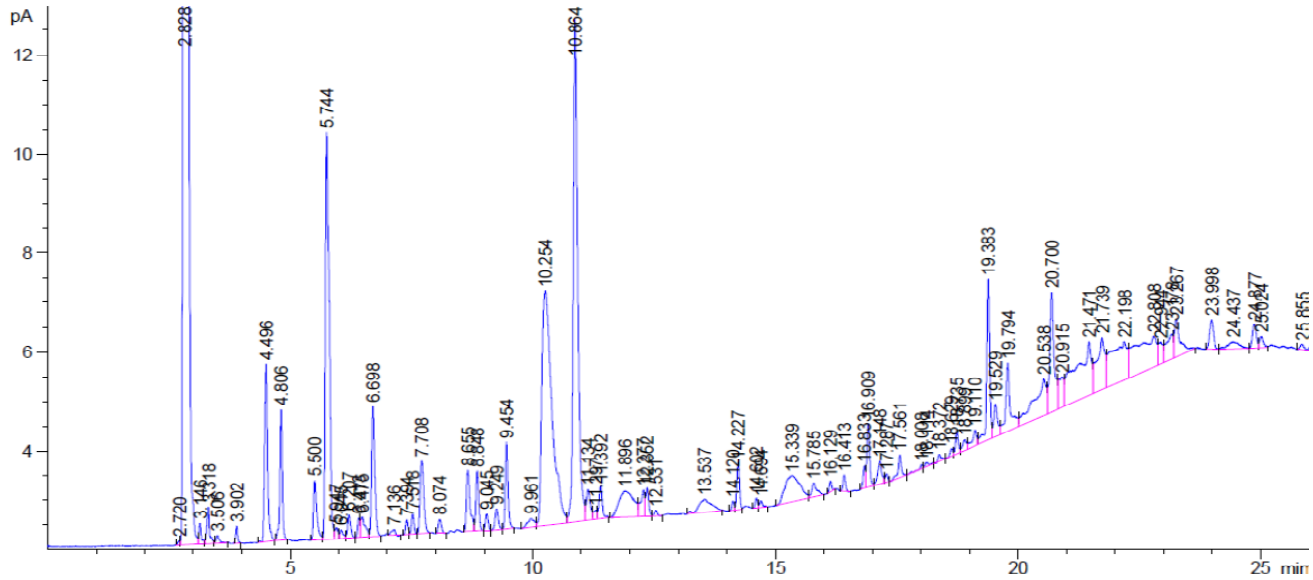

Figure 8.22: GC analysis catalyst 7

As we can see, the most important peaks are in the following times: 2,841 min, 5,517 min, 5,766 min, 7,702 min, 10,885 min, 14,228 min, 14,698 min, 19,791 min and 21,232 min,

Comparing these times with the time of the pure components (Appendix G), we can decide which kind of chemicals are. These chemicals are:

- Peak 2,841 min: 2-propanol (3,156 min).
- Peak 5,517 min: 1-hexanol (6,256 min).
- Peak 7,702 min: 1-hexanol (6,256 min).
- Peak 10,885 min: EG and PG (10,305 min).
- Peak 14,228 min: 1,3-propandiol (13,537 min)
- Peak 14,698 min: 1,3-propandiol (13,537 min)
- Peak 19,791 min: dodecanol (18,103 min)
- Peak 21,232 min: glicerol (21,855 min)

- Catalyst 8: the graph that is obtained with the GC is the following figure:

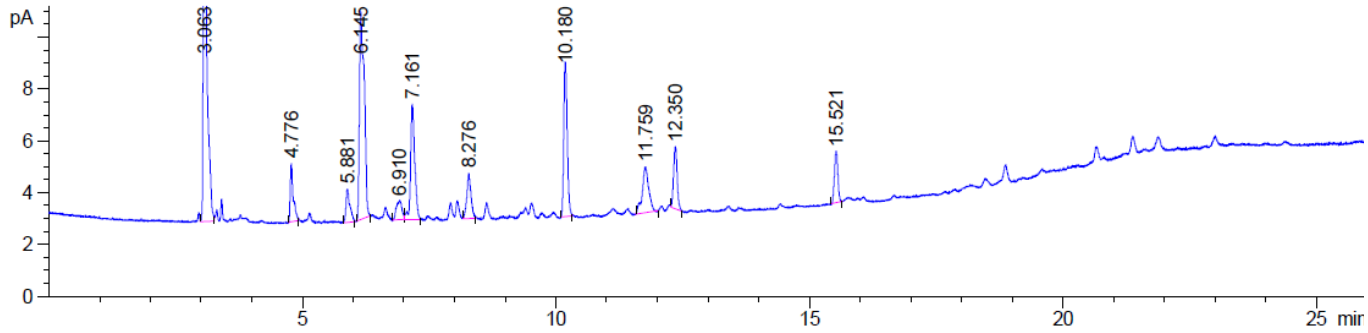

Figure 8.23: GC analysis catalyst 8

As we can see, the most important peaks are in the following times: 3,063 min, 6,145 min, 7,161 min, 10,180 min and 11,759 min.

Comparing these times with the time of the pure components (Appendix G), we can decide which kind of chemicals are. These chemicals are:

- Peak 3,063 min: 2-propanol (3,156 min).
- Peak 6,145 min: 1-hexanol (6,256 min).
- Peak 7,161 min: 1-hexanol (6,256 min).
- Peak 10,180 min: EG and PG (10,305 min).
- Peak 11,759 min: EG (11,712 min)

7. Recommendations for further work

It must be emphasized that the validity of these results is limited because the results are based on one series of experiments. It is recommended to continue the investigation of the catalyst and the testing conditions.

After see the results, I discovered that we have to pay special attention in the adition of the Ni and ZnO together.

For the BET results, the surface area decrease a lot in comparison with the rest of the catalysts. Also with the chemisorption the dispersion decreases so much, but the particle size increase very much. These differences may be caused by the different electrical charges between the Ni and Zn.

With XRD resuts something similar occurs. The particle size decrease if we added this two components together.

CONCLUSION

CONCLUSIONS

In this study, the combination between Pechini method and incipient wetness impregnation were used to prepare Ni-ZnO/CNT catalysts. In total 8 samples were prepared. The ZnO loading for each catalyst was proved in this proyect. Two of the samples, as it is described before, they only contain Ni or ZnO.

The BET analysis demonstrate that the BET surface decrease if the ZnO loading is higher. We can also say that after the Ni is added the BET surface are increase so much.

With the chemisorption analysis, we can see that the dispersion of the Ni decreases if there is more ZnO loading and the particle size increases when the ZnO loading is higher.

The XRD results shown that zinc nickel oxide is formed, or at least it is very hard to separate nickel from zinc oxide. In relation with the catalyst 7, the particle size decrease if the Nickel isn't added. So the adition of Ni increase the particle size. This conclusion is also suported by the results of the chemisorption.

TGA shows that several pretreatments produce a reduction in the remaining mass % from TGA analysis, thus reduction in remaining growft catalysts and impurities from production.

CO_2-TPD results indicate that catalyst 1 had the highest CO_2 desorption before nickel was added, however, after nickel addition the same catalyst had less CO_2 desorption. It is proposed that these findings might be related to the strong acidity of the nickel precursor, which might have destroyed parts of the ZnO-layer on the catalyst.

For the catalyst test, we can observe that with the catalyst 5 and 8, a lot of polyols are obtained than with the catalysts 6 and 7. The products obtained from catalyst 5 and 8 are more pure and more easily to separate each other.

BIBLIOGRAPHY

BIBLIOGRAPHY

[1] Administration, U.S.E.I., International Energy Outlook. 2010.

[2] Vyas, A.P., J.L. Verma, and N. Subrahmanyam, A review on FAME production processes. Fuel, 2010. 89(1): p. 1-9.

[3] He, J. and W. Zhang, Techno-economic evaluation of thermo-chemical biomass-to-ethanol. Applied Energy, 2011. 88(4): p. 1224-1232.

[4] Li, C., et al., One-pot catalytic hydrocracking of raw woody biomass into chemicals over supported carbide catalysts: simultaneous conversion of cellulose, hemicellulose and lignin. Energy & Environmental Science, 2012. 5(4): p. 6383-6390.

[5] Carlos Serrano-Ruiz, J. and J.A. Dumesic, Catalytic routes for the conversion of biomass into liquid hydrocarbon transportation fuels. Energy & Environmental Science, 2011. 4(1): p. 83-99.

[6] Fukuoka, A. and P.L. Dhepe, Catalytic conversion of cellulose into sugar alcohols. Angewandte Chemie-International Edition, 2006. 45(31): p. 5161-5163.

[7] Ji, N., et al., Direct Catalytic Conversion of Cellulose into Ethylene Glycol Using Nickel-Promoted Tungsten Carbide Catalysts. Angewandte Chemie-International Edition, 2008. 47(44): p. 8510-8513.

[8] Pang, J., et al., Catalytic Hydrogenation of Corn Stalk to Ethylene Glycol and 1,2-Propylene Glycol. Industrial & Engineering Chemistry Research, 2011. 50(11): p. 6601-6608.

[9] Zhang, Y., A. Wang, and T. Zhang, A new 3D mesoporous carbon replicated from commercial silica as a catalyst support for direct conversion of cellulose into ethylene glycol. Chemical Communications, 2010. 46(6): p. 862-864.

[10] Tai, Z., et al., Temperature-controlled phase-transfer catalysis for ethylene glycol production from cellulose. Chemical Communications, 2012. 48(56): p. 7052-7054.

[11] Liu, Y., C. Luo, and H. Liu, Tungsten Trioxide Promoted Selective Conversion of Cellulose into Propylene Glycol and Ethylene Glycol on a Ruthenium Catalyst. Angewandte Chemie-International Edition, 2012. 51(13): p. 3249-3253.

[12] Wang, X., et al., Efficient conversion of microcrystalline cellulose to 1,2-alkanediols over supported Ni catalysts. Green Chemistry, 2012. 14(3): p. 758-765.

[13] S. Brunauer, P. H. Emmett, and E. Teller. Adsorption of gases in multimolecular layers. Journal of the American Chemical Society, 60:309–319, 1938.

[14] K. S. W. Sing. The use of nitrogen adsorption for the characterisation of porous materials. Colloids and Surfaces A: Physicochemical and Engineering Aspects, 187-188:3–9, 2001.

[15] K. S. W. Sing, D. H. Everett, R. A. W. Haul, L. Moscou, R. A. Pierotti, J. Rouquérol, and T. Siemieniewska. Reporting physisorption data for gas/solid systems with special reference to the determination of surface area and porosity. Pure & Applied Chemistry, 57:603–619, 1985.

[16] I. Chorkendorff and J. W. Niemantsverdriet. Concepts of modern catalysis and kinetics. WILEY-VCH Verlag GmbH & Co., 2nd edition, 2007.

[17] J. Rouquerol, D. Avnir, C. W. Fairbridge, D. H. Everett, J. H. Haynes, N. Pernicone, J. D. F. Ramsay, K. S. W. Sing, and K. K. Unger. Recommendations for the characterization of porous solids. Pure & Applied Chemistry, 66:1739–1758, 1994.

[18] K. S. W. Sing. Adsorption methods for the characterization of porous materials. Advances in Colloid and Interface Science, 76-77:3–11, 1998.

[19] R. Di Monte, P. Fornasiero, J. Kaspar, P. Rumori, G. Gubitosa, and M. Graziani. Pd/Ce0.6Zr0.4O2/Al2O3 as advanced materials for three-way catalysts. Part 1. Catalyst characterisation, thermal stability and catalytic activity in the reduction of NO by CO. Applied Catalysis B: Environmental, 24:157–167, 2000.

[20] P. A. Sermon and G. C. Bond. Hydrogen spillover. Catalysis Reviews, 8:211– 239, 1974.

[21] S. P. Rane. Relation between catalyst properties and selectivity in Fischer- Tropsch synthesis. PhD thesis, Norwegian University of Science and Technology, 2011.

[22] M. Boudart. Turnover rates in heterogeneous catalysis. Chemical Review, 95:661–666, 1995.

[23] S. Bernal, J. J. Calvino, G. A. Cifredo, A. Laachir, V. Perrichon, and J. M. Herrmann. Influence of the reduction/evacuation conditions on the rate of hydrogen spillover on Rh/CeO2 catalysts. Langmuir, 10:717–722, 1994.

[24] C. H. Bartholomew. Hydrogen adsorption on supported cobalt, iron and nickel. Catalysis Letters, 7:27–52, 1990.

SYMBOLS AND ABREVIATIONS

A_0: Area occupied by N_2 at 77 K (0.162 nm^2)

d: Lattice spacing [Å]

D: Dispersion [%]

m_i: Mass of i [g]

M_i: Molar mass of i [g/mol]

n Order of reflection

ni: Mole of i [mol]

N_A: Avogadro's number (6.022·1023 atoms/mol)

P: Pressure [bar]

P_0: Equilibrium pressure [bar]

r: Rate of reaction

S_{BET}: BET surface area [m^2/g]

T: Temperature [K] [°C]

T_{calc}: Calcination temperature [K]

v_{ads}: Volume gas adsorbed (chemisorption) [cm^3/g STP]

V_a: Total volume adsorbed (BET) [cm^3/g STP]

α: Slope of BET plot

β: Full width at half maximum (FWHM)

η: Intersection of y-axis of BET plot

θ: Adsorption layer

θ: Angle

λ: Wavelength

ρ: Density (kg/m^3)

BET: Brunauer Emmett Teller

BJH: Barrett Joyner Halenda

CA: Citric acid

EG: Ethylene glycol

FWHM: Full width at half maximum

GC: Gas chromatograph

M: Metal

PG: Polyethylene glycol

TPD: Temperature programmed desorption

TGA: Thermal gravimetric analysis

XRD: X-ray diffraction

APPENDIX A

APPENDIX A: CALCULATION FOR THE COMPLEX METAL SOLUTION

In all the catalysts, the ZnO loading and the total amount of the catalyst were supposed.

- **CATALYSTS 1 AND 2:** ZnO loading: 20%.

$$m_{total} = 3g$$

$m(ZnO) = \%(ZnO) \cdot m_{total} = 0{,}2 \cdot 3 = 0{,}6g\ ZnO.$

$\boldsymbol{m(CNT)} = \%(CNT) \cdot m_{total} = 0{,}8 \cdot 3 = \boldsymbol{2{,}4g\ CNT}.$

$$n(ZnO) = \frac{m(ZnO)}{M_m(ZnO)} = \frac{0{,}6}{81{,}39} = 0{,}0073\ mol\ ZnO.$$

$$\boldsymbol{m(Zn(NO_3)_2 \cdot 6H_2O)} = \frac{m(ZnO) \cdot M_m(Zn(NO_3)_2 \cdot 6H_2O)}{M_m(ZnO)} = \frac{0{,}6 \cdot 297{,}49}{81{,}39}$$

$$= \boldsymbol{2{,}1930\ g\ Zn(NO_3)_2 \cdot 6H_2O}$$

Due to the ratio between the conponents is molar ratio, the number of mol is calculated.

$$n(Zn(NO_3)_2 \cdot 6H_2O) = \frac{m(Zn(NO_3)_2 \cdot 6H_2O)}{M_m(Zn(NO_3)_2 \cdot 6H_2O)} = 0{,}0073\ mol\ Zn(NO_3)_2 \cdot 6H_2O$$

The molar ratio between CA and Zn is 7:8.

$$\frac{n(Zn(NO_3)_2 \cdot 6H_2O)}{n(CA)} = \frac{0{,}0073}{n(CA)} = \frac{7}{8} \rightarrow n(CA) = 0{,}00842\ mol$$

$\boldsymbol{m(CA)} = n(CA) \cdot M_m(CA) = \boldsymbol{1{,}7690g\ CA}$

The molar ratio between CA and EG is 8:8.

$n(EG) = n(CA) = 0{,}00842\ mol$

$\boldsymbol{m(EG)} = n(EG) \cdot M_m(EG) = \boldsymbol{0{,}5222g\ EG}$

2 ml of the complex metal solution was impregnated on the CNT1.

1,8 ml of the complex metal solution was impregnated on the CNT2.

- **CATALYSTS 3 AND 4:** ZnO loading: 10%.

$$m_{total} = 3g$$

$m(ZnO) = \%(ZnO) \cdot m_{total} = 0{,}1 \cdot 3 = 0{,}3g\ ZnO.$

$\boldsymbol{m(CNT)} = \%(CNT) \cdot m_{total} = 0{,}9 \cdot 3 = \boldsymbol{2{,}7g\ CNT}.$

$$n(ZnO) = \frac{m(ZnO)}{M_m(ZnO)} = \frac{0{,}3}{81{,}39} = 0{,}0036\ mol\ ZnO.$$

$$\boldsymbol{m(Zn(NO_3)_2 \cdot 6H_2O)} = \frac{m(ZnO) \cdot M_m(Zn(NO_3)_2 \cdot 6H_2O)}{M_m(ZnO)} = \frac{0{,}3 \cdot 297{,}49}{81{,}39}$$

$$= \boldsymbol{1{,}0965\ g\ Zn(NO_3)_2 \cdot 6H_2O}$$

Due to the ratio between the conponents is molar ratio, the number of mol is calculated.

$$n(Zn(NO_3)_2 \cdot 6H_2O) = \frac{m(Zn(NO_3)_2 \cdot 6H_2O)}{M_m(Zn(NO_3)_2 \cdot 6H_2O)} = 0{,}00368\ mol\ Zn(NO_3)_2 \cdot 6H_2O$$

The molar ratio between CA and Zn is 7:8.

$$\frac{n(Zn(NO_3)_2 \cdot 6H_2O)}{n(CA)} = \frac{0{,}00368}{n(CA)} = \frac{7}{8} \rightarrow n(CA) = 0{,}00421 mol$$

$$\boldsymbol{m(CA) = n(CA) \cdot M_m(CA) = 0{,}8841 g\ CA}$$

The molar ratio between CA and EG is 8:8.

$$n(EG) = n(CA) = 0{,}00421 mol$$

$$\boldsymbol{m(EG) = n(EG) \cdot M_m(EG) = 0{,}2610 g\ EG}$$

2 ml of the complex metal solution was impregnated on the CNT3.

1,8 ml of the complex metal solution was impregnated on the CNT4.

- **<u>CATALYST 5:</u>** ZnO loading: 26%.

$$m_{total} = 3g$$

$$m(ZnO) = \%(ZnO) \cdot m_{total} = 0{,}26 \cdot 3 = 0{,}78 g\ ZnO.$$

$$\boldsymbol{m(CNT) = \%(CNT) \cdot m_{total} = 0{,}74 \cdot 3 = 2{,}2 g\ CNT.}$$

$$n(ZnO) = \frac{m(ZnO)}{M_m(ZnO)} = \frac{0{,}78}{81{,}39} = 0{,}0095\ mol\ ZnO.$$

$$\boldsymbol{m(Zn(NO_3)_2 \cdot 6H_2O)} = \frac{m(ZnO) \cdot M_m(Zn(NO_3)_2 \cdot 6H_2O)}{M_m(ZnO)} = \frac{0{,}78 \cdot 297{,}49}{81{,}39}$$

$$= \boldsymbol{2{,}8509\ g\ Zn(NO_3)_2 \cdot 6H_2O}$$

Due to the ratio between the conponents is molar ratio, the number of mol is calculated.

$$n(Zn(NO_3)_2 \cdot 6H_2O) = \frac{m(Zn(NO_3)_2 \cdot 6H_2O)}{M_m(Zn(NO_3)_2 \cdot 6H_2O)} = 0{,}0095\ mol\ Zn(NO_3)_2 \cdot 6H_2O$$

The molar ratio between CA and Zn is 7:8.

$$\frac{n(Zn(NO_3)_2 \cdot 6H_2O)}{n(CA)} = \frac{0{,}0095}{n(CA)} = \frac{7}{8} \rightarrow n(CA) = 0{,}0109 mol$$

$$\boldsymbol{m(CA) = n(CA) \cdot M_m(CA) = 2{,}2999 g\ CA}$$

The molar ratio between CA and EG is 8:8.

$$n(EG) = n(CA) = 0{,}0109\ mol$$

$$\boldsymbol{m(EG) = n(EG) \cdot M_m(EG) = 0{,}6758 g\ EG}$$

2 ml of the complex metal solution was impregnated on the CNT5.

- **CATALYST 6:** in this catalyst the Zn and the Ni were added together, then the catalyst was calcined and after this, the Ni was reduced with pure H_2. To make the complex solution, the molar ratio had been calculated due to the electric charges. The nex molar ratio between Ni:Zn:CA:EG is 1:1:4:4.

  ZnO loading: 20%.

  Ni loading: 20%.

  $m_{total} = 3g$

$m(ZnO) = \%(ZnO) \cdot m_{total} = 0{,}2 \cdot 3 = 0{,}6g\ ZnO.$

$m(Ni) = \%(Ni) \cdot m_{total} = 0{,}2 \cdot 3 = 0{,}6g\ ZnO.$

$\boldsymbol{m(CNT) = \%(CNT) \cdot m_{total} = 0{,}6 \cdot 3 = 1{,}8g\ CNT.}$

$$n(ZnO) = \frac{m(ZnO)}{M_m(ZnO)} = \frac{0{,}6}{81{,}39} = 0{,}0073\ mol\ ZnO.$$

Due to the molar ratio between Ni and Zn is 1:1:

$n(ZnO) = n(Ni) = 0{,}0073 mol\ Ni.$

$$\boldsymbol{m(Zn(NO_3)_2 \cdot 6H_2O)} = \frac{m(ZnO) \cdot M_m(Zn(NO_3)_2 \cdot 6H_2O)}{M_m(ZnO)} = \frac{0{,}6 \cdot 297{,}49}{81{,}39}$$

$$= \boldsymbol{2{,}1930\ g\ Zn(NO_3)_2 \cdot 6H_2O}$$

Due to the ratio between the conponents is molar ratio, the number of mol is calculated.

$$n(Zn(NO_3)_2 \cdot 6H_2O) = \frac{m(Zn(NO_3)_2 \cdot 6H_2O)}{M_m(Zn(NO_3)_2 \cdot 6H_2O)} = 0{,}0073\ mol\ Zn(NO_3)_2 \cdot 6H_2O$$

The molar ratio between CA and Zn is 4:1.

$$\frac{n(Zn(NO_3)_2 \cdot 6H_2O)}{n(CA)} = \frac{0{,}0073}{n(CA)} = \frac{1}{4} \rightarrow n(CA) = 0{,}0292 mol$$

$\boldsymbol{m(CA) = n(CA) \cdot M_m(CA) = 6{,}132g\ CA}$

The molar ratio between CA and EG is 4:4.

$n(EG) = n(CA) = 0{,}0292\ mol$

$\boldsymbol{m(EG) = n(EG) \cdot M_m(EG) = 1{,}81g\ EG}$

$\boldsymbol{m(Ni(NO_3)_2 \cdot 6H_2O) = n(Ni) \cdot M_m(Ni(NO_3)_2 \cdot 6H_2O)}$

$$= \boldsymbol{2{,}122g\ Ni(NO_3)_2 \cdot 6H_2O}$$

6 ml of the complex metal solution was impregnated on the CNT6.

- **CATALYST 7:** ZnO loading: 20%.

$$m_{total} = 3g$$

$m(ZnO) = \%(ZnO) \cdot m_{total} = 0{,}2 \cdot 3 = 0{,}6g\ ZnO.$

$\boldsymbol{m(CNT)} = \%(CNT) \cdot m_{total} = 0{,}8 \cdot 3 = \boldsymbol{2{,}4g\ CNT}.$

$n(ZnO) = \frac{m(ZnO)}{M_m(ZnO)} = \frac{0{,}6}{81{,}39} = 0{,}0073\ mol\ ZnO.$

$$\boldsymbol{m(Zn(NO_3)_2 \cdot 6H_2O)} = \frac{m(ZnO) \cdot M_m(Zn(NO_3)_2 \cdot 6H_2O)}{M_m(ZnO)} = \frac{0{,}6 \cdot 297{,}49}{81{,}39}$$

$$= \boldsymbol{2{,}1930\ g\ Zn(NO_3)_2 \cdot 6H_2O}$$

Due to the ratio between the conponents is molar ratio, the number of mol is calculated.

$$n(Zn(NO_3)_2 \cdot 6H_2O) = \frac{m(Zn(NO_3)_2 \cdot 6H_2O)}{M_m(Zn(NO_3)_2 \cdot 6H_2O)} = 0{,}0073\ mol\ Zn(NO_3)_2 \cdot 6H_2O$$

The molar ratio between CA and Zn is 7:8.

$$\frac{n(Zn(NO_3)_2 \cdot 6H_2O)}{n(CA)} = \frac{0{,}0073}{n(CA)} = \frac{7}{8} \rightarrow n(CA) = 0{,}00842\ mol$$

$$\boldsymbol{m(CA)} = n(CA) \cdot M_m(CA) = \boldsymbol{1{,}7690g\ CA}$$

The molar ratio between CA and EG is 8:8.

$n(EG) = n(CA) = 0{,}00842\ mol$

$$\boldsymbol{m(EG)} = n(EG) \cdot M_m(EG) = \boldsymbol{0{,}5222g\ EG}$$

8 ml of the complex metal solution was impregnated on the CNT7.

- **<u>CATALYST 8:</u>** This catalyst only contain 20% Ni, so it will be explained in the appendix B.

APPENDIX B

APPENDIX B: CALCULATIONS FOR Ni IMPREGNATION

All catalysts has 20% of Ni loading.

- **CATALYSTS 1 AND 2:** Ni loading: 20%.

$$m_{total} = 1{,}73g$$

$$\boldsymbol{m(ZnO/CNT)} = \%(ZnO/CNT) \cdot m_{total} = 0{,}8 \cdot 1{,}73 = \boldsymbol{1{,}384g\ ZnO/CNT}$$

$$m(Ni) = \%(Ni) \cdot m_{total} = 0{,}2 \cdot 1{,}73 = 0{,}34g\ Ni$$

$$n(Ni) = \frac{m(Ni)}{M_m(Ni)} = \frac{0{,}34}{58{,}693} = 0{,}005\ mol\ Ni.$$

2ml destillated water was used per g of ZnO/CNT catalyst. So the total amount of water was:

$$\boldsymbol{m(water)} = 2 \cdot 1{,}384 = \boldsymbol{2{,}77ml\ water}$$

$$\boldsymbol{m(Ni(NO_3)_2 \cdot 6H_2O)} = n(Ni) \cdot M_m(Ni(NO_3)_2 \cdot 6H_2O) = 0{,}005 \cdot 290{,}79$$
$$= \boldsymbol{1{,}7178g\ Ni(NO_3)_2 \cdot 6H_2O}$$

- **CATALYSTS 3 AND 4:** Ni loading: 20%.

$$m_{total} = 1{,}67g$$

$$\boldsymbol{m(ZnO/CNT)} = \%(ZnO/CNT) \cdot m_{total} = 0{,}8 \cdot 1{,}67 = \boldsymbol{1{,}336g\ ZnO/CNT}$$

$$m(Ni) = \%(Ni) \cdot m_{total} = 0{,}2 \cdot 1{,}67 = 0{,}334g\ Ni$$

$$n(Ni) = \frac{m(Ni)}{M_m(Ni)} = \frac{0{,}334}{58{,}693} = 0{,}0052\ mol\ Ni.$$

2ml destillated water was used per g of ZnO/CNT catalyst. So the total amount of water was:

$$\boldsymbol{m(water)} = 2 \cdot 1{,}336 = \boldsymbol{2{,}68ml\ water}$$

$$\boldsymbol{m(Ni(NO_3)_2 \cdot 6H_2O)} = n(Ni) \cdot M_m(Ni(NO_3)_2 \cdot 6H_2O) = 0{,}0052 \cdot 290{,}79$$
$$= \boldsymbol{1{,}6602g\ Ni(NO_3)_2 \cdot 6H_2O}$$

- **CATALYST 5:** Ni loading: 20%.

$$m_{total} = 1{,}9g$$

$$\boldsymbol{m(ZnO/CNT)} = \%(ZnO/CNT) \cdot m_{total} = 0{,}8 \cdot 1{,}9 = \boldsymbol{1{,}5196g\ ZnO/CNT}$$

$$m(Ni) = \%(Ni) \cdot m_{total} = 0{,}2 \cdot 1{,}9 = 0{,}379g\ Ni$$

$$n(Ni) = \frac{m(Ni)}{M_m(Ni)} = \frac{0{,}379}{58{,}693} = 0{,}006\ mol\ Ni.$$

2ml destillated water was used per g of ZnO/CNT catalyst. So the total amount of water was:

$$\boldsymbol{m(water)} = 2 \cdot 1{,}5196 = \boldsymbol{3{,}03ml\ water}$$

$$\boldsymbol{m(Ni(NO_3)_2 \cdot 6H_2O)} = n(Ni) \cdot M_m(Ni(NO_3)_2 \cdot 6H_2O) = 0{,}006 \cdot 290{,}79$$
$$= \boldsymbol{1{,}8821g\ Ni(NO_3)_2 \cdot 6H_2O}$$

- **CATALYST 6:** the amount of Ni of this catalyst was explained in appendix A.
- **CATALYST 7:** this catalyst doesn't contain Ni. It is a ZnO/CNT catalyst.
- **CATALYST 8:** this catalyst is Ni/CNT.

  Ni loading: 20%.

  $m_{total} = 3g$

$$\boldsymbol{m(CNT)} = \%(CNT) \cdot m_{total} = 0{,}8 \cdot 3 = \boldsymbol{2{,}4g\ ZnO/CNT}$$

$$m(Ni) = \%(Ni) \cdot m_{total} = 0{,}2 \cdot 3 = 0{,}6g\ Ni$$

$$n(Ni) = \frac{m(Ni)}{M_m(Ni)} = \frac{0{,}6}{58{,}693} = 0{,}0102\ mol\ Ni.$$

2ml destillated water was used per g of CNT catalyst. So the total amount of water was:

$$\boldsymbol{m(water)} = 2 \cdot 2{,}4 = \boldsymbol{4{,}8ml\ water}$$

$$\boldsymbol{m(Ni(NO_3)_2 \cdot 6H_2O)} = n(Ni) \cdot M_m(Ni(NO_3)_2 \cdot 6H_2O) = 0{,}0102 \cdot 290{,}79$$
$$= \boldsymbol{2{,}97g\ Ni(NO_3)_2 \cdot 6H_2O}$$

APPENDIX C

APPENDIX C: BET AND BJH PLOTS

- **CATALYST 1:** 20%Ni-20%ZnO/CNT

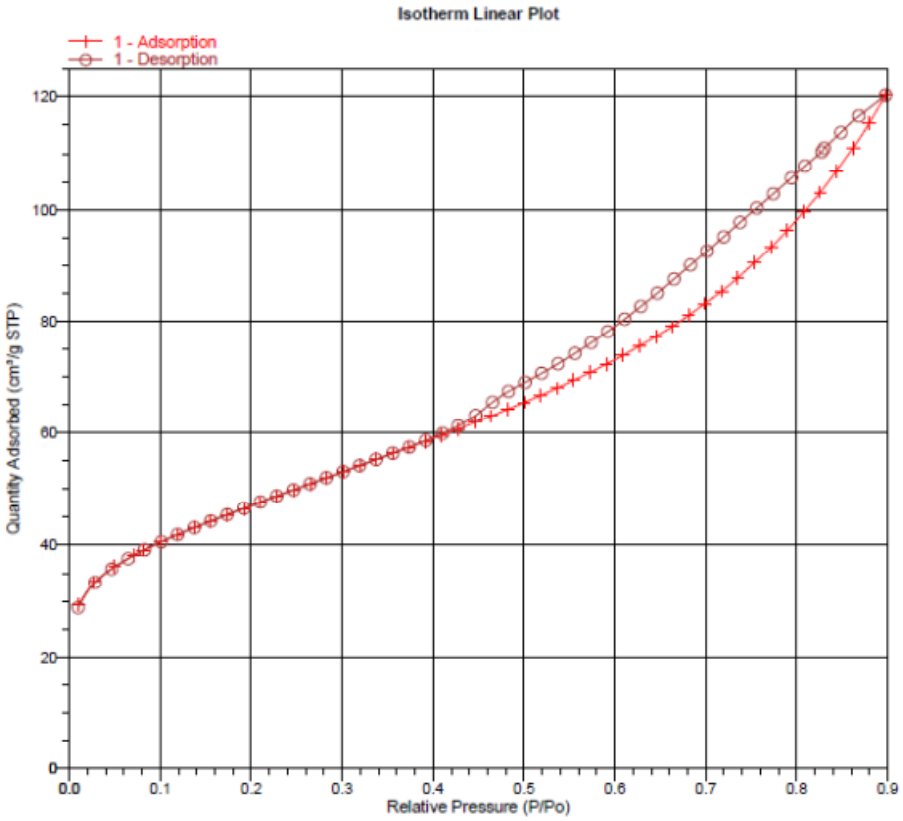

Figure C.1: adsorption-desorption isotherm catalyts 1

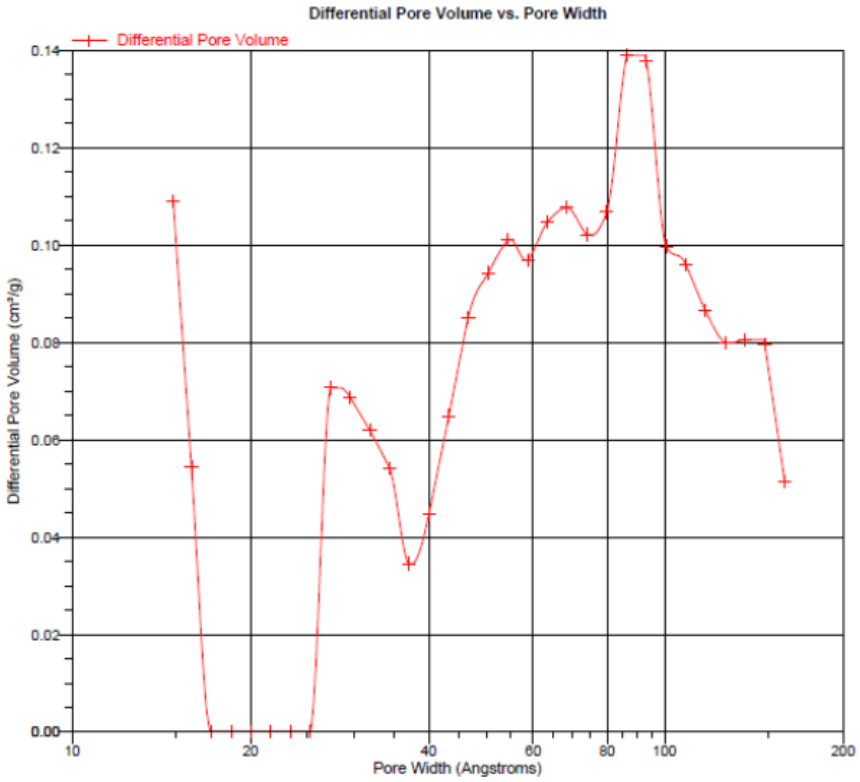

Figure C.2: differential pore volume vs pore width catalyst 1

- **CATALYST 2:** 20%Ni-20%ZnO/CNT

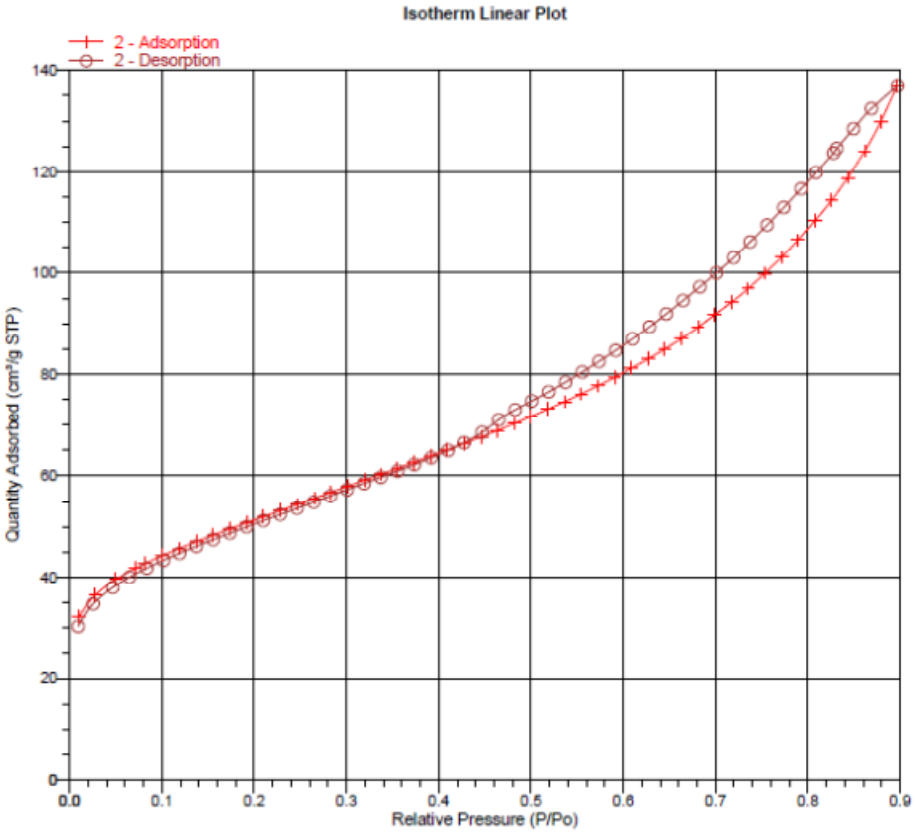

Figure C.3: adsorption-desorption isotherm catalyst 2

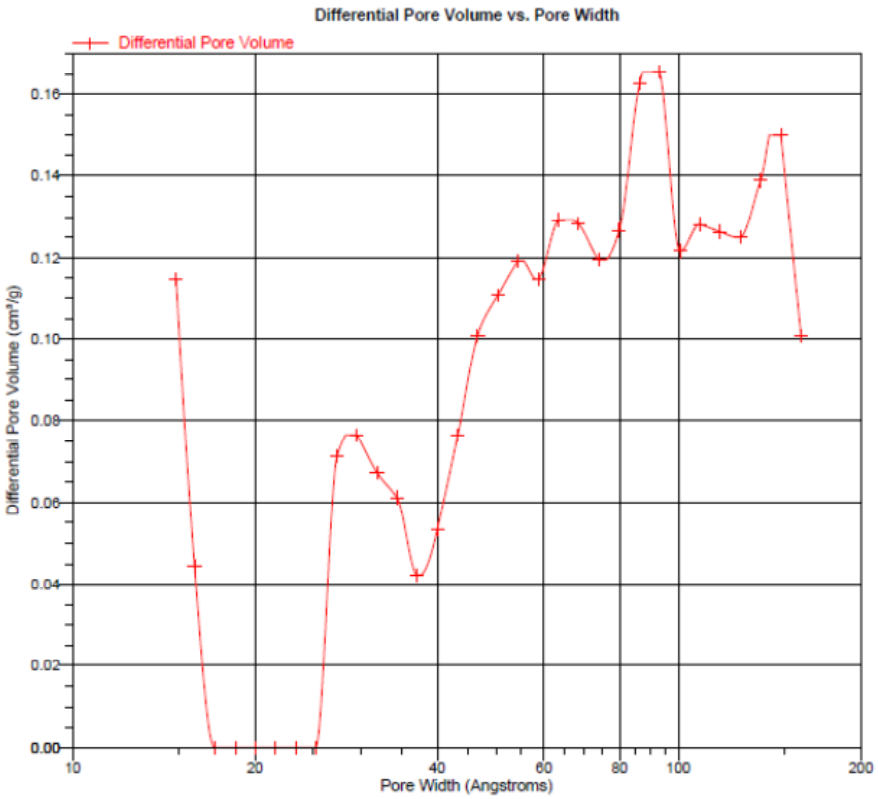

Figure C.4: differential pore volume vs pore width catalyst 2

- **CATALYST 3:** 20%Ni-10%ZnO/CNT

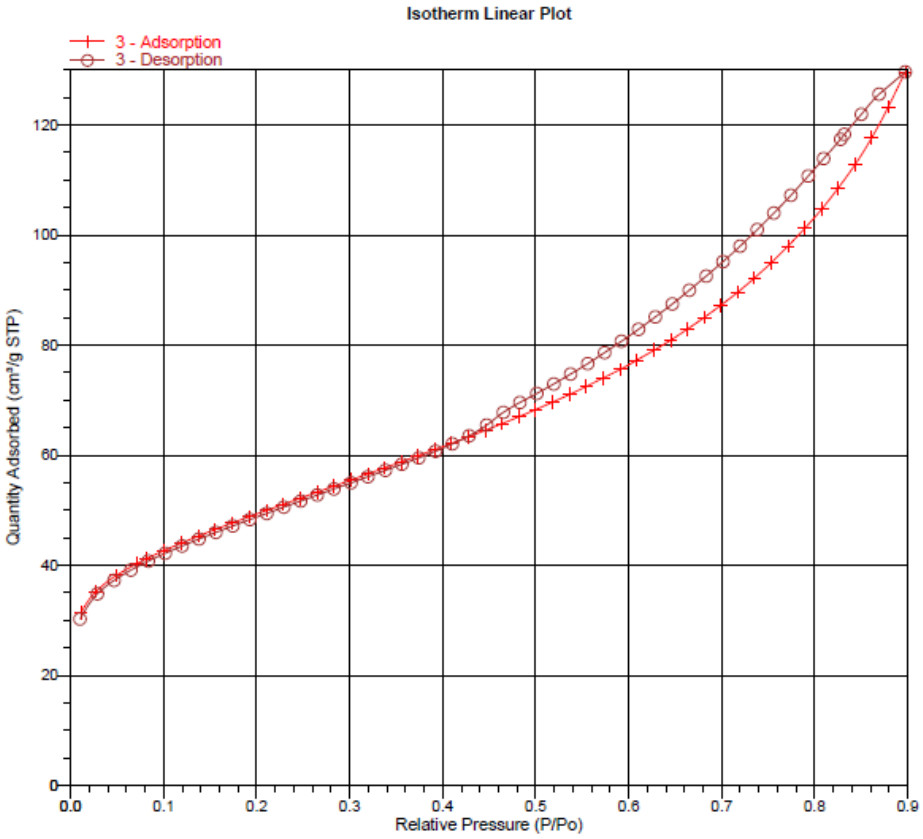

Figure C.5: adsorption-desorption isotherm catalyst 3

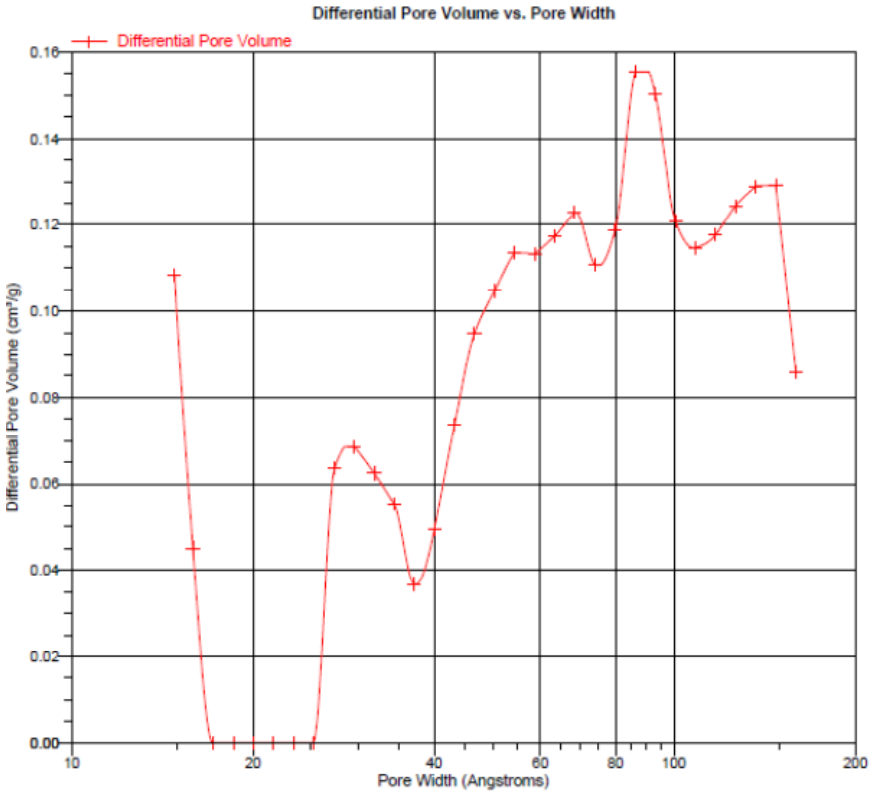

Figure C.6: differential pore volume vs pore width catalyst 3

- **CATALYST 4:** 20%Ni-10%ZnO/CNT

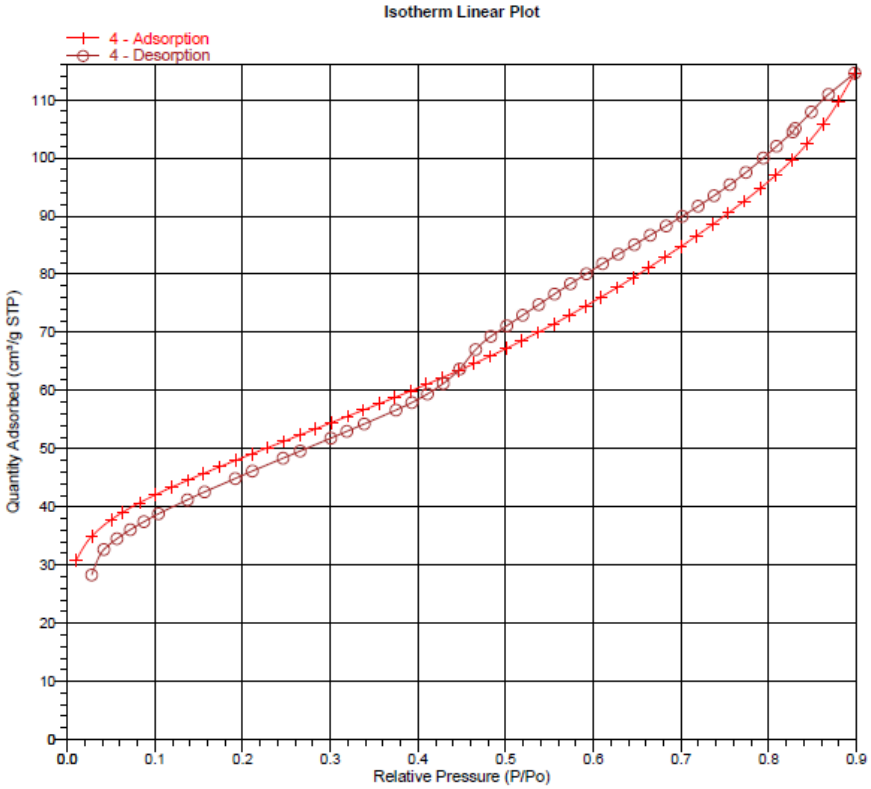

Figure C.7: adsorption-desorption isotherm catalyst 4

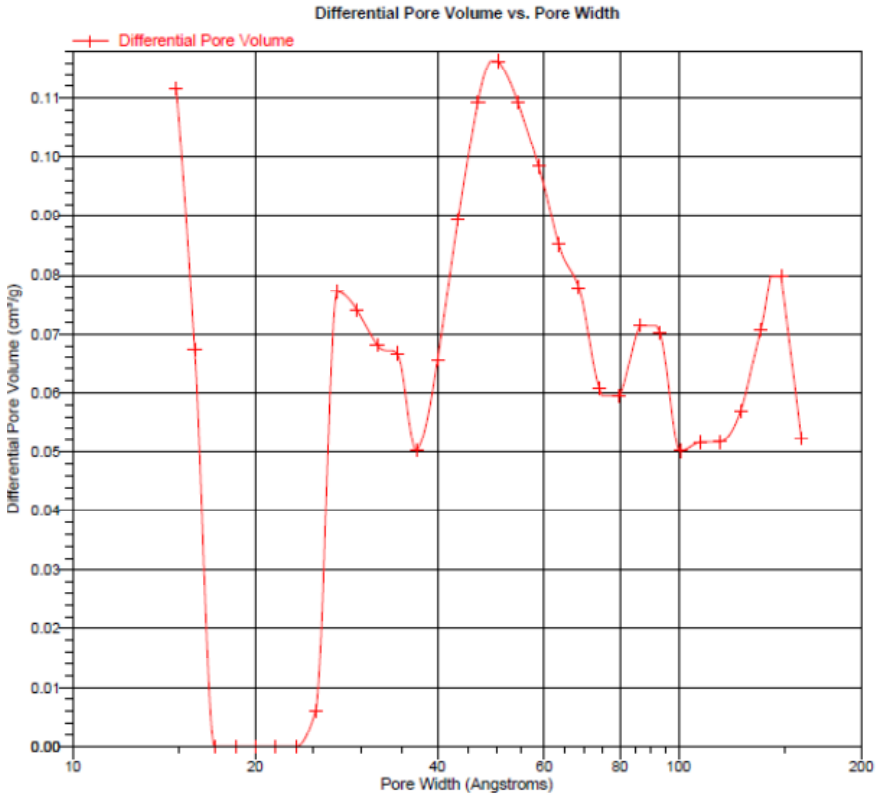

Figure C.8: differential pore volume vs pore width catalyst 4

- **CATALYST 5:** 20%Ni-26%ZnO/CNT

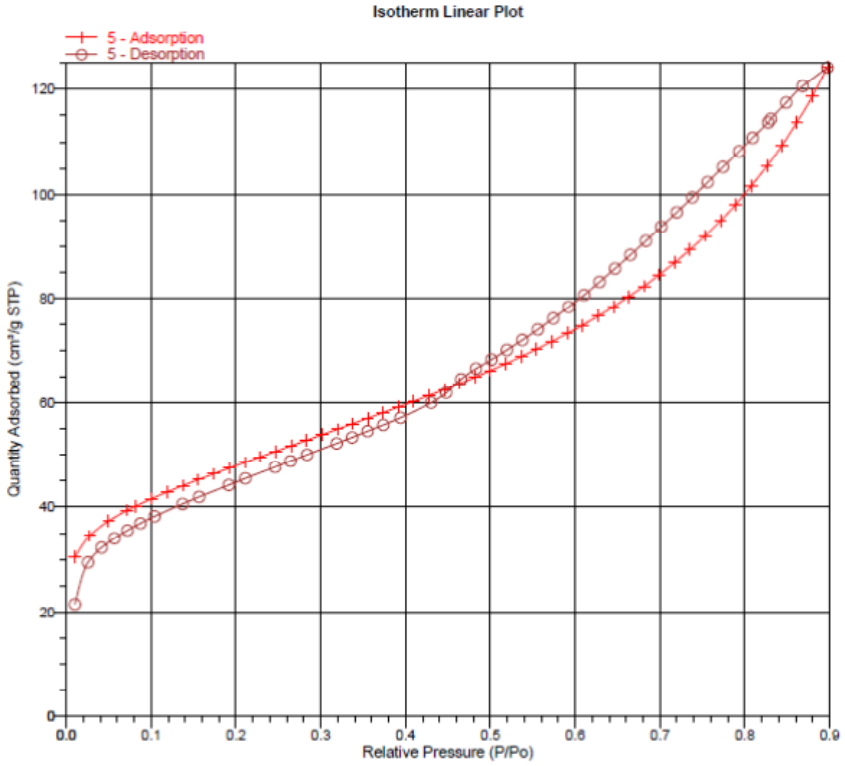

Figure C.9: adsorption-desorption isotherm catalyst 5

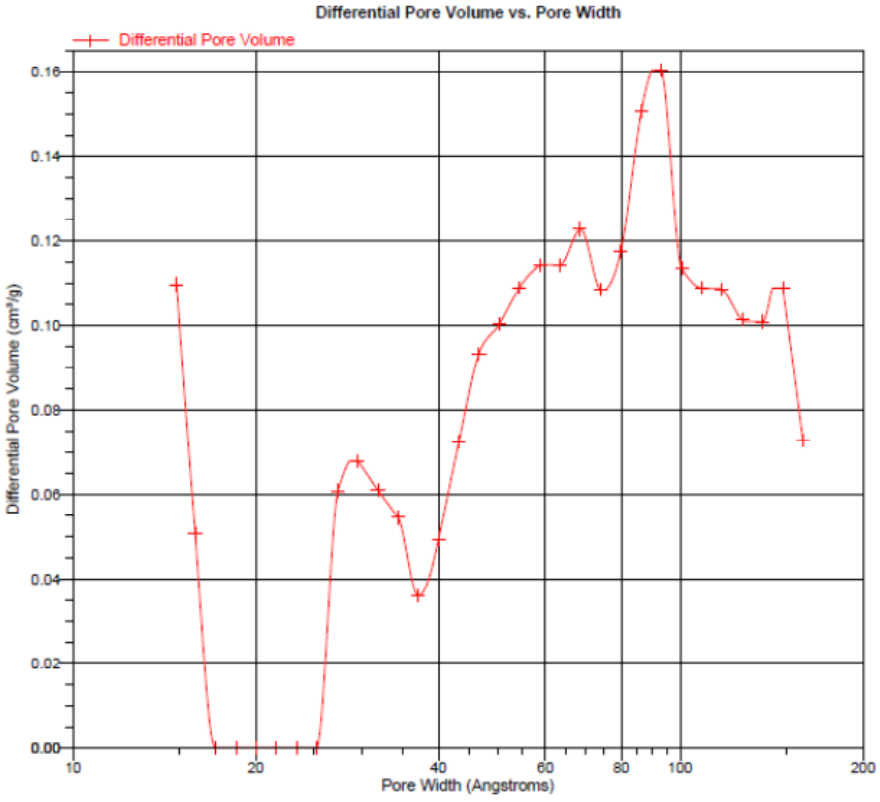

Figure C.10: differential pore volume vs pore width catalyst 5

- **CATALYST 6:** 20%Ni-20%ZnO/CNT added together

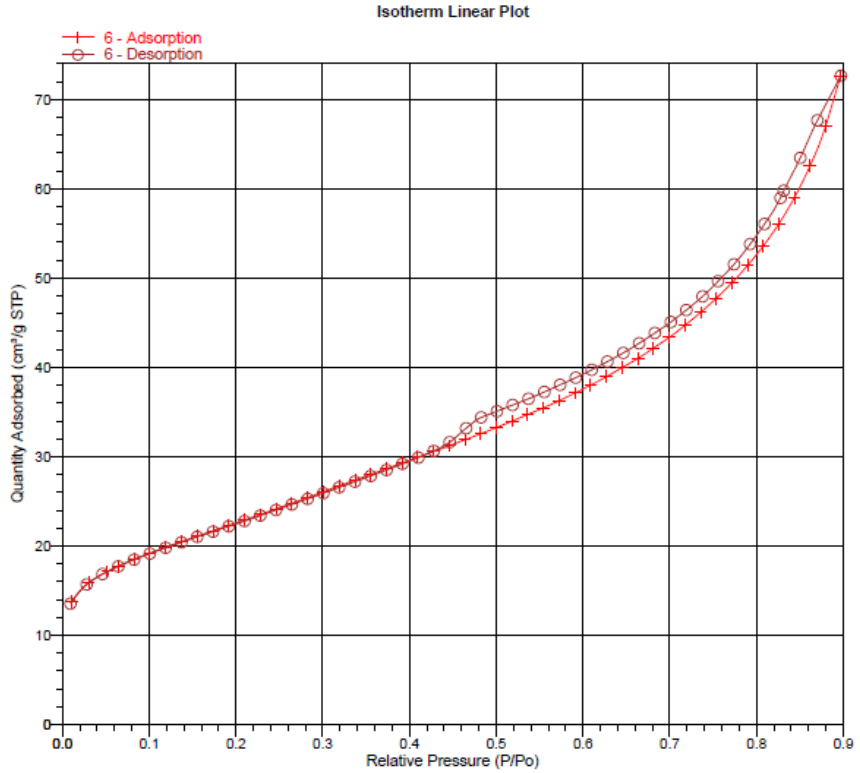

Figure C.11: adsorption-desorption isotherm catalyst 6

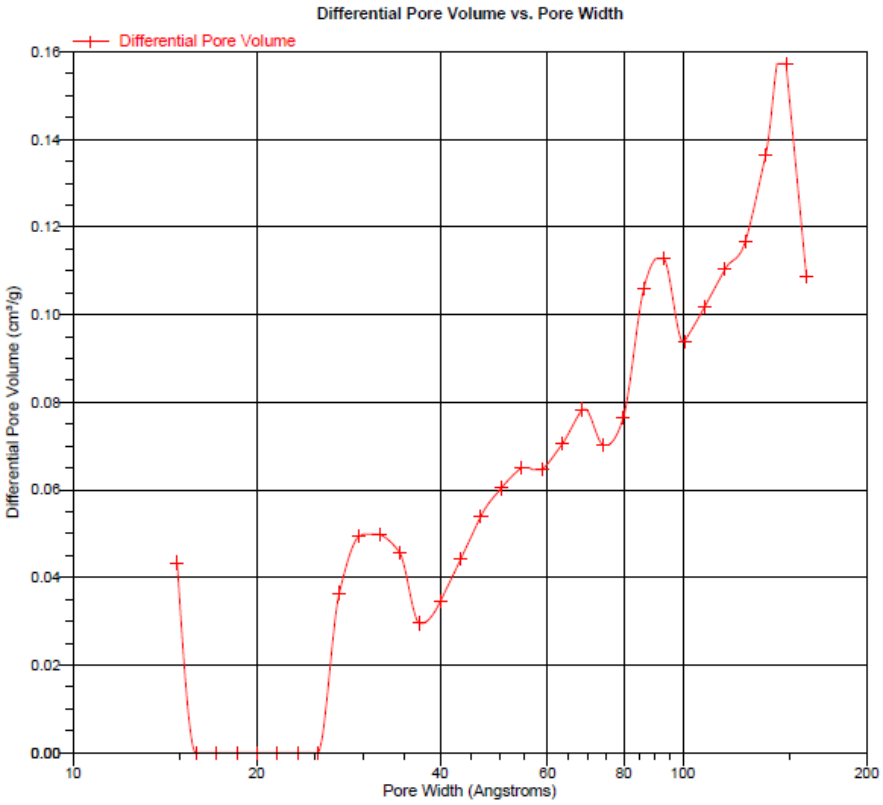

Figure C.12: differential pore volume vs pore width catalyst 6

- **CATALYST 7:** 20%ZnO/CNT

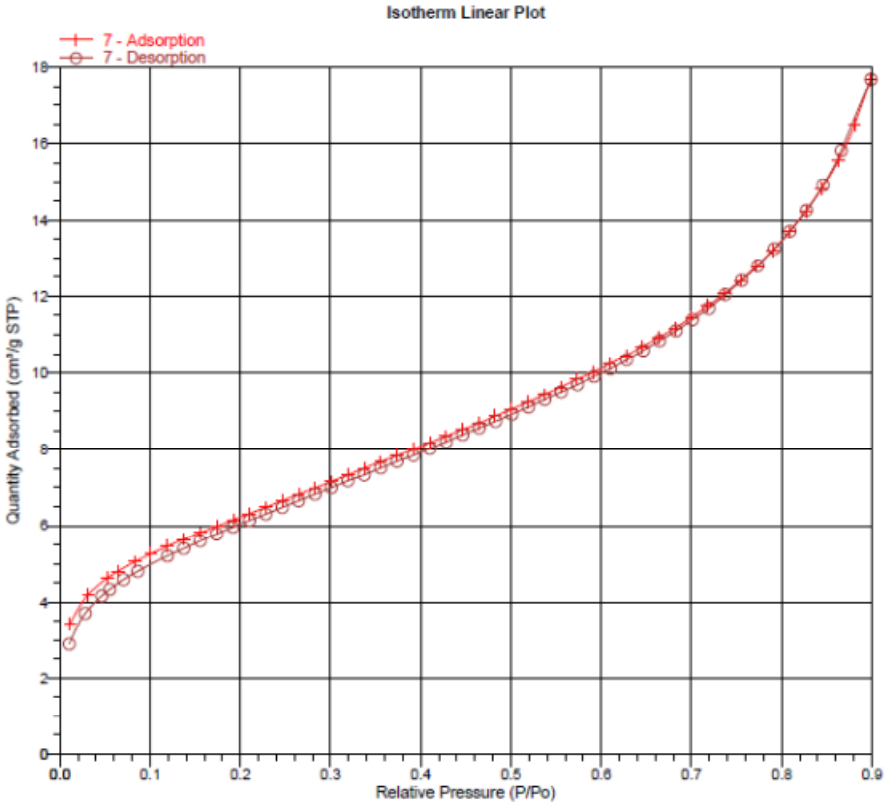

Figure C.13: adsorption-desorption isotherm catalyst 7

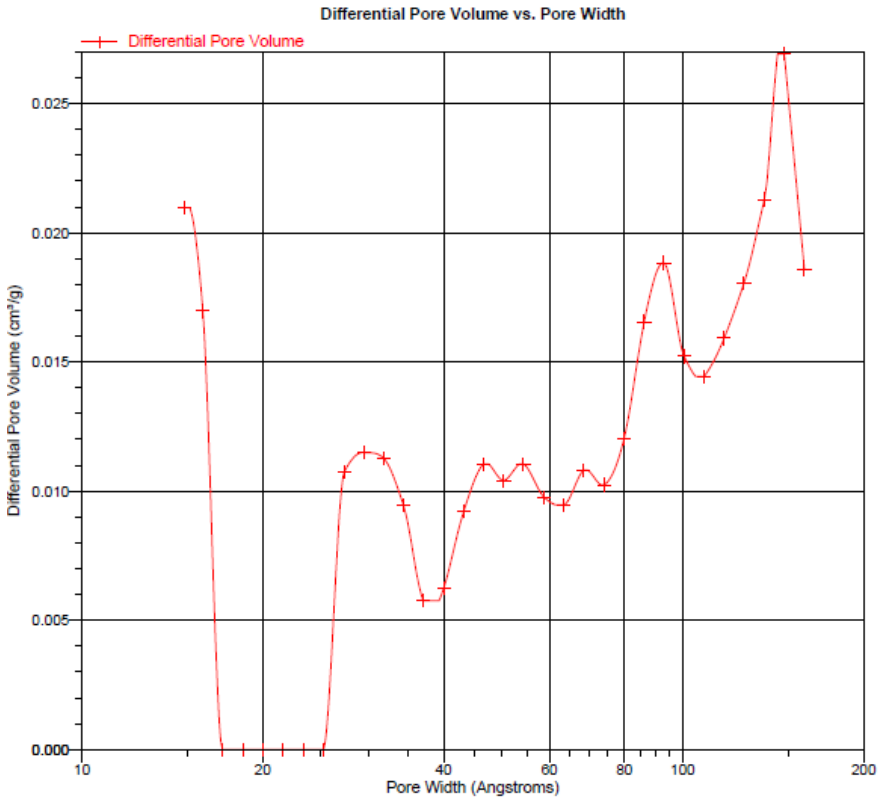

Figure C.14: differential pore volume vs pore width catalyst 7

- **CATALYST 8:** 20%Ni/CNT

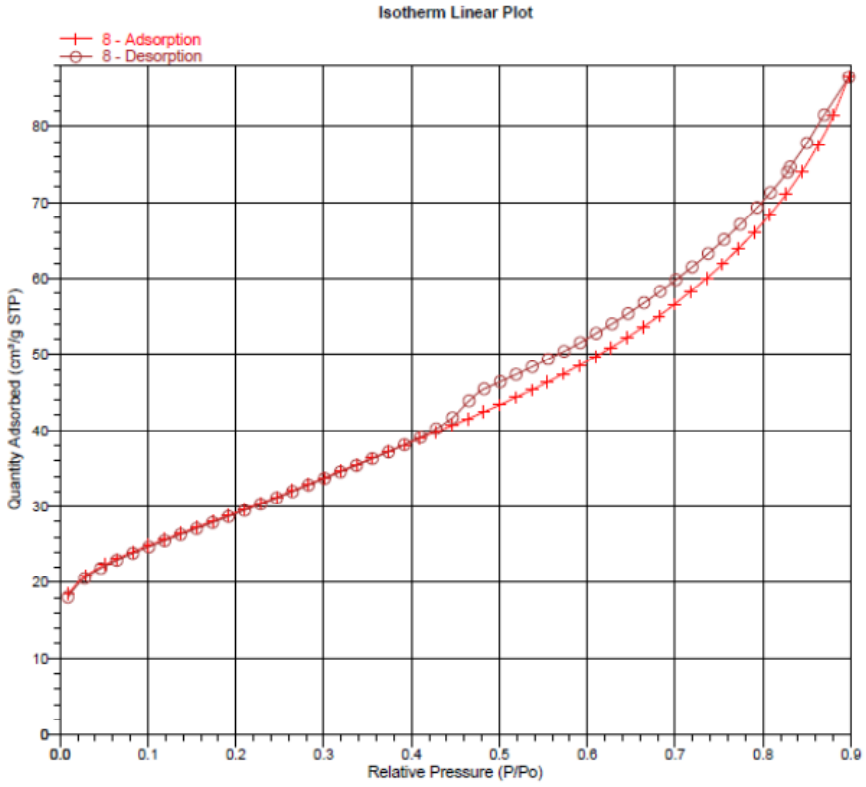

Figure C.15: adsorption-desorption isotherm catalyst 8

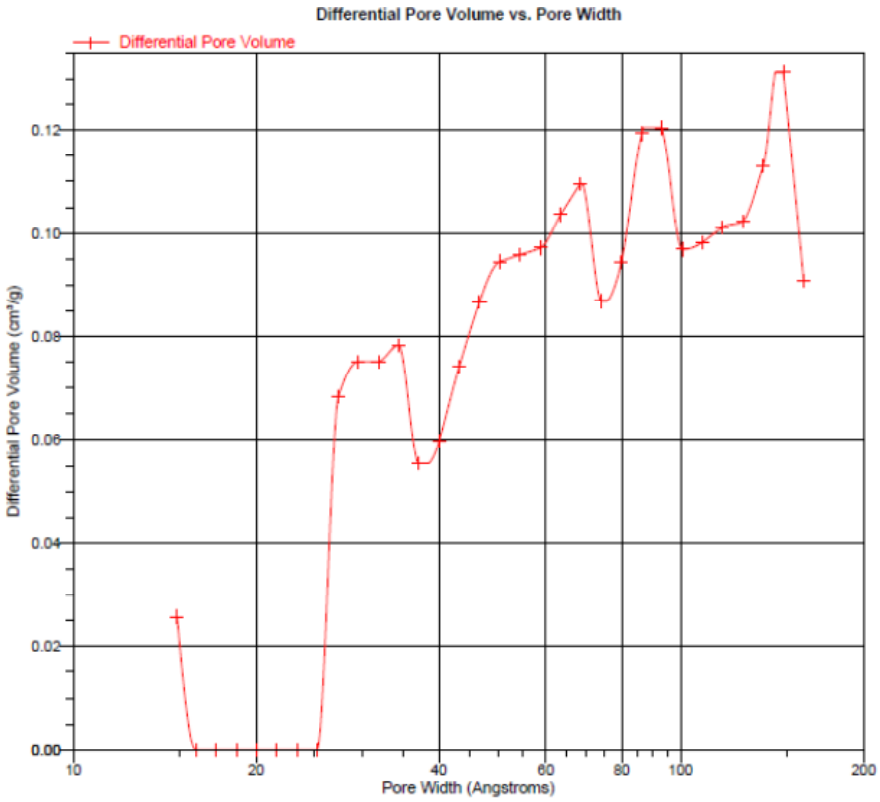

Figure C.16: differential pore volume vs pore width catalyst 8

APPENDIX D

APPENDIX D: CHEMISORPTION PLOTS

- **CATALYST 1:** 20%Ni-20%ZnO/CNT

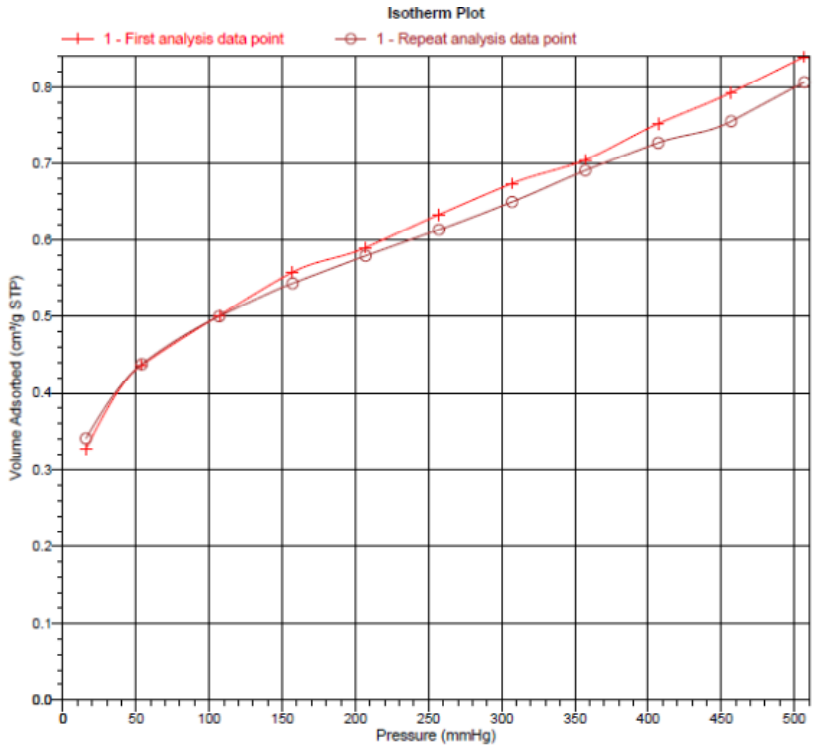

Figure D.1: adsorption-desorption isotherm catalyst 1

- **CATALYST 2:** 20%Ni-20%ZnO/CNT

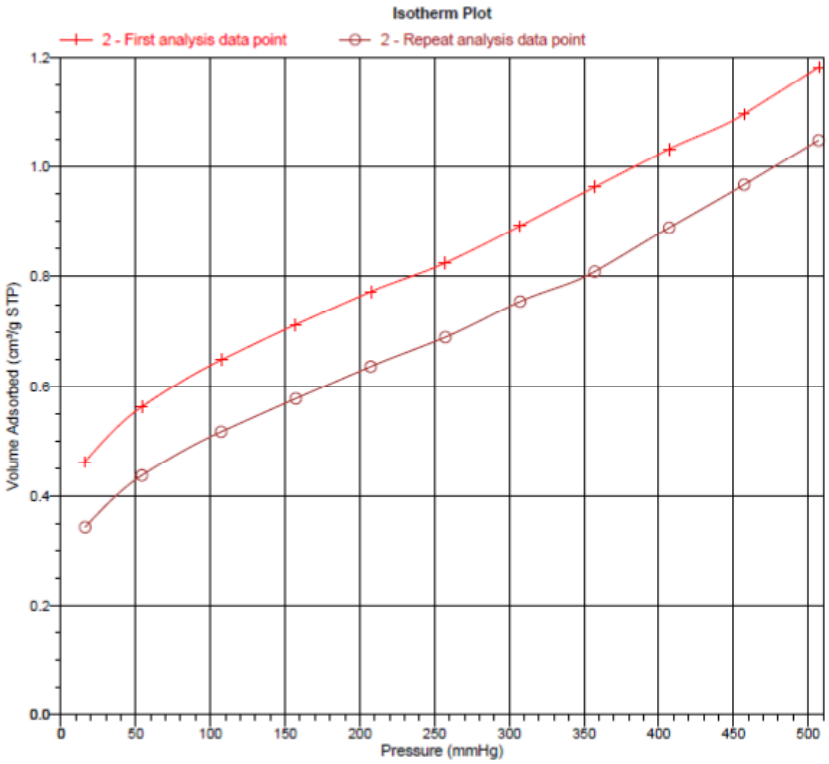

Figure D.2: adsorption-desorption isotherm catalyst 2

- **CATALYST 3:** 20%Ni-10%ZnO/CNT

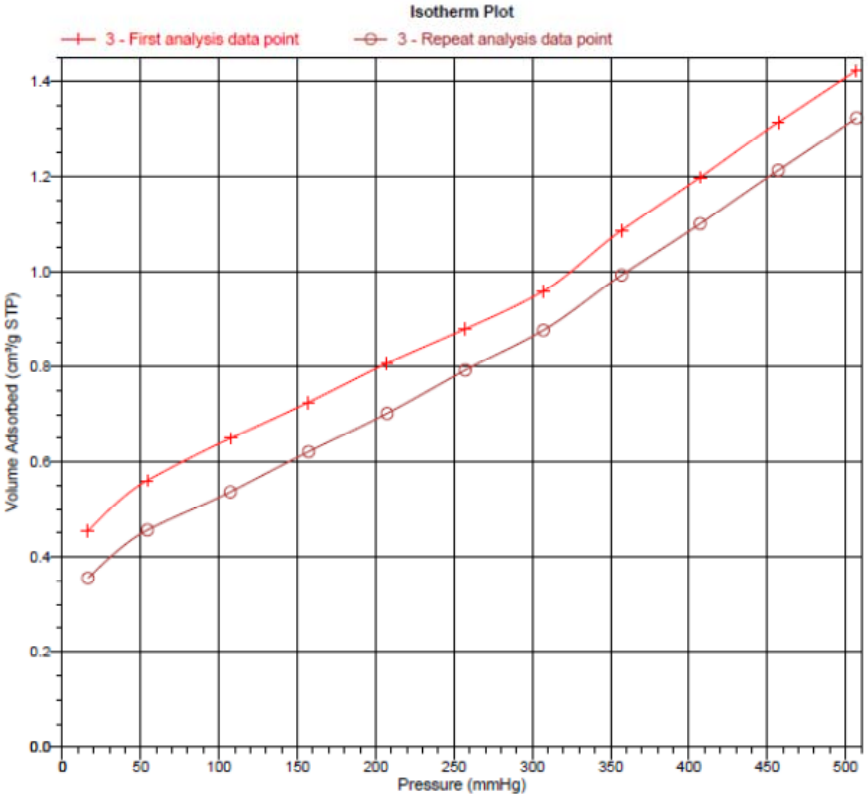

Figure D.3: adsorption-desorption isotherm catalyst 3

- **CATALYST 4:** 20%Ni-10%ZnO/CNT

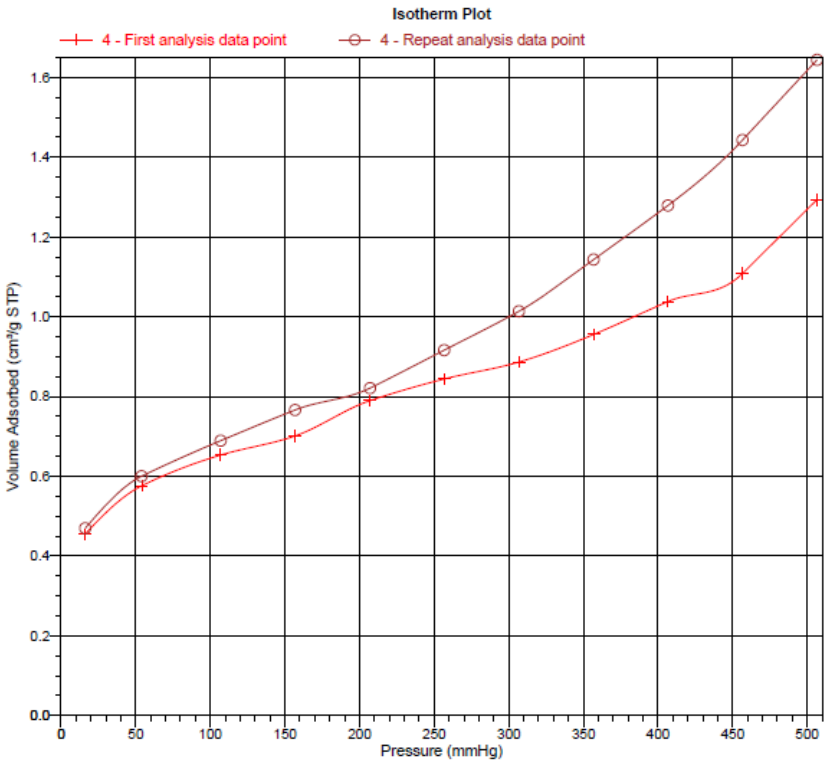

Figure D.4: adsorption-desorption isotherm catalyst 4

- **CATALYST 5:** 20%Ni-26%ZnO/CNT

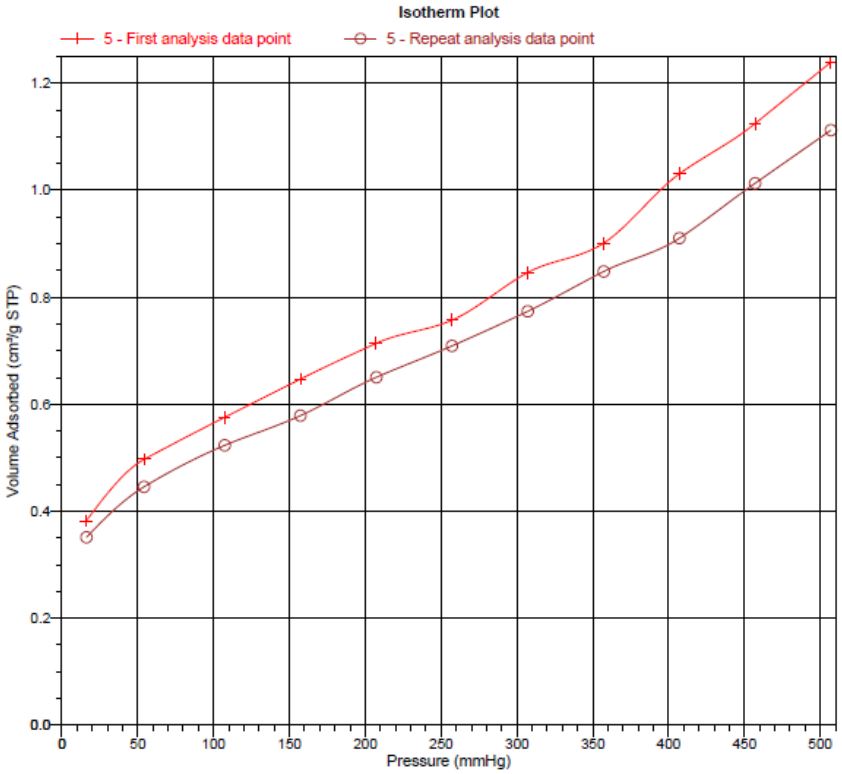

Figure D.5: adsorption-desorption isotherm catalyst 5

- **CATALYST 6:** 20%Ni-20%ZnO/CNT added together

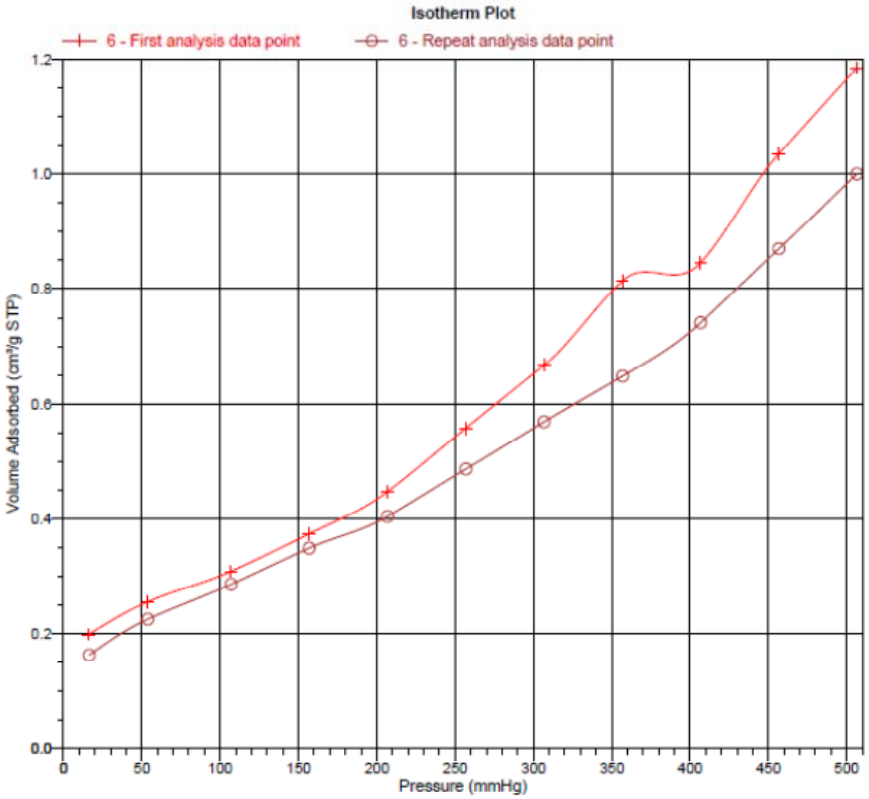

Figure D.6: adsorption-desorption isotherm catalyst 6

- **CATALYST 7:** 20%ZnO/CNT

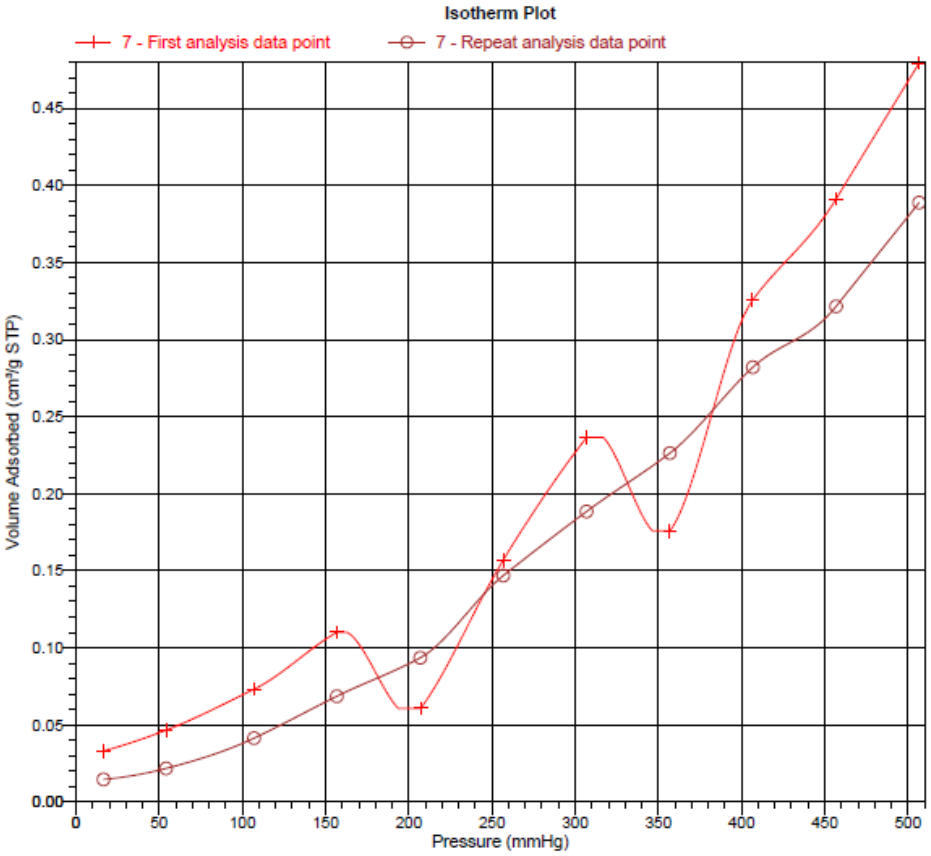

Figure D.7: adsorption-desorption isotherm catalyst 7

- **CATALYST 8:** 20%Ni/CNT

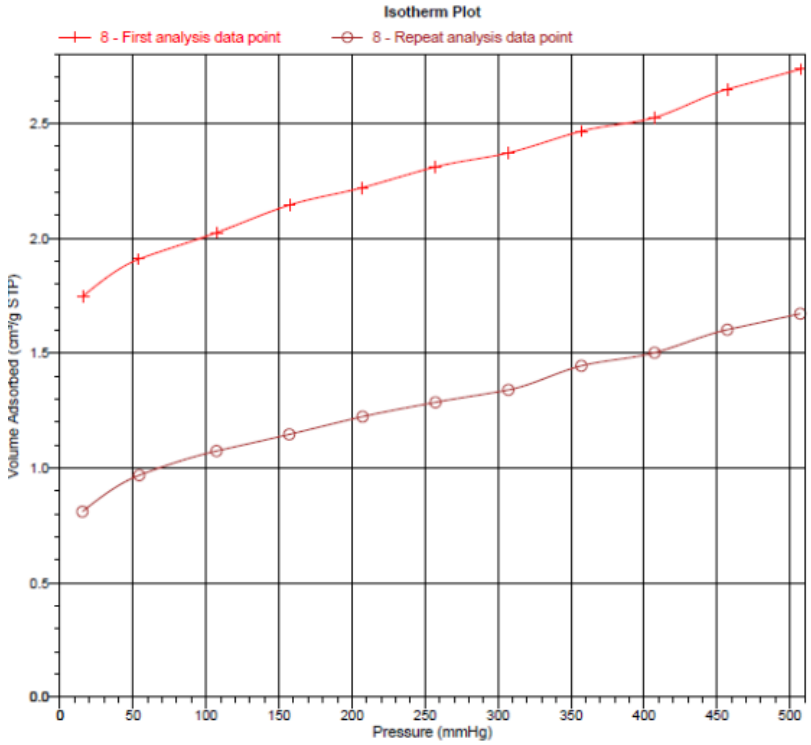

Figure D.8: adsorption-desorption isotherm catalyst 8

APPENDIX E

APPENDIX E: XRD PLOTS

- **CATALYST 1:** 20%Ni-20%ZnO/CNT

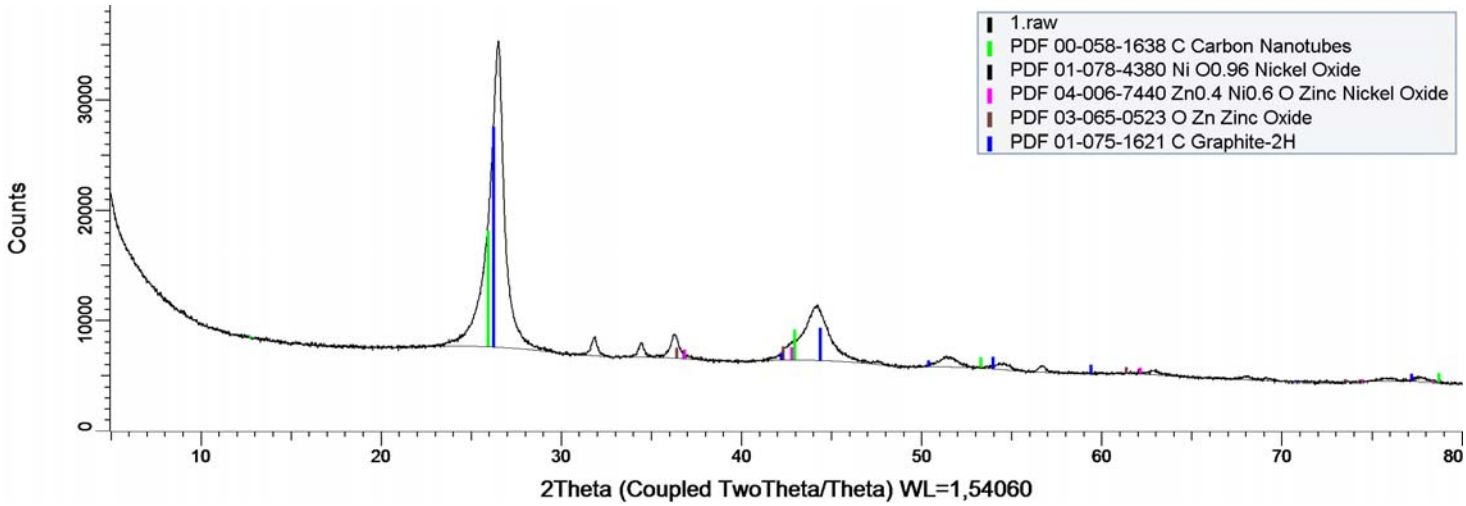

Figure E.1: The XRD patterns for the catalyst 1

- **CATALYST 2:** 20%Ni-20%ZnO/CNT

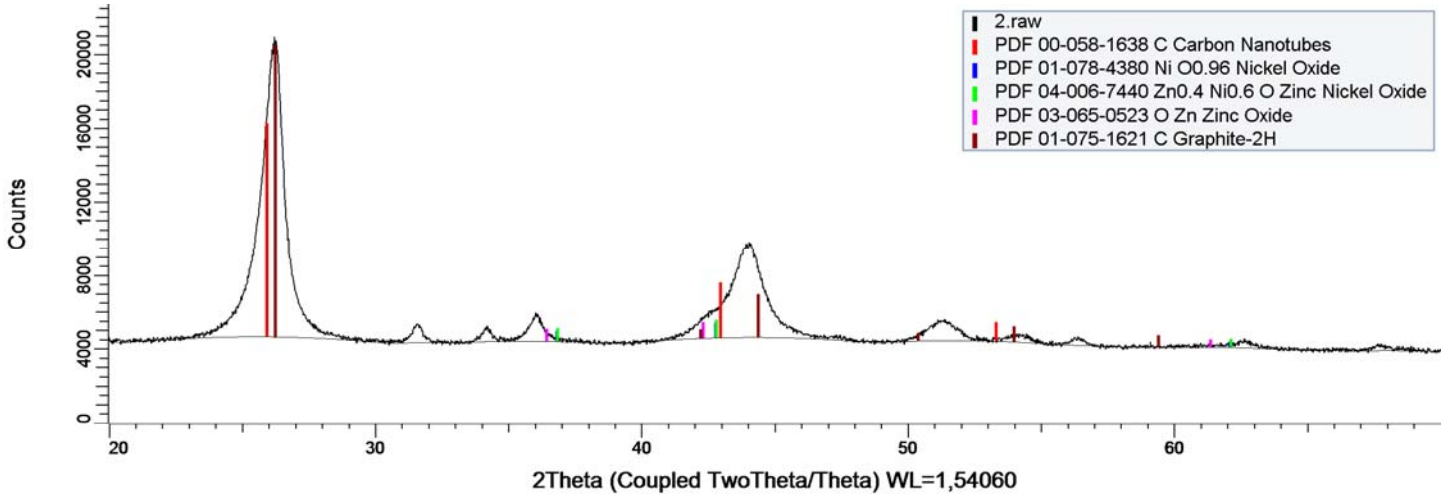

Figure E.2: The XRD patterns for the catalyst 2

- **CATALYST 3:** 20%Ni-10%ZnO/CNT

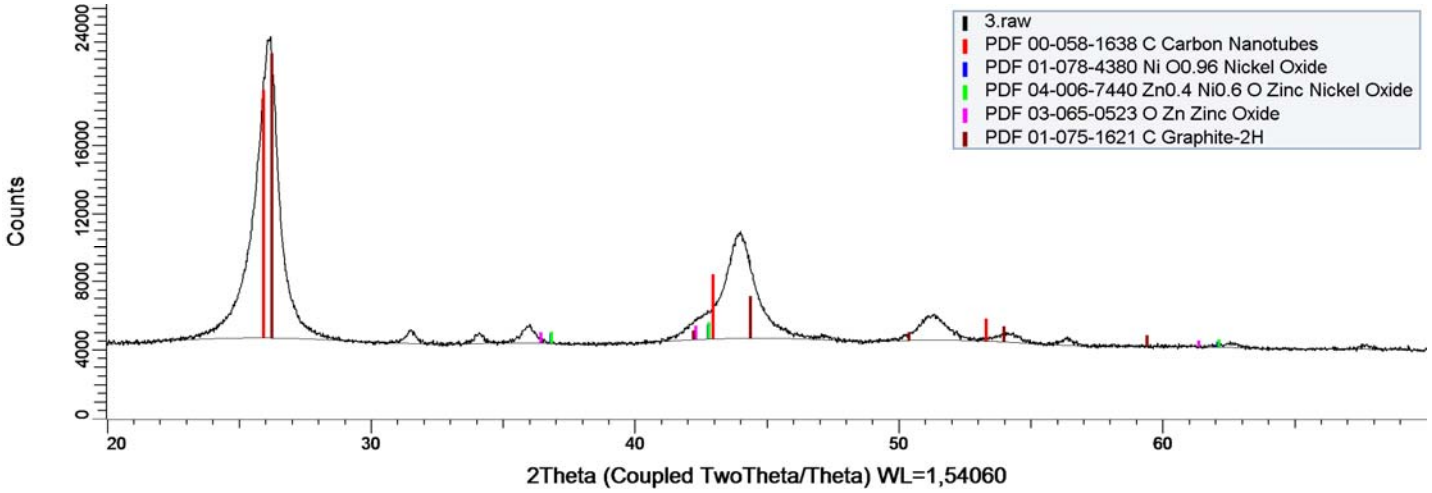

Figure E.3: The XRD patterns for the catalyst 3

- **CATALYST 4:** 20%Ni-10%ZnO/CNT

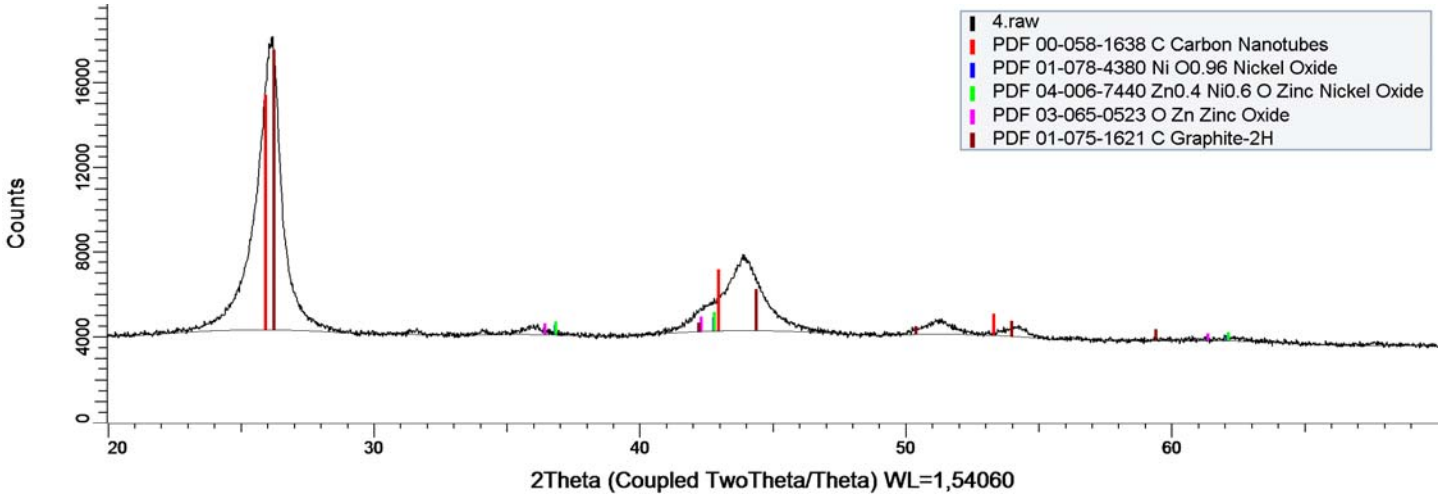

Figure E.4: The XRD patterns for the catalyst 4

- **CATALYST 5:** 20%Ni-26%ZnO/CNT

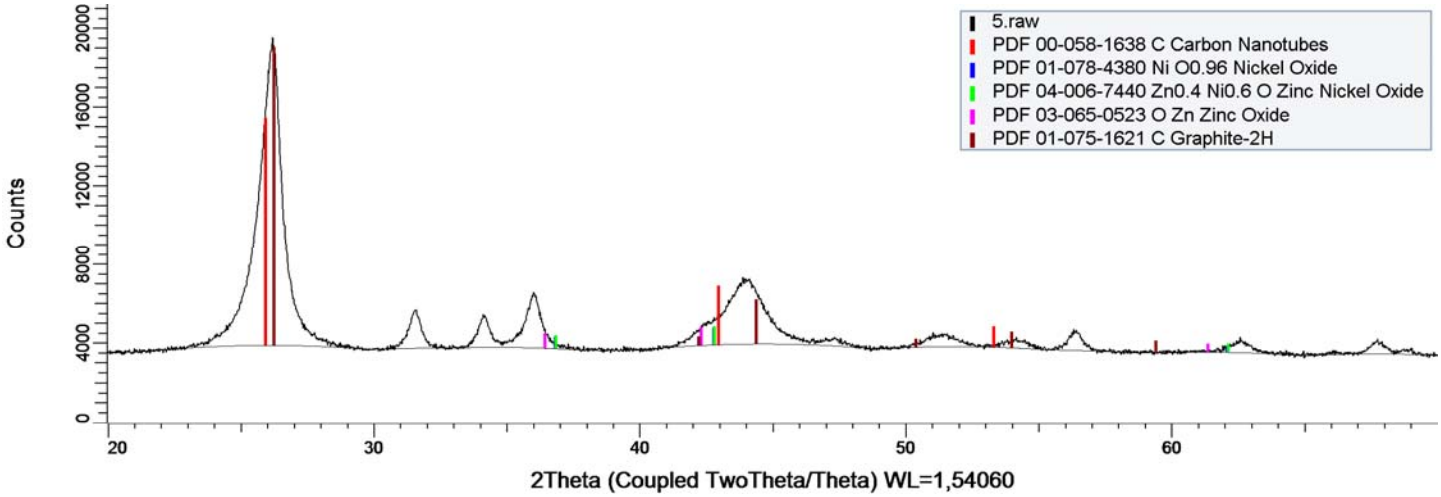

Figure E.5: The XRD patterns for the catalyst 5

- **CATALYST 6:** 20%Ni-20%ZnO/CNT added together

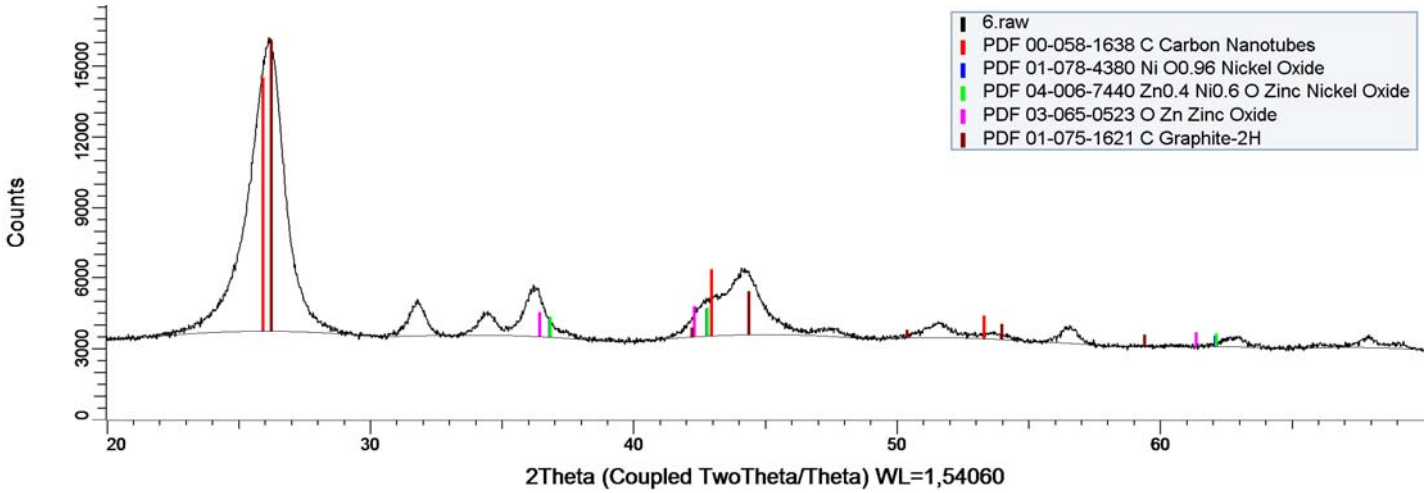

Figure E.6: The XRD patterns for the catalyst 6

APPENDIX F

APPENDIX F: LOADING ACCORDING TGA RESULTS

- **CATALYST 2:** 20%Ni-20%ZnO/CNT

% mass CNT: 7,64%.

% mass TGA: 28,8%.

Ratio:

$$\frac{molar\ mass\ precursor}{molar\ mass\ ZnO} = \frac{297{,}49 g/mol}{81{,}39 g/mol} = 3{,}655$$

ZnO precursor: P_{WO3} = 3,655 ZnO.

Ratio:

$$\frac{molar\ mass\ precursor}{molar\ mass\ ZnO} = \frac{290{,}79 g/mol}{165{,}38 g/mol} = 1{,}758$$

Ni precursor: P_{Ni} = 1,758 Ni_2O_3

Use this in:

$$\frac{m(ZnO) + m(Ni_2O_3) + m(metal\ on\ CNT)}{m(P_{ZnO}) + m(P_{Ni_2O}) + m(CNT) + m(metal\ on\ CNT)} = 0{,}288$$

Where:

m (ZnO) = 0,0324m (CNT)

m (metal CNT) = 0,0764m (CNT)

m (P_{ZnO}) = 3,655m (ZnO)

m (P_{Ni2O3}) = 1,758m (Ni_2O_3)

$$\frac{0{,}0324m(CNT) + m(Ni_2O_3) + 0{,}0764m(CNT)}{3{,}655m(ZnO) + 1{,}758m(Ni_2O_3) + m(CNT) + 0{,}0764m(CNT)} = 0{,}288$$

$$\frac{0{,}1088m(CNT) + m(Ni_2O_3)}{(3{,}655 \cdot 0{,}0324)m(ZnO) + 1{,}758m(Ni_2O_3) + m(CNT) + 0{,}0764m(CNT)} = 0{,}288$$

$$m(Ni_2O_3) = 0{,}4741m(CNT)$$

Real loading:

$$\frac{m(ZnO) + m(Ni_2O_3)}{m(ZnO) + m(Ni_2O_3) + m(CNT) + m(metal\ on\ CNT)} =$$

$$= \frac{0{,}0324 + 0{,}4741}{0{,}0324 + 0{,}4741 + 1 + 0{,}0764} = \mathbf{31{,}99\%}$$

- **CATALYST 4:** 20%Ni-10%ZnO/CNT

% mass CNT: 7,64%.

% mass TGA: 28,51%.

Ratio:

$$\frac{molar\ mass\ precursor}{molar\ mass\ ZnO} = \frac{297{,}49 g/mol}{81{,}39 g/mol} = 3{,}655$$

ZnO precursor: P_{WO3} = 3,655 ZnO.

Ratio:

$$\frac{molar\ mass\ precursor}{molar\ mass\ ZnO} = \frac{290{,}79 g/mol}{165{,}38 g/mol} = 1{,}758$$

Ni precursor: P_{Ni} = 1,758 Ni_2O_3

Use this in:

$$\frac{m(ZnO) + m(Ni_2O_3) + m(metal\ on\ CNT)}{m(P_{ZnO}) + m(P_{Ni_2O}) + m(CNT) + m(metal\ on\ CNT)} = 0{,}2851$$

Where:

m (ZnO) = 0,0324m (CNT)

m (metal CNT) = 0,0764m (CNT)

m (P_{ZnO}) = 3,655m (ZnO)

m (P_{Ni2O3}) = 1,758m (Ni_2O_3)

$$\frac{0{,}0324m(CNT) + m(Ni_2O_3) + 0{,}0764m(CNT)}{3{,}655m(ZnO) + 1{,}758m(Ni_2O_3) + m(CNT) + 0{,}0764m(CNT)} = 0{,}2851$$

$$\frac{0{,}1088m(CNT) + m(Ni_2O_3)}{(3{,}655 \cdot 0{,}0324)m(ZnO) + 1{,}758m(Ni_2O_3) + m(CNT) + 0{,}0764m(CNT)} = 0{,}2851$$

$$m(Ni_2O_3) = 0{,}4629m(CNT)$$

Real loading:

$$\frac{m(ZnO) + m(Ni_2O_3)}{m(ZnO) + m(Ni_2O_3) + m(CNT) + m(metal\ on\ CNT)} =$$

$$= \frac{0{,}0324 + 0{,}4629}{0{,}0324 + 0{,}4629 + 1 + 0{,}0764} = \mathbf{31{,}51\%}$$

- **CATALYST 5:** 20%Ni-26%ZnO/CNT

% mass CNT: 5,65%.

% mass TGA: 20,47%.

Ratio:

$$\frac{molar\ mass\ precursor}{molar\ mass\ ZnO} = \frac{297{,}49 g/mol}{81{,}39 g/mol} = 3{,}655$$

ZnO precursor: P_{WO3} = 3,655 ZnO.

Ratio:

$$\frac{molar\ mass\ precursor}{molar\ mass\ ZnO} = \frac{290{,}79 g/mol}{165{,}38 g/mol} = 1{,}758$$

Ni precursor: P_{Ni} = 1,758 Ni_2O_3

Use this in:

$$\frac{m(ZnO) + m(Ni_2O_3) + m(metal\ on\ CNT)}{m(P_{ZnO}) + m\left(P_{Ni_2O}\right) + m(CNT) + m(metal\ on\ CNT)} = 0{,}2047$$

Where:

m (ZnO) = 0,0324m (CNT)

m (metal CNT) = 0,0565m (CNT)

m (P_{ZnO}) = 3,655m (ZnO)

m (P_{Ni2O3}) = 1,758m (Ni_2O_3)

$$\frac{0{,}0324m(CNT) + m(Ni_2O_3) + 0{,}0565m(CNT)}{3{,}655m(ZnO) + 1{,}758m(Ni_2O_3) + m(CNT) + 0{,}0565m(CNT)} = 0{,}2047$$

$$\frac{0{,}0889m(CNT) + m(Ni_2O_3)}{(3{,}655 \cdot 0{,}0324)m(ZnO) + 1{,}758m(Ni_2O_3) + m(CNT) + 0{,}0565m(CNT)} = 0{,}2047$$

$$m(Ni_2O_3) = 0{,}2360m(CNT)$$

Real loading:

$$\frac{m(ZnO) + m(Ni_2O_3)}{m(ZnO) + m(Ni_2O_3) + m(CNT) + m(metal\ on\ CNT)} =$$

$$= \frac{0{,}0324 + 0{,}2360}{0{,}0324 + 0{,}2360 + 1 + 0{,}0565} = \mathbf{20{,}24\%}$$

- **CATALYST 6:** 20%Ni-20%ZnO/CNT added together

% mass CNT: 5,65%.

% mass TGA: 25,2%.

Ratio:

$$\frac{molar\ mass\ precursor}{molar\ mass\ ZnO} = \frac{297{,}49 g/mol}{81{,}39 g/mol} = 3{,}655$$

ZnO precursor: P_{WO3} = 3,655 ZnO.

Ratio:

$$\frac{molar\ mass\ precursor}{molar\ mass\ ZnO} = \frac{290{,}79 g/mol}{165{,}38 g/mol} = 1{,}758$$

Ni precursor: P_{Ni} = 1,758 Ni_2O_3

Use this in:

$$\frac{m(ZnO) + m(Ni_2O_3) + m(metal\ on\ CNT)}{m(P_{ZnO}) + m\left(P_{Ni_2O}\right) + m(CNT) + m(metal\ on\ CNT)} = 0{,}252$$

Where:

m (ZnO) = 0,0324m (CNT)

m (metal CNT) = 0,0565m (CNT)

m (P_{ZnO}) = 3,655m (ZnO)

m (P_{Ni2O3}) = 1,758m (Ni_2O_3)

$$\frac{0{,}0324m(CNT) + m(Ni_2O_3) + 0{,}0565m(CNT)}{3{,}655m(ZnO) + 1{,}758m(Ni_2O_3) + m(CNT) + 0{,}0565m(CNT)} = 0{,}252$$

$$\frac{0{,}0889m(CNT) + m(Ni_2O_3)}{(3{,}655 \cdot 0{,}0324)m(ZnO) + 1{,}758m(Ni_2O_3) + m(CNT) + 0{,}0565m(CNT)} = 0{,}252$$

$$m(Ni_2O_3) = 0{,}3732m(CNT)$$

Real loading:

$$\frac{m(ZnO) + m(Ni_2O_3)}{m(ZnO) + m(Ni_2O_3) + m(CNT) + m(metal\ on\ CNT)} =$$

$$= \frac{0{,}0324 + 0{,}3732}{0{,}0324 + 0{,}3732 + 1 + 0{,}0565} = \mathbf{27{,}74\%}$$

- **CATALYST 7:** 20%ZnO/CNT

% mass CNT: 5,65%.

% mass TGA: 8,236%.

Ratio:

$$\frac{molar\ mass\ precursor}{molar\ mass\ ZnO} = \frac{297{,}49 g/mol}{81{,}39 g/mol} = 3{,}655$$

ZnO precursor: P_{WO3} = 3,655 ZnO.

Use this in:

$$\frac{m(ZnO) + m(metal\ on\ CNT)}{m(P_{ZnO}) + m(CNT) + m(metal\ on\ CNT)} = 0{,}08236$$

$$\frac{m(ZnO) + 0{,}0565m(CNT)}{3{,}655m(ZnO) + m(CNT) + 0{,}0565m(CNT)} = 0{,}08236$$

$$m(ZnO) + 0{,}0565m(CNT) = 0{,}301m(ZnO) + 0{,}0877m(CNT)$$

$$0{,}699m(ZnO) = 0{,}0227m(CNT)$$

$$m(ZnO) = 0{,}0324m(CNT)$$

Real loading:

$$\frac{m(ZnO)}{m(ZnO) + m(CNT) + m(metal\ on\ CNT)} = \frac{0{,}0324}{0{,}0324 + 1 + 0{,}0565} = \mathbf{2{,}98\%}$$

- **CATALYST 8:** 20%Ni/CNT

% mass CNT: 5,65%.

% mass TGA: 25,72%.

Ratio:

$$\frac{molar\ mass\ precursor}{molar\ mass\ ZnO} = \frac{297{,}49 g/mol}{81{,}39 g/mol} = 3{,}655$$

ZnO precursor: P_{WO3} = 3,655 ZnO.

Ratio:

$$\frac{molar\ mass\ precursor}{molar\ mass\ ZnO} = \frac{290{,}79 g/mol}{165{,}38 g/mol} = 1{,}758$$

Ni precursor: P_{Ni} = 1,758 Ni_2O_3

Use this in:

$$\frac{m(ZnO) + m(Ni_2O_3) + m(metal\ on\ CNT)}{m(P_{ZnO}) + m\left(P_{Ni_2O}\right) + m(CNT) + m(metal\ on\ CNT)} = 0{,}2572$$

Where:

m (ZnO) = 0,0324m (CNT)

m (metal CNT) = 0,0565m (CNT)

m (P_{ZnO}) = 3,655m (ZnO)

m (P_{Ni2O3}) = 1,758m (Ni_2O_3)

$$\frac{0{,}0324m(CNT) + m(Ni_2O_3) + 0{,}0565m(CNT)}{3{,}655m(ZnO) + 1{,}758m(Ni_2O_3) + m(CNT) + 0{,}0565m(CNT)} = 0{,}2572$$

$$\frac{0{,}0889m(CNT) + m(Ni_2O_3)}{(3{,}655 \cdot 0{,}0324)m(ZnO) + 1{,}758m(Ni_2O_3) + m(CNT) + 0{,}0565m(CNT)} = 0{,}2572$$

$$m(Ni_2O_3) = 0{,}3906m(CNT)$$

Real loading:

$$\frac{m(ZnO) + m(Ni_2O_3)}{m(ZnO) + m(Ni_2O_3) + m(CNT) + m(metal\ on\ CNT)} =$$

$$= \frac{0{,}0324 + 0{,}3906}{0{,}0324 + 0{,}3906 + 1 + 0{,}0565} = \mathbf{28{,}59\%}$$

APPENDIX G

APPENDIX G: GC ANALYSIS OF THE PURE COMPONENTS

1-HEXANOL

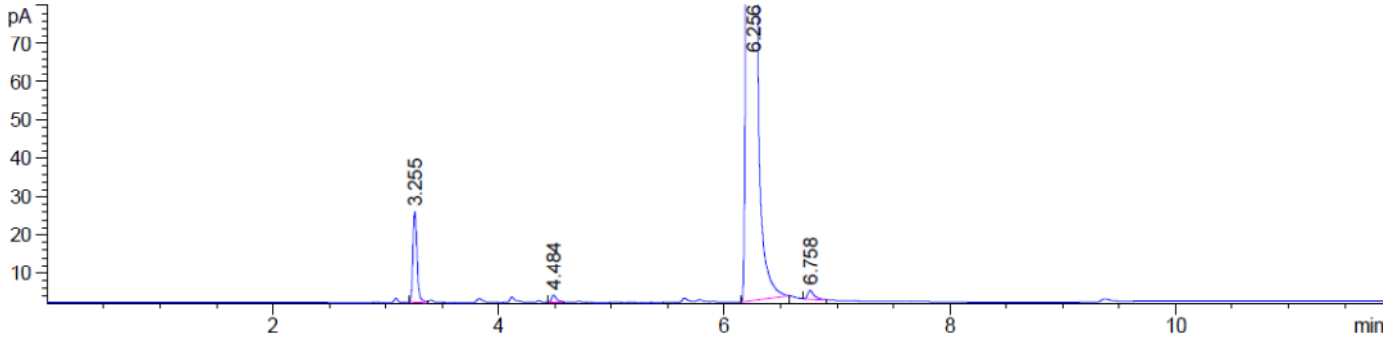

Figure G.1: GC results 1-hexano

3-PENTANOL

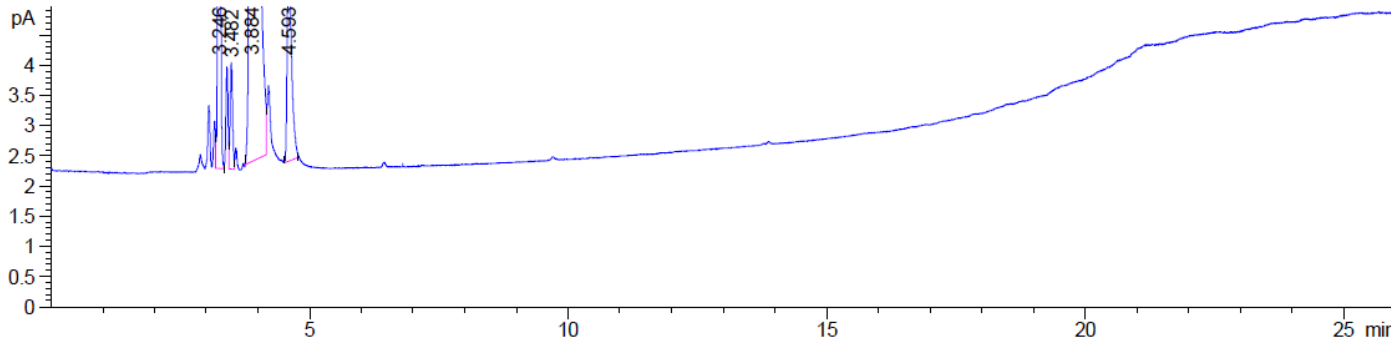

Figure G.2: GC results 3-pentanol

1,3-PROPANDIOL

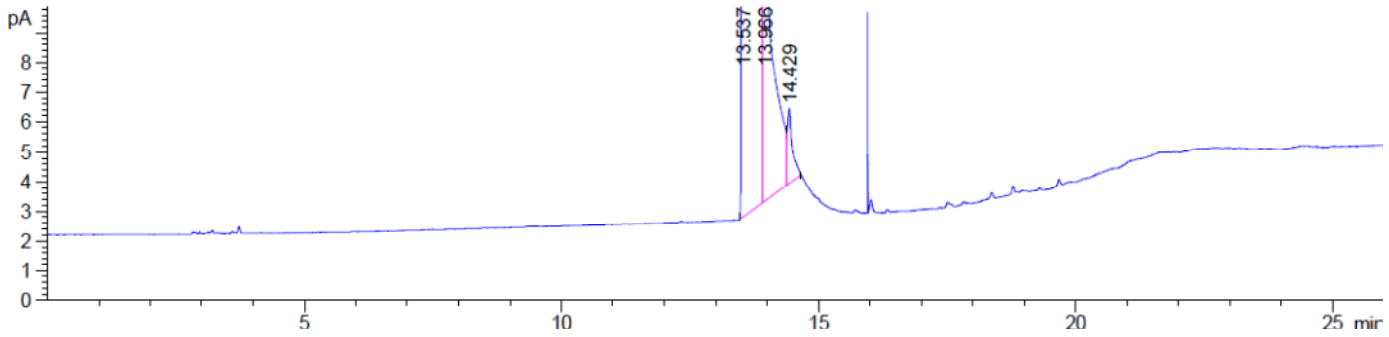

Figure G.3: GC results 1,3-propandiol

DODECANOL

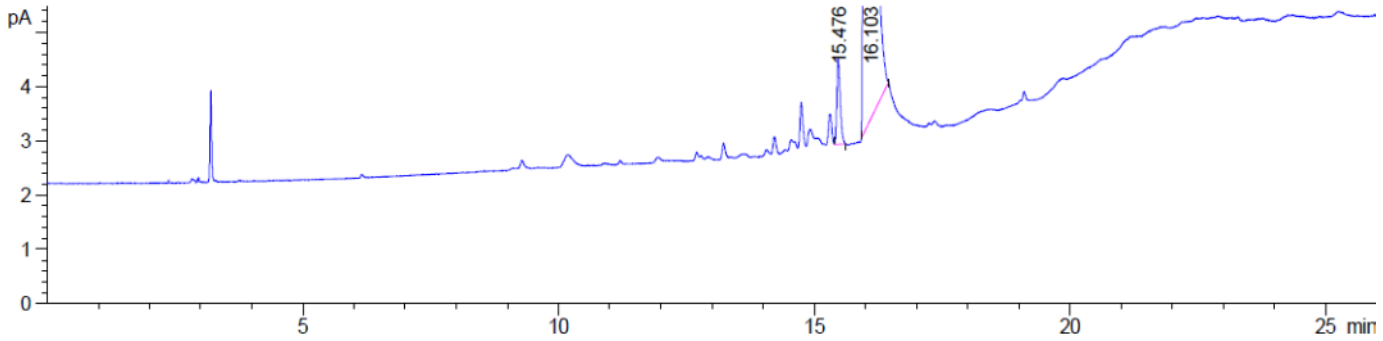

Figure G.4: GC results dodecanol

EG AND PG

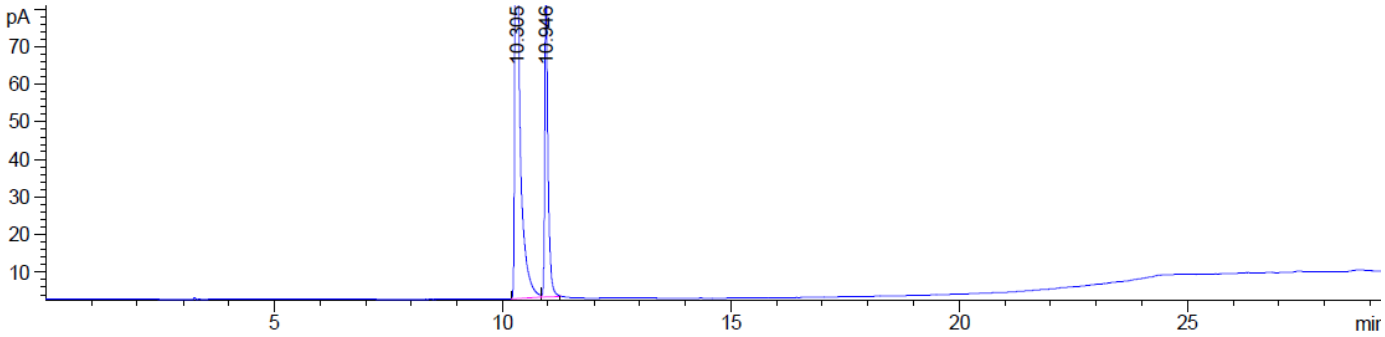

Figure G.5: GC results EG and PG

EG

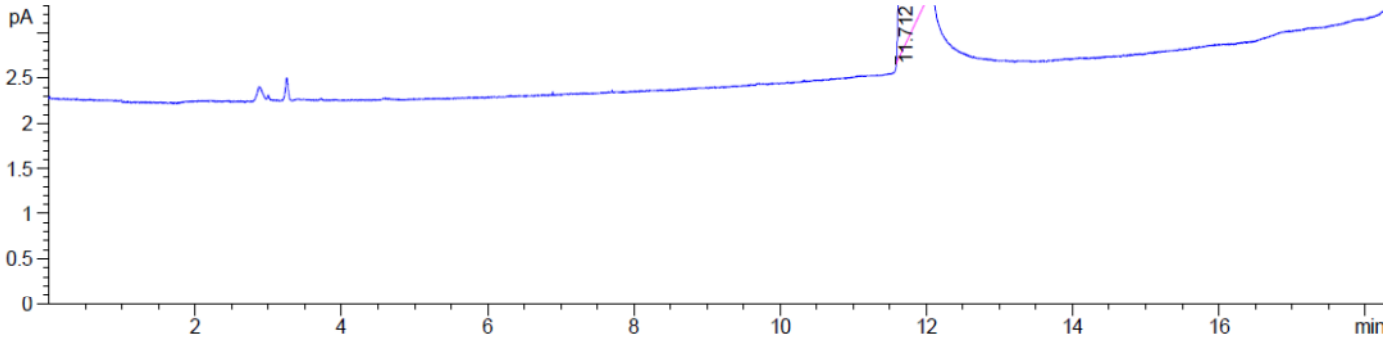

Figure G.6: GC results EG

ETHANOL

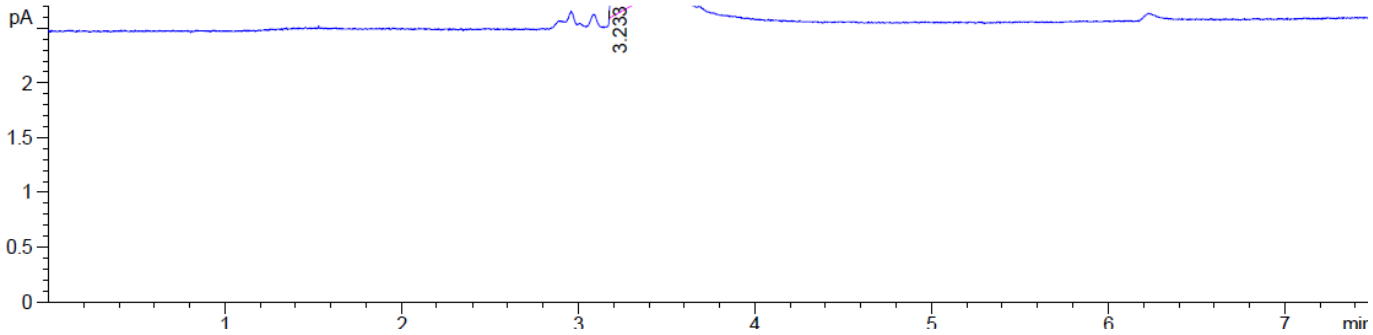

Figure G.7: GC results ethanol

GLYCEROL

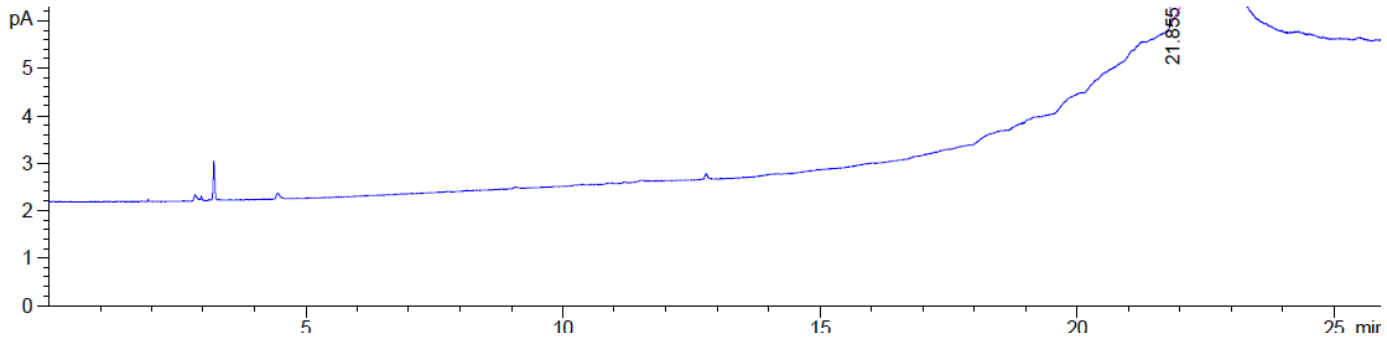

Figure G.8: GC results glycerol

PG

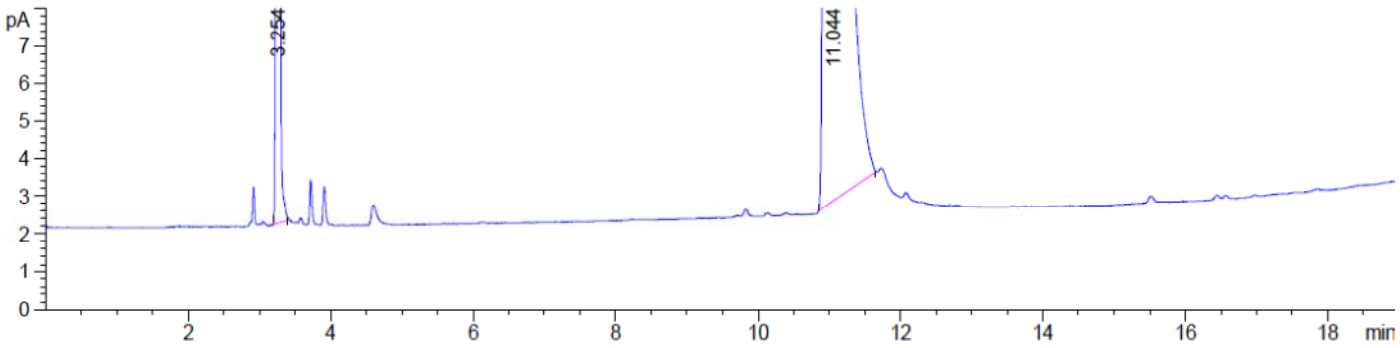

Figure G.9: GC results PG

1-PROPANOL

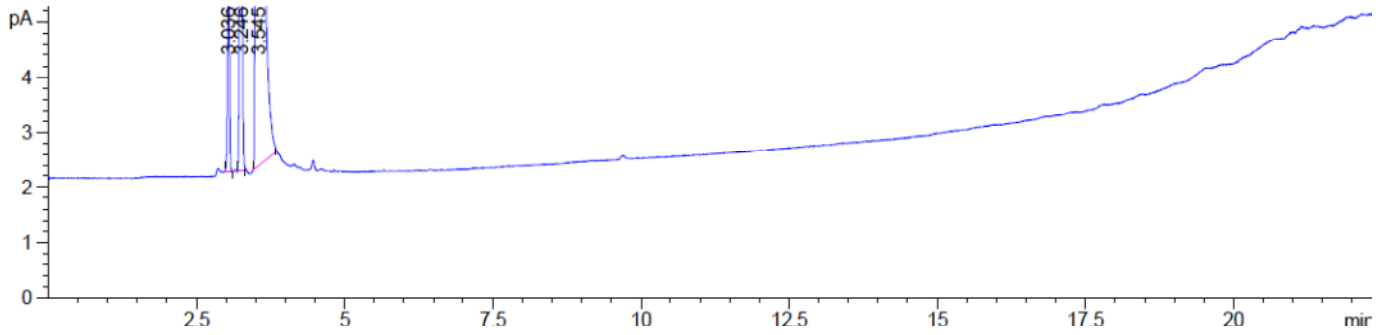

Figure G.10: GC results 1-propanol

2-PROPANOL

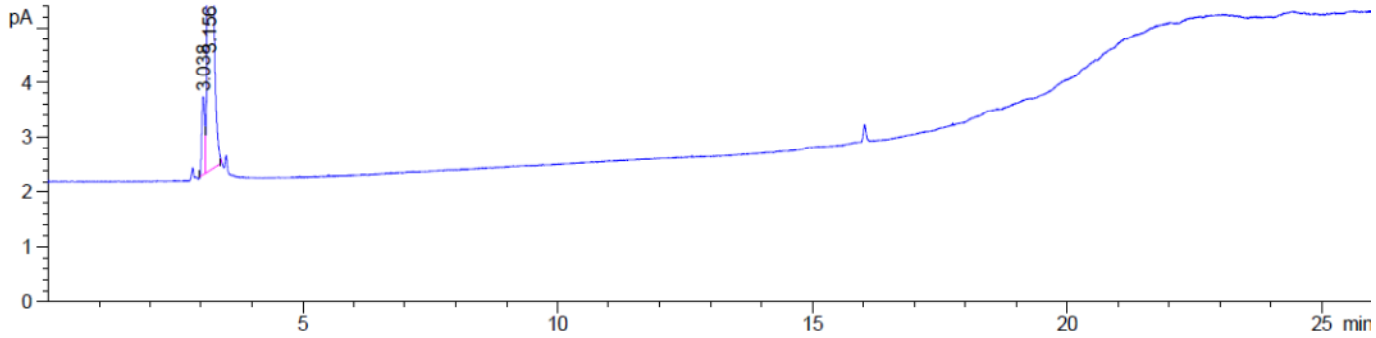

Figure G.11: GC results 2-propanol

APPENDIX H

APPENDIX H: DSC AND DTG AS A FUNCTION OF TEMPERATURE (FROM THE CO_2-TPD)

BEFORE NI IMPREGNATION

CATALYST 1

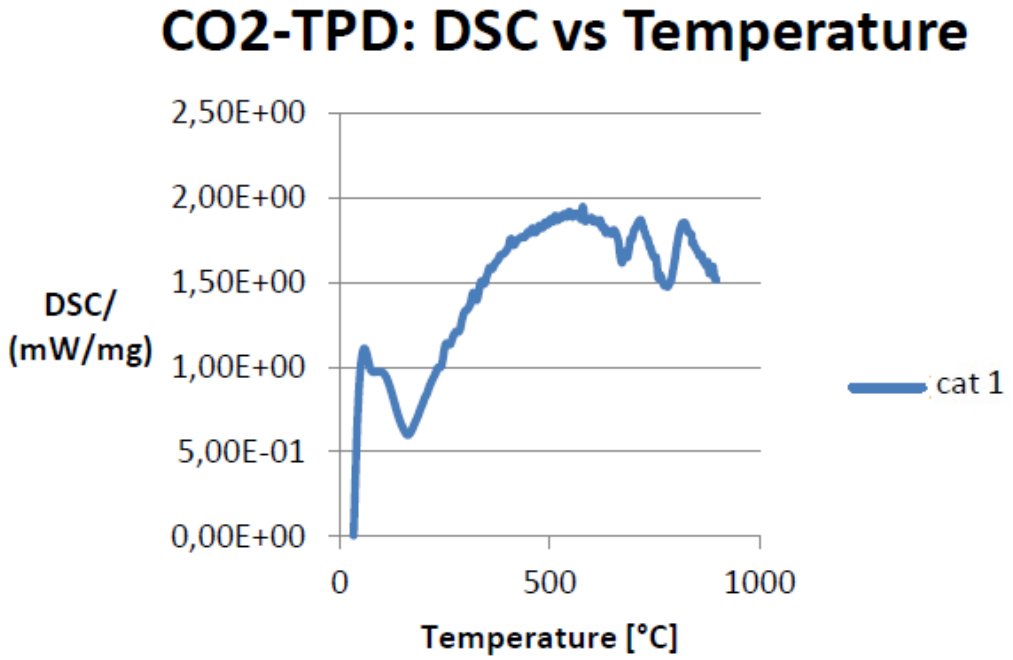

Figure H.1: DSC catalyst 1

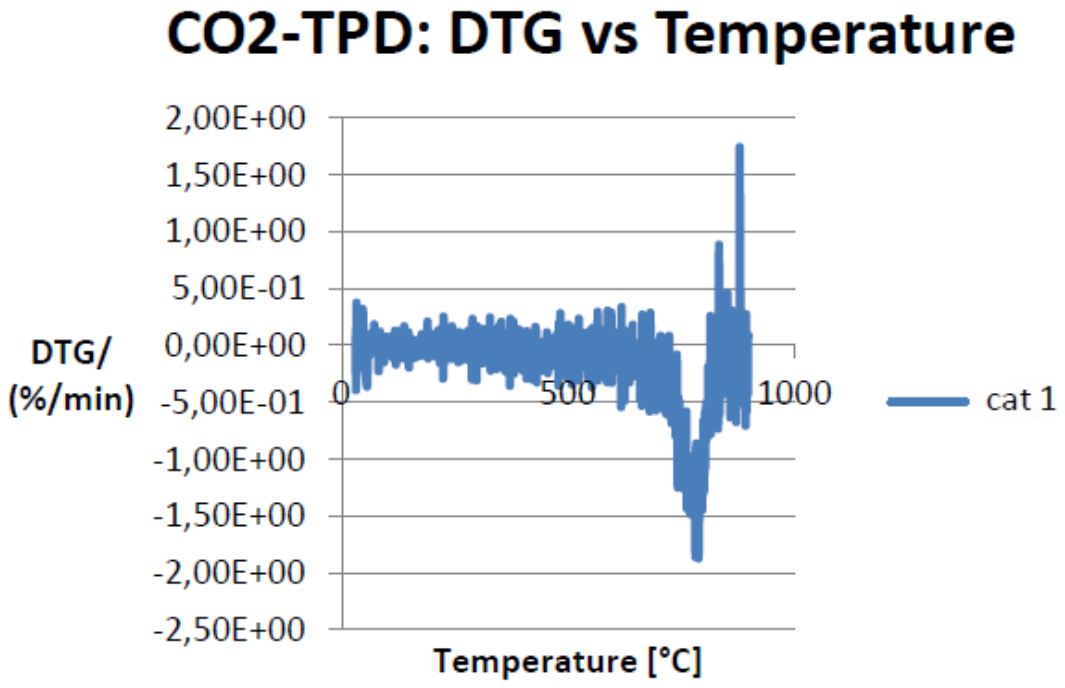

Figure H.2: DTG catalyst 1

CATALYST 3

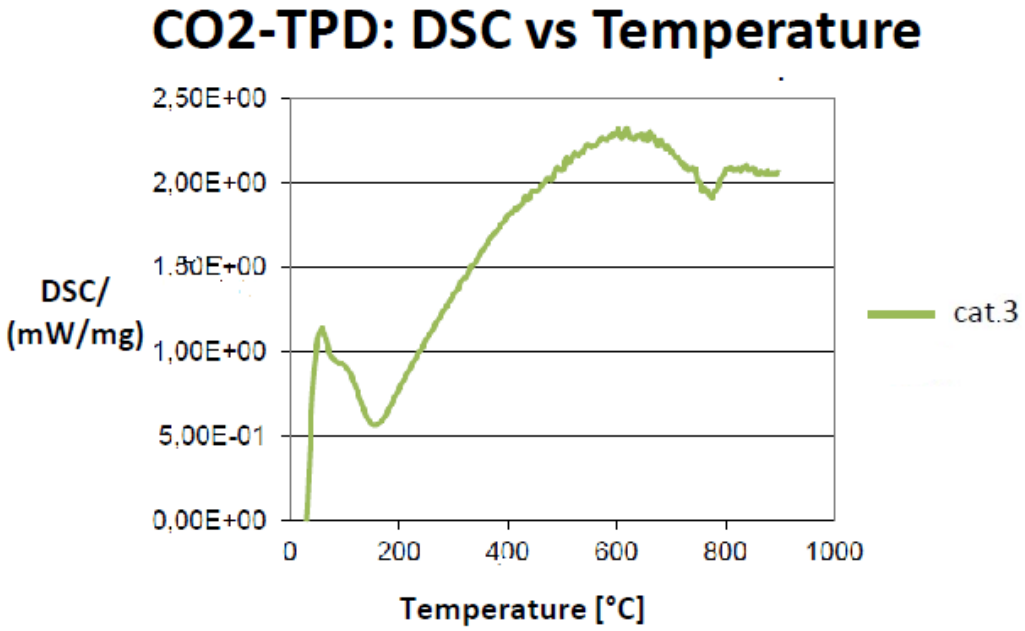

Figure H.3: DSC catalyst 3

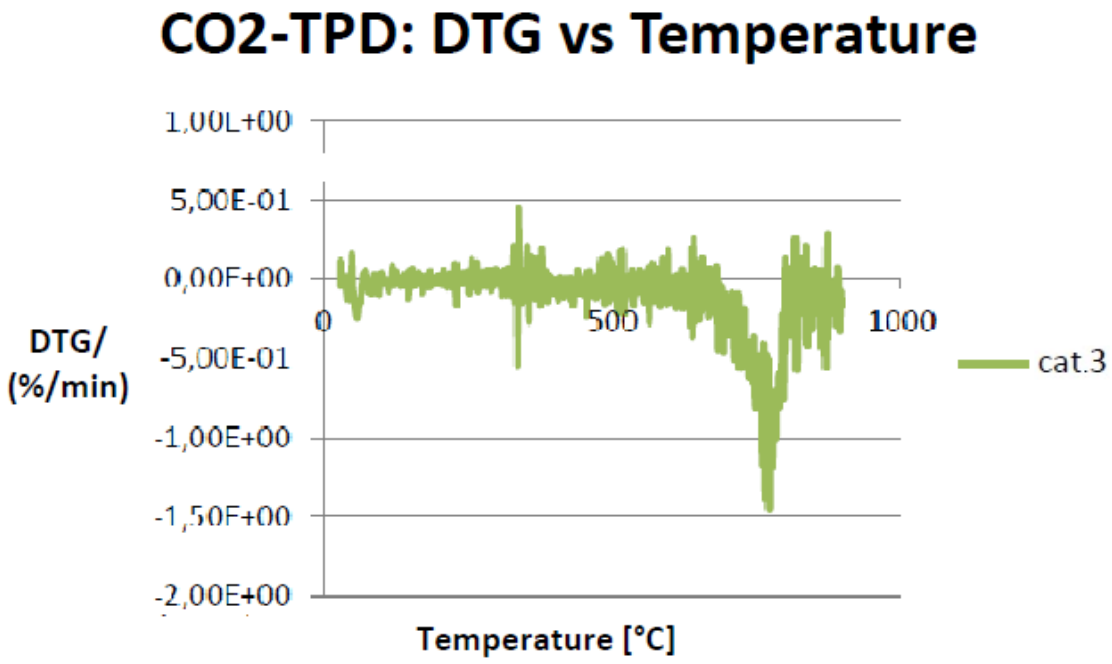

Figure H.4: DTG catalyst 3

CATALYST 5

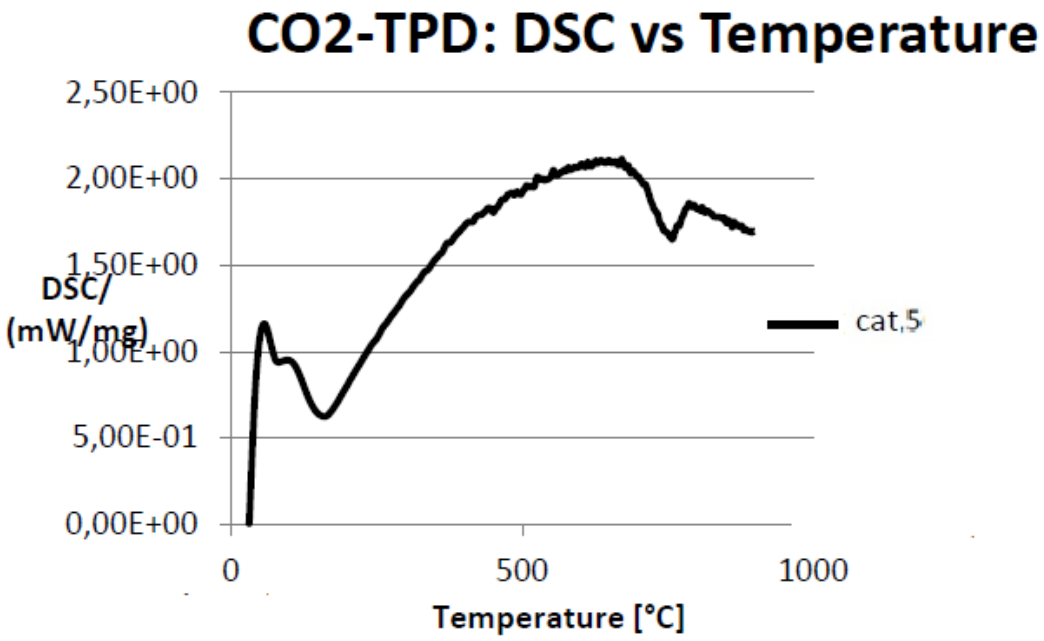

Figure H.5: DSC catalyst 5

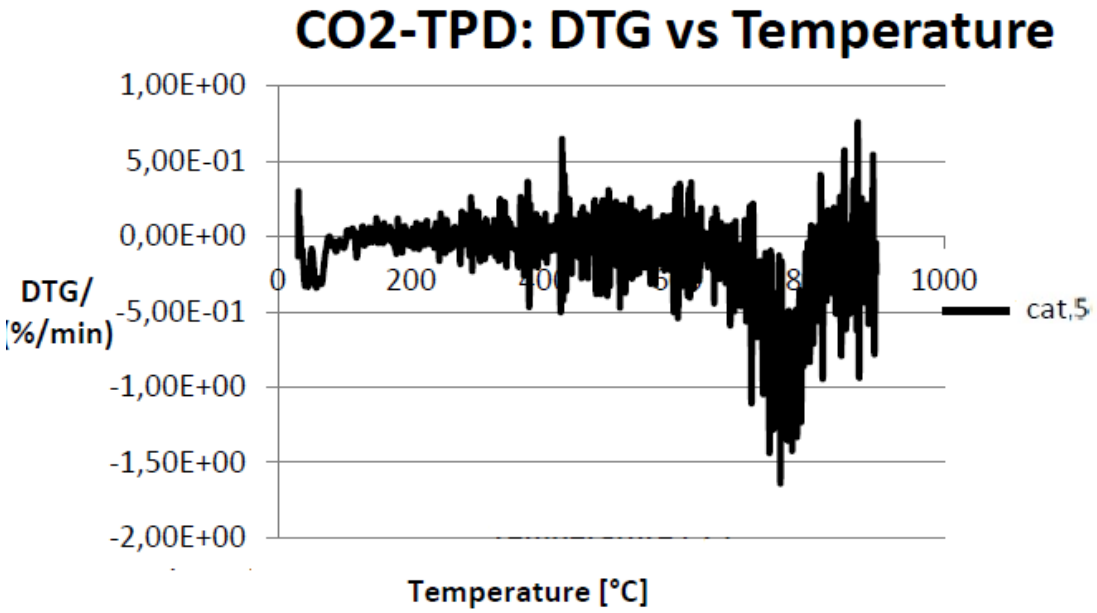

Figure H.6: DTG catalyst 5

AFTER NI IMPREGNATION

CATALYST 1

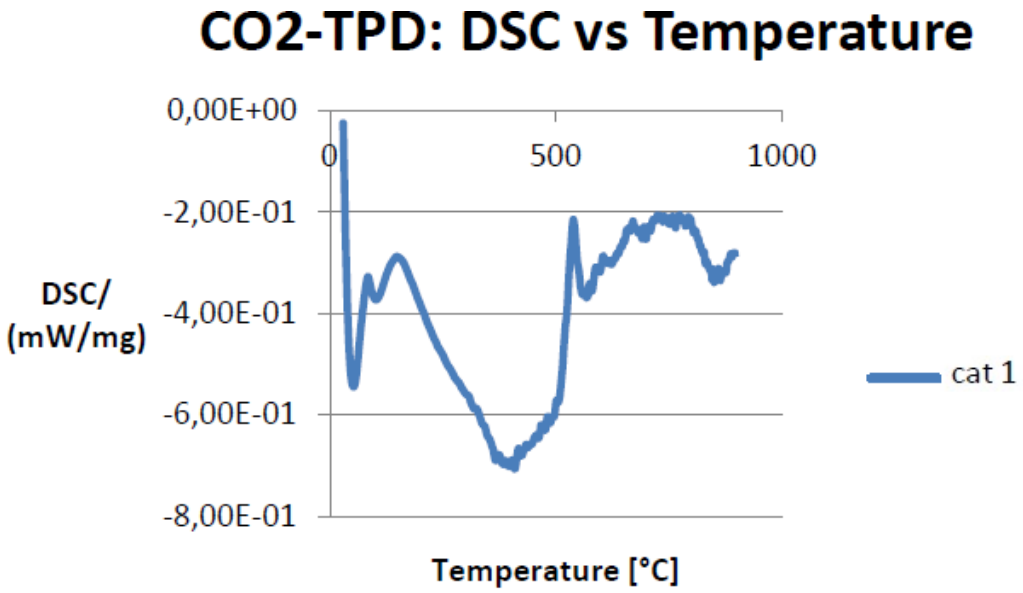

Figure H.7: DSC catalyst 1

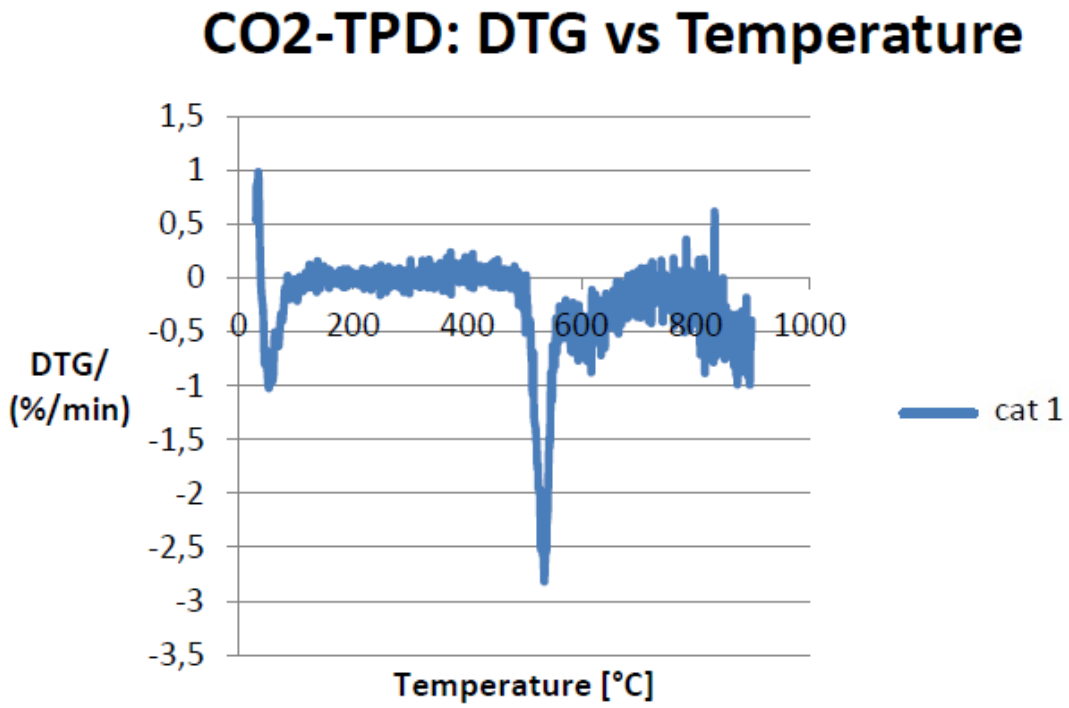

Figure H.8: DTG catalyst 1

CATALYST 3

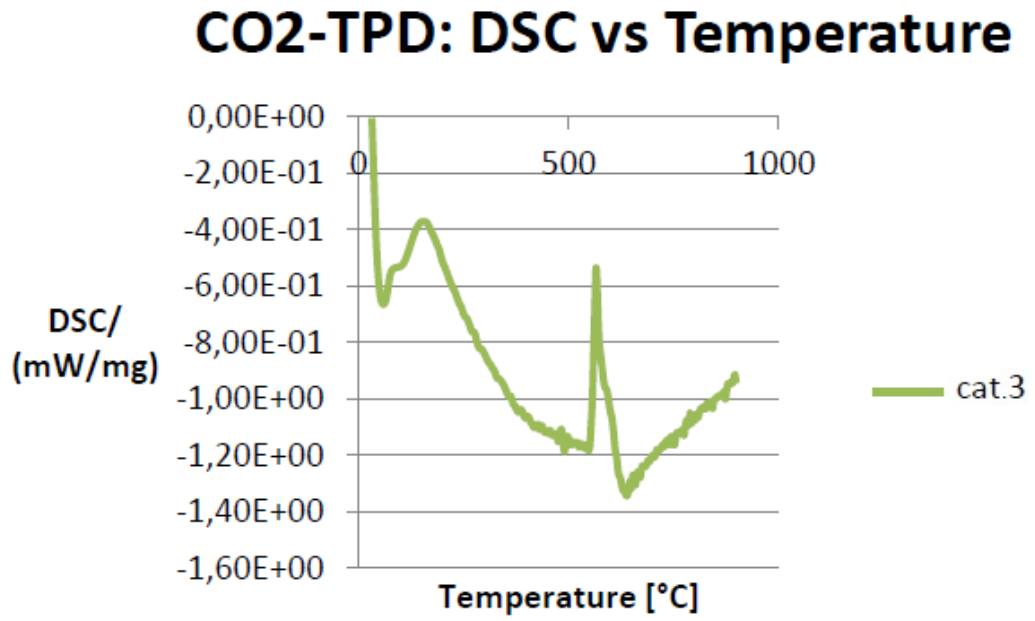

Figure H.9: DSC catalyst 3

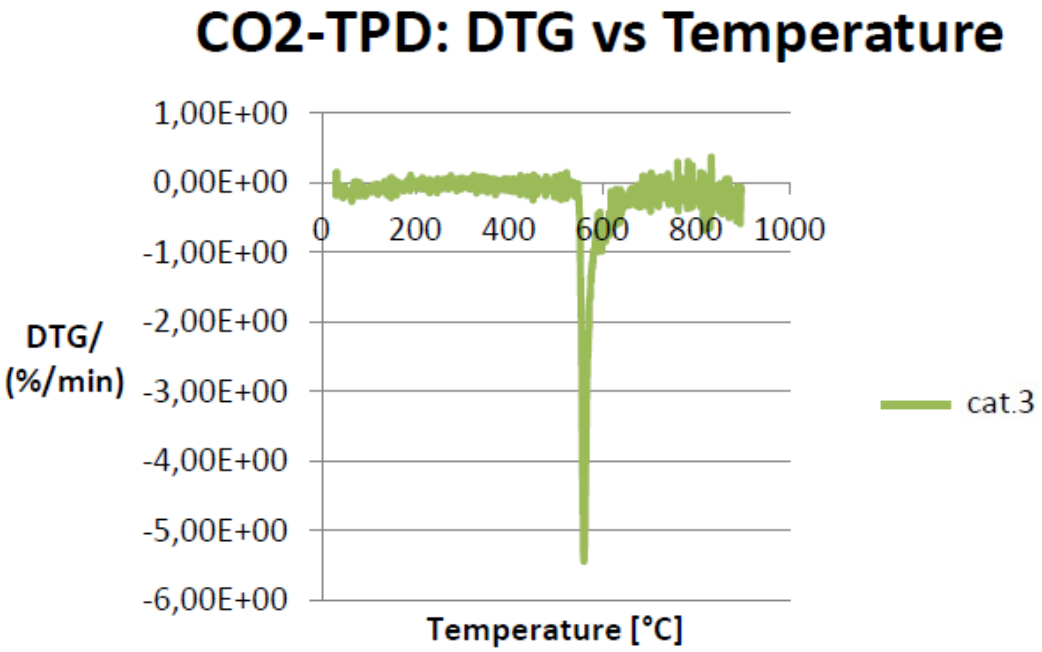

Figure H.10: DTG catalyst 3

CATALYST 5

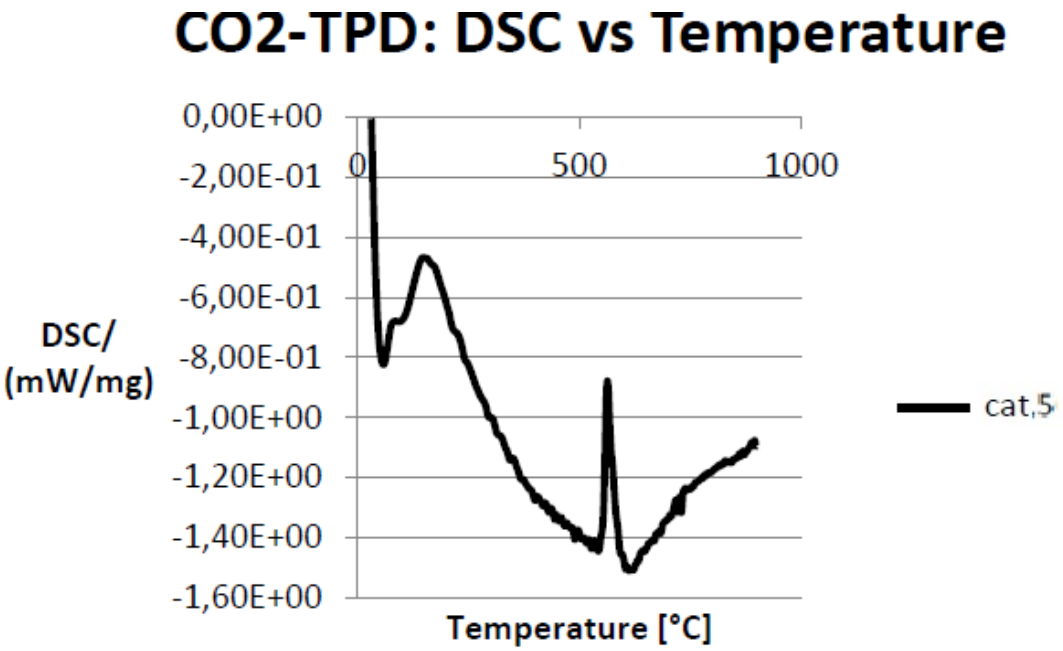

Figure H.11: DSC catalyst 5

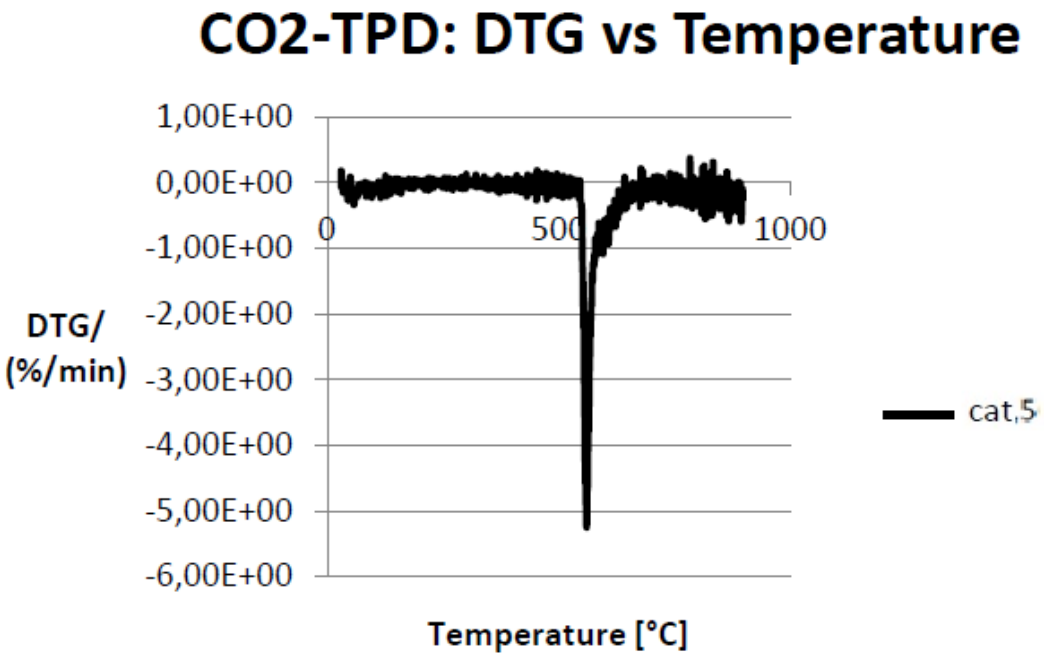

Figure H.12: DTG catalyst 5

CATALYST 8

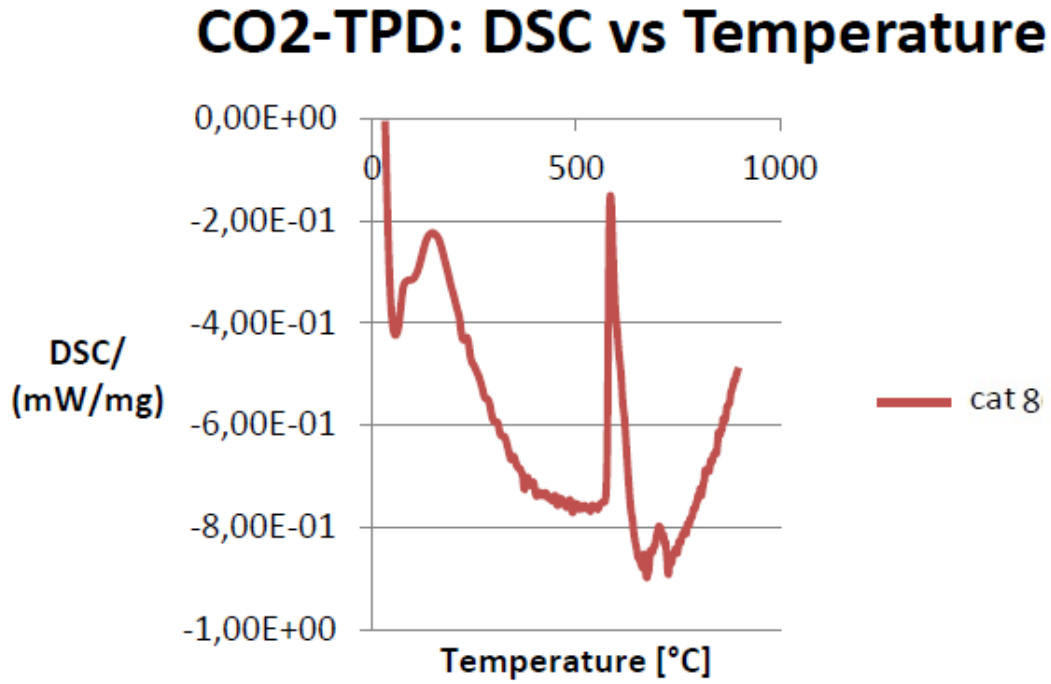

Figure H.13: DSC catalyst 8

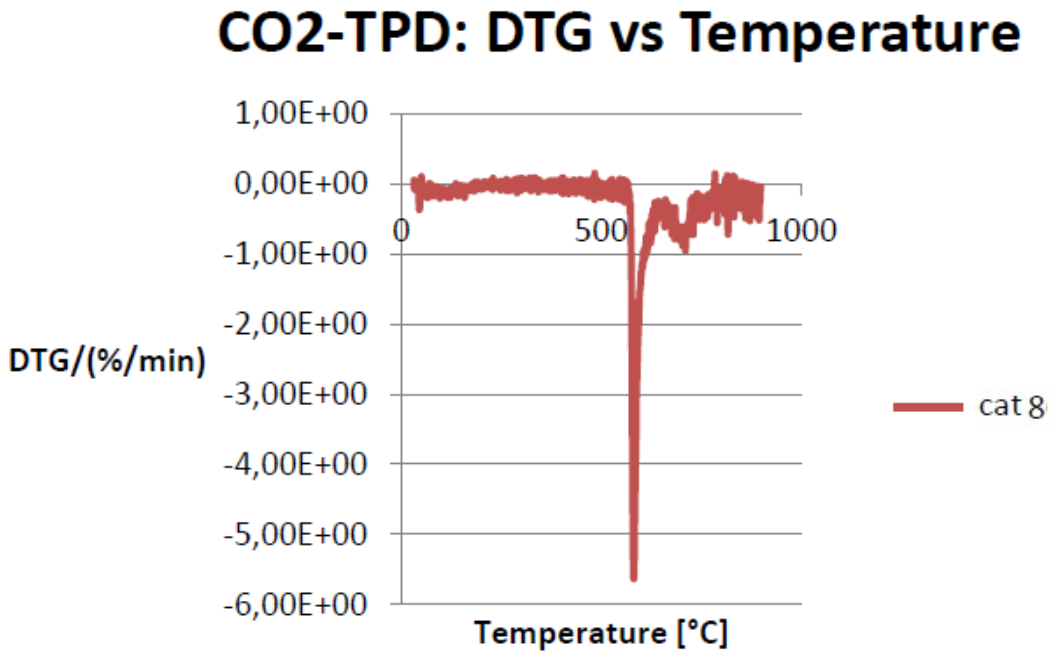

Figure H.14: DTG catalyst 8

CALCULATION OF THE CHANGE OF MASS IN THE CO_2-TPD PEAKS

After Ni impregnation

- Catalyst 1:

441ºC: 102% and 685ºC: 89 % → Difference: 13%

- Catalyst 8:

550ºC: 95,75% and 755ºC: 77,75% → Difference: 18%

- Catalyst 3:

548ºC: 95,77% and 692ºC: 83,07% → Difference: 12,7%

- Catalyst 5:

545ºC: 96,12% and 640ºC: 84,32% → Difference: 11,8%

Before Ni impregnation

- Catalyst 1:

1st peak: Start: 300ºC: 94%; Slutt: 530ºC: 93% → Difference: 1%

2nd peak: Start: 530ºC: 95,64%; Slutt: 730ºC: 92,64% → Difference: 3%

3rd peak: Start: 730ºC: 92,9%; slutt: 880ºC: 83,40% → Difference: 9,5%

Total: 13,5%

- Catalyst 3:

1st peak: start: 320ºC: 97,3%; slutt: 470ºC: 96,08% → Difference: 0,5%

2nd peak: start: 490ºC: 96,00%; slutt: 695ºC: 94,8% → Difference: 1,2%

3rd peak: start: 702ºC: 94,7%; slutt: 830ºC: 88,2% → Difference 6,5%

Total: 8,2%

- Catalyst 5:

1st peak: start: 315ºC: 97,15%; slutt: 510ºC: 96,75% → Difference: 0,4%

2nd peak: start: 550ºC: 96,55%; slutt: 705ºC: 95,05% → Difference 1,5%

3rd peak: start: 710C: 95,49%; slutt: 847ºC: 89,19% → Difference: 6,3 %

Total: 8,2%

RISK ASSESMENT

HMS	Hazardous activity identification process	HMS-avd.	HMSRV2601	
		Godkjent av	Side	Erstatter

Unit: *Kjemisk prosessteknologi* **Date:**

Line manager: *Øyvind Gregersen*

Participants in the identification process (including their funct

Short description of the main activity/main process:

ID no.	Activity/process	Responsible person	Laws, regulations etc.	Existing documentation	Existing safety measures	Comment
1	Use of toxic and flammable gases (H2)	Jun Zhu and De chen		Safety data sheet EIGA067A (H2)	Room detector, local detector, leak testing, gloves,	
2	Assembling/use of toxic gases CO	Jun Zhu and De chen		Safety data sheet: EIGA019	Room detector, local detector, leak testing, gloves	
3	Assembling/use of non toxic and inert gases: $CO_2/N_2/Ar/He$	Jun Zhu and De chen		Safety data sheet: EIGA018A CO2; EIGA089A N2;	Leak testing, gloves, gogles, lab coat.	
4	Use of acetone for cleaning proceedures	Jun Zhu and De chen		Safety data sheet	Gloves, lab coat, gogles.	
5	Carbon nanotubes	Jun Zhu and De chen		Safety data sheet	Gloves, lab coat, gogles, gas mask	
6	Handling chemicals	Jun Zhu and De chen		Safety data sheet	Gloves, lab coat, gogles	
7	Synthesis of catalysts	Jun Zhu and De chen		Safety data sheet	Gloves, lab coat, gogles	
8	Use of nitric acid	Jun Zhu and De chen		Safety data sheet	Gloves, lab coat, gogles	

NTNU	Risk assessment	Utarbeidet av	Nummer	Dato
		HMS-avd.	HMSRV2603	04/02/2011
		Godkjent av	Side	Erstatter
HMS/KS				

Unit: *Kjemisk prosessteknologi* **Date:** 0

Line manager: *Øyvind Gregersen*

Participants in the identification process (including th *0*

Signatures:

ID no.	Activity from the identification process form	Potential undesirable incident/strain	Likelihood:	Consequence:				Risk value	Comments/status Suggested measures
			Likelihood (1-5)	Human (A-E)	Environment (A-E)	Economy / material	Reputation (A-E)	Human	
1	Use of toxic and flammable gases (H2)	Leaks, fire, explosion	2	B	A	A		2B	Leak testing with noble gases and room and local detectors
2	Assembling/use of toxic gases CO	Leaks, fire	1	C	B	A		1C	Leak testing with noble gases and room and local detectors
3	Assembling/use of non toxic and inert gases: CO_2/N_2/Ar/He	Leaks	2	B	B	A		2B	Use of gloves, lab coat, gogles.
4	Use of acetone for cleaning proceedures	Spill, fire	3	A	A	A		2B	Use of gloves, lab coat, gogles.
5	Carbon nanotubes		3	C				3C	Use of gloves, lab coat, gogles, gas mask
6	Handling chemicals	Spill	2	C	A	A		2C	Use of gloves, lab coat, gogles
7	Synthesis of catalysts	Spill	2	B	A	A		2B	Use of gloves, lab coat, gogles
8	Use of nitric acid	Spill	2	C	A	A		2C	Use of gloves, lab coat, gogles